Master's thesis

A simulation study of beam backgrounds at the KEKB and Super KEKB colliders

Department of Physics,

Tohoku university

Hiroshi Nakano

2011

Abstract

To search new physics beyond the standard model, upgrade project of KEKB-factory is on the move. In order to gain luminosity, IP beam size become nanometer order.

Increment of backgrounds is expected due to gain in beam current and beam density.

For the purpose of IR designing, Touschek effect and gas scattering background were simulated for current KEKB and SuperKEKB. The result of current KEKB simulation was compared with experimental data.

We confirmed the validity of our simulation framework and obtained detailed understanding of the background mechanism.

Acknowledgment

First, I would like to thank Yamamoto Hitoshi-sensei [1] for giving me such a worthwhile and challenging work. His advice based on his overwhelming sense of physics was always accurate. It was good opportunity to discuss with him for the work.

Nakayama Hiroyuki-san told me how to manage work. He guided me with his excellent leadership as sometimes IR leader and sometimes senior. Hara Takanori-san helped me to debug simulation code whenever I had trouble. I was helped and encouraged uncountable times by his great kindness. Karim Trabelsi-san had taught me simulation basic without holiday for a month at the beginning of the work. Without him, my simulation study couldn't be started. Tanaka Shuji-san taught me IR mechanics and gave me useful advices. Tsuboyama-san helped me about how to compare simulation result with SVD data. Kanazawa-san kindly answered my many questions about vacuum. Funakoshi-san answered my questions about KEKB accelerator while he was busy on controlling KEKB. Iwasaki-san, former IR leader, gave me advices. Onishi-san's Touschek simulation helped my understanding. I also thank Shibata-san, Haba-san, Tajima-san, Abe-san, and many other people in KEK group. And Sugihara-kun gave me background study data which is comparable to simulation result.

Sanuki-san sometimes became counselor about my career. Nagamine-san helped me about computer problem. Takubo-san advised me about manner of presentation and how

[1] Japanese prefix. "-sensei" is used for teacher. "-san" or "-senpai" are added with respect. "-kun" is added with intimateness.

a person should be as a physicist. Onuki-san taught me about SVD. Kobayashi-san helped me as laboratory's secretary. Horii-san gave me many advices for career to be physicist. D1 students, my "senpai" ,were always kindly answered my question. Especially, I got the skill about ROOT and shell script from Yutaro-san and Zenmei-san. I was stimulated to work hard by smart and powerful rival, Saito-kun, Negishi-kun, Honda-kun and M1 students. I am thankful to everyone in the laboratory.

I want to say thank you to my parents.

Finally, I am much obliged to Yamamoto-sensei, Sanuki-san, Nakayama-san and Kato-san for castigating my master's thesis.

Contents

List of Figures

List of Tables

Chapter 1

Introduction

KEKB collider had made large amount of B mesons. By the end of running, 30 June 2010, KEKB achieved its peak luminosity as 2×10^{34} [$\mathrm{cm^2 s^{-1}}$] and integrated luminosity exceeded 1000 $\mathrm{fb^{-1}}$. Both of them are world records. Using such a high luminosity, belle experiment had pioneered luminosity frontier of particle physics with Babar experiment.

The aim of Belle II experiment is searching new physics. For this purpose, we need much more integrated luminosity for precise measurement. Therefore, KEKB will be upgraded to SuperKEKB. Design luminosity of SuperKEKB is about 40 times higher than one of KEKB.

After upgrade, beam size will be much smaller than before to increase luminosity. This change will also induce increment of beam background. Especially a kind of scattering, caused by collision of beam particle each other within a bunch ,called "Touschek effect" will be increased.

In order to decrease beam background, heavy metal mask will be placed near the interaction point. Simulation study of beam background is necessary for designing of heavy metal mask and estimation of background in SuperKEKB.

We compared simulation results of beam-gas scattering and Touschek background with experimental data and confirmed a validity of the simulation method. Preliminary

estimation of background amount for SuperKEKB was also done.

In Chapter 2, physics motivation of Belle II experiment is mentioned. The way to increase luminosity of KEKB collider is described in Chapter 3. In Chapter 4, beam background mechanism especially Beam-gas scattering and Touschek effect are mentioned. Chapter 5 describes interaction region of KEKB and SuperKEKB. The method of simulation study of Beam-gas scattering and Touschek effect for KEKB and SuperKEKB colliders are represented and the results are shown in Chapter 6. Summary and future prospects are in Chapter 7. Accelerator things are described in Appendix A.

Chapter 2

Physics motivation of Belle II

2.1 Sign of new physics seen at Belle experiment

Belle experiment was started for the purpose of searching CP violation of B meson decay. Time dependent CP violation was observed by using $B^0 \to J/\psi K^0$ decay mode. From this, one of the angle of the unitarity triangle $\sin 2\phi_1$ was measured.

One of a new physics (NP) sign was seen at measurement of $\sin 2\phi_1^{\rm eff}$ by using $b \to sq\bar{q}$ process. The results of the measurement by B factories are summarized in Fig. 2.1 In the standard model (SM), results of these values should be same. If the results are deviated from the result of $B^0 \to J/\psi K^0$ mode, there is new CP-violating phase. Now, there is not enough statistics to decide whether there is deviation or not. Thus, precise measurement with high luminosity is expected.

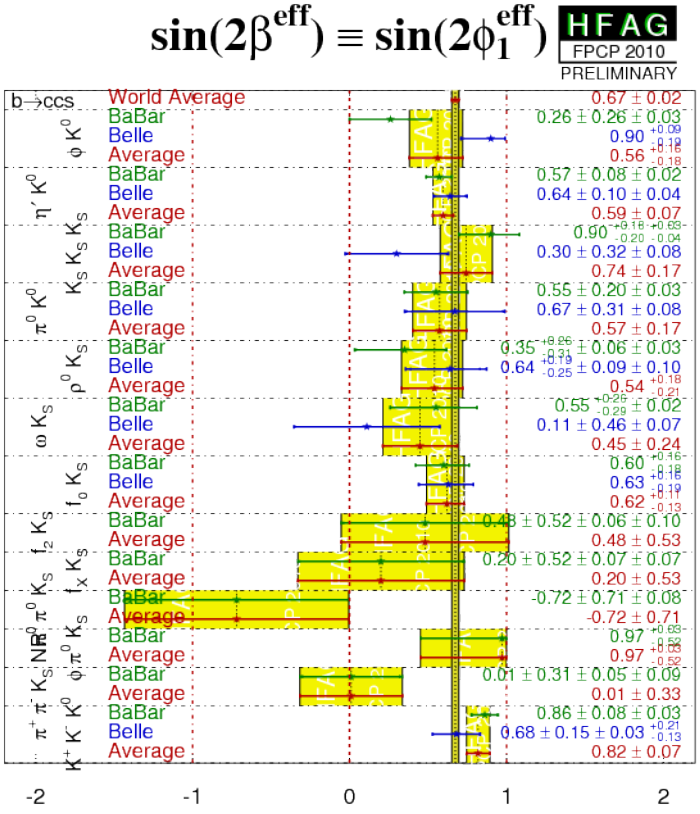

Figure 2.1: Time-dependent CP asymmetries in $b \to q\bar{q}$ transitions [1]

2.2 Expected physics at Belle II experiment

Increment of the luminosity allows us searching NP sign described above. Figure 2.2 shows the CP asymmetries for $B^0 \to \phi K_s^0$ decay and $B^0 \to J/\psi K_s^0$ decay at 50 ab^{-1}. Input values $\mathcal{S}_{\phi K_s^0} = 0.39$ and $\mathcal{A}_{\phi K_s^0} = 0.0$ are used for $B^0 \to \phi K_s^0$. In the SM, results of these two decays should be same. If these results are different, this means existence of new physics. Figure 2.3 shows the relationship between error of ϕ_1 for $B^0 \to \phi K_s^0$ and luminosity. The dotted (red) and dashed (green) curves show the statistical and systematic errors respectively. And the solid (black) curve shows the total of them ($\sigma_{tot}^2 = \sigma_{stat}^2 + \sigma_{syst}^2$). While statistical error decreases as luminosity gained, systematic error has lower limit. At 50 ab^{-1} statistics, statistical error fall below systematic error and systematic error becomes dominant. These figures show that if there is NP contribution to sin2$\phi_1^{\rm eff}$, Belle II experiment will observe the difference from SM.

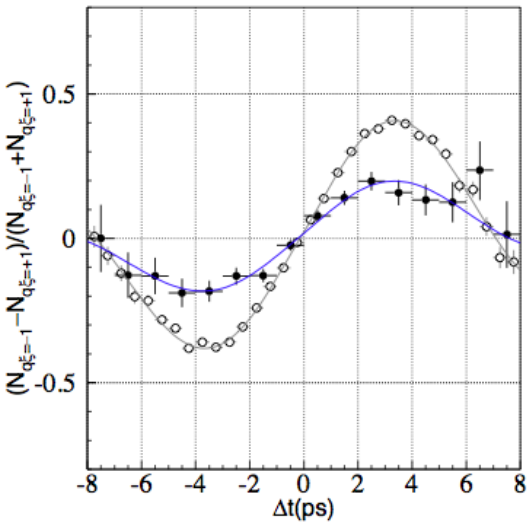

Figure 2.2: Raw asymmetries for $B^0 \to \phi K_s^0$ and $B^0 \to J/\psi K_s^0$ at 50 ab^{-1} [2].

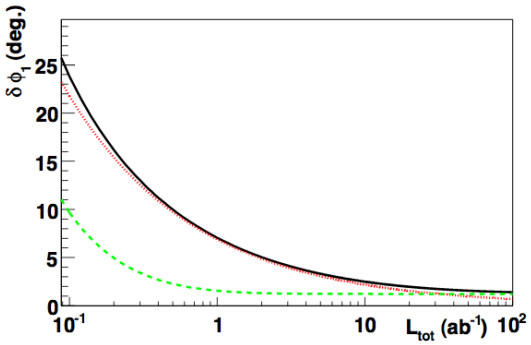

Figure 2.3: Estimated uncertainties as a function of the integrated luminosity in $B^0 \to \phi K_s^0$ decay [2].

There is two way to search NP beyond the SM. One is searching the deviation from SM with precise measurement. The other is searching the event which is strongly suppressed in the SM. Here are the examples of promising way to searching NP sign at Belle II

experiment [2].

Searching deviation from the SM

- Precise measurement of Wilson coefficients by using $b \to s\gamma$ decays. Wilson coefficients are the coefficients of the effective hamiltonian $\mathcal{H}_{\text{eff}}$.
- Searching for charged Higgs is possible from measurement of the branching fraction of $B \to \tau\nu_\tau$ and $B \to \bar{D}\tau\nu_\tau$.
- Measurement of the angles of the unitarity triangle ϕ_1, ϕ_2 and ϕ_3.

Strongly suppressed event in the SM

- Searching for lepton flavor violation of τ.
- Direct CP violation of $B^\pm \to \phi\phi X_s^\pm$ decay.
- Direct CP violation of $B^0 \to K^{*0}\gamma$ decay.

The phase of B physics is being shifted from verification of CP violation to finding NP sign. In order to achieve this, we need more statistics. Therefore, KEKB must be upgraded to SuperKEKB.

Chapter 3

KEKB-factory upgrade

For searching beyond the standard model, KEKB-factory has set it's goal to an integrated luminosity of $50ab^{-1}$. In this chapter, we mention the KEKB collider and its upgrade scheme. Basic terminology of accelerator are described in Appendix A.

3.1 KEKB and its luminosity

At this point in time (KEKB operation closed in 2010 June), integrated luminosity at c.m. energy of 10.58 GeV is about 700 fb^{-1} as shown in Fig. 3.1. Cross section of $\Upsilon(4s)$ at c.m. energy of 10.58 GeV is about 1 nb^{-1}. The amount of $\Upsilon(4s)$ event i.e. $B\bar{B}$ pair event is

$$\sim 1 \text{ [nb]} \times 700 \text{ [fb}^{-1}\text{]} = 700 \text{ million.} \tag{3.1}$$

There are two methods for collecting a lot of events. One is taking longer operation time. Second is increment of luminosity. Next aim of integrated luminosity is 50 ab^{-1} (50000 fb^{-1}). Now, assuming that luminosity is 20 $\text{nb}^{-1}\text{s}^{-1}$ and operation time per year is 10^7 s, KEKB-factory has an ability to store 200 fb^{-1} of integrated luminosity per year. So, if we were to continue operating in the former method, it would takes 250 years to collect 50 ab^{-1}. On the other hand, if we increase luminosity 50 times larger, only 5 years

are needed.

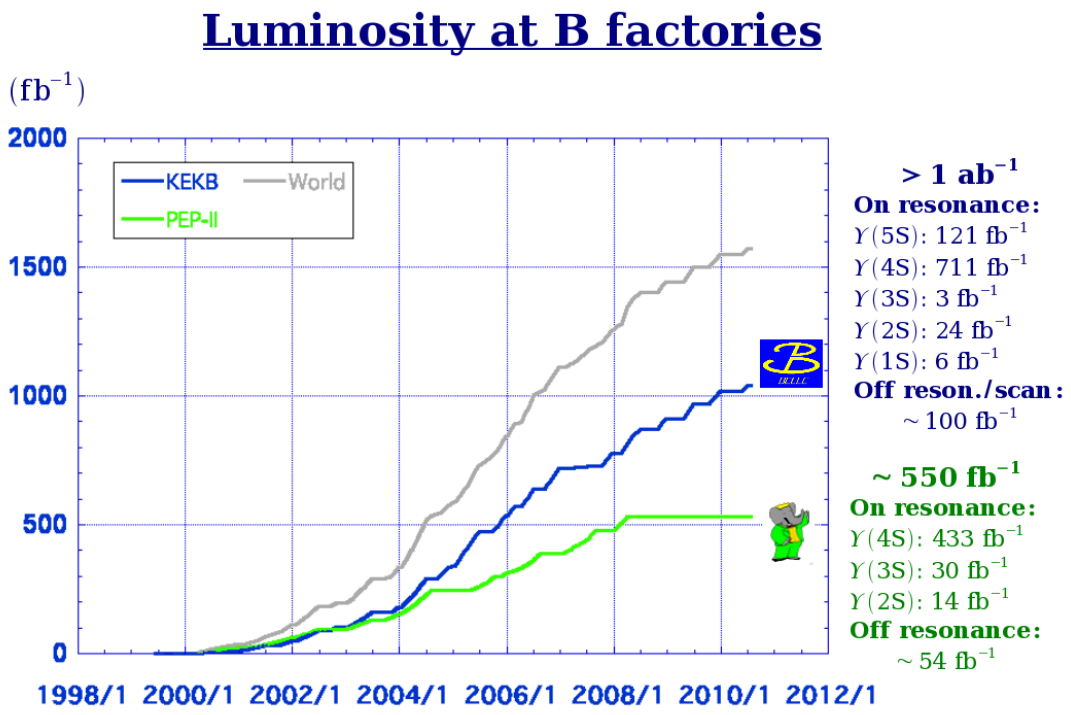

Figure 3.1: Integrated luminosity of B factories [3]

Before we talk about the upgrade scheme, we will look at the means as to achieve such a high luminosity at the current KEKB. Figure 3.2 shows the overview of KEKB ring. First, electrons and positrons were made and accelerated at linac. Next, 8.0 GeV electron beam and 3.5 GeV positron beam are injected to "high energy ring (HER)" and "low energy ring (LER)" respectively. After injection, each beam particle circles the rings which have 3 km of circumference. At each curve, the beam particles emit synchrotron radiation and decreases its energy; accelerating cavities compensate their loss of energy. This process acts as a damping ring. LER's damping speed is slower than HER's one. So, LER has wiggler to decrease beam energy more faster. Wiggler is a sequence of bending magnets which helps LER beams to emit synchrotron radiation. At the interaction region

(**IR**), LER beam and HER beam cross and collide with each other.

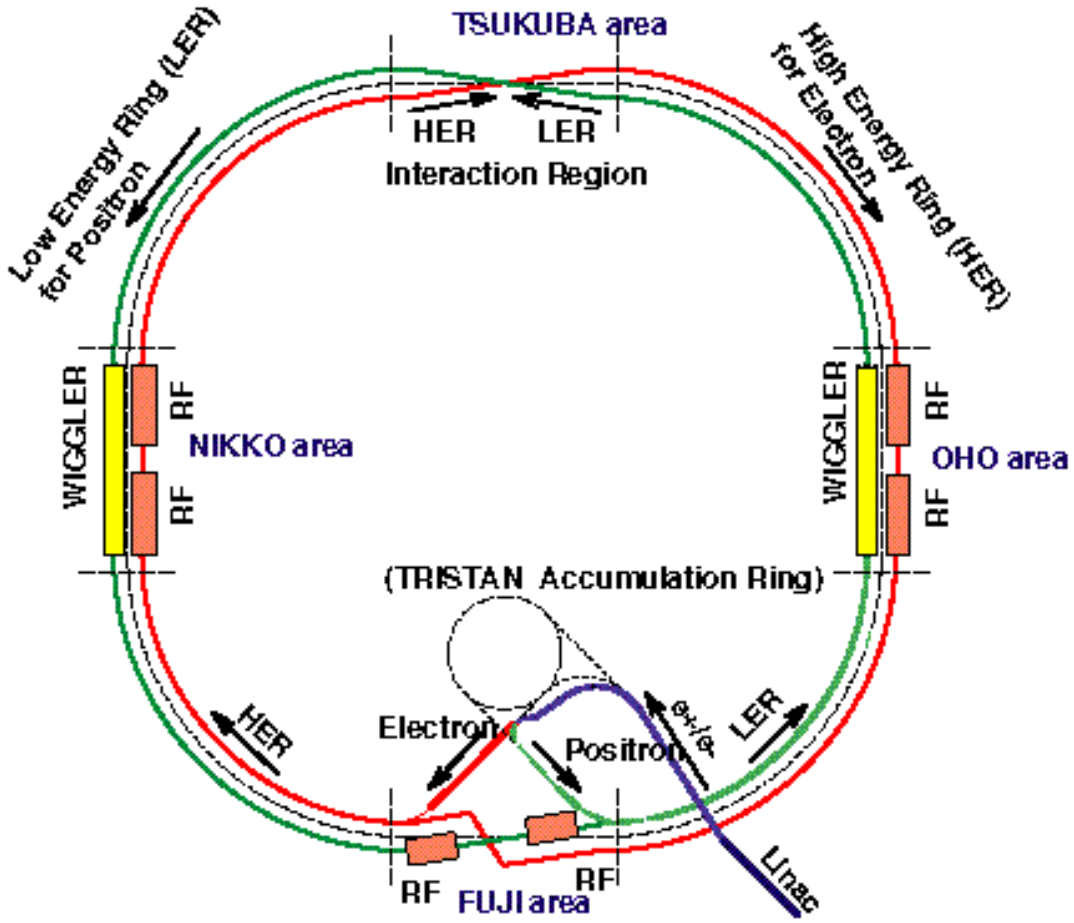

Figure 3.2: KEKB ring [4]

KEKB adopts a scheme where the crossing angle at interaction point (IP) is non-zero. The existence of crossing angle decreases luminosity (see A.3.6). To remove this effect, KEKB adopted collision method called "crab crossing" (Fig. 3.3).

3.2 Upgrade scheme for SuperKEKB

KEKB design parameters, KEKB parameters with crab crossing when luminosity record was achieved and SuperKEKB design parameters of nano-beam scheme are listed in table 3.1. Here, $\beta^*_{x,y}$ is the beta functions at IP, ϵ_x is the horizontal emittance, $\sigma^*_{x,y}$ is the beam

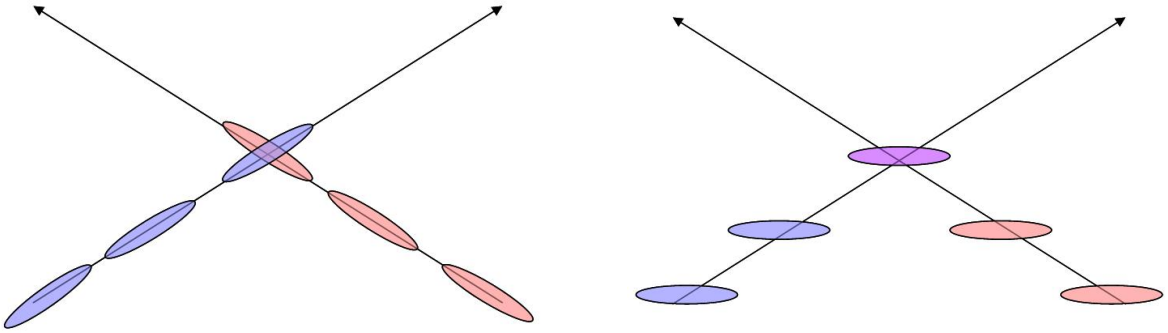

Figure 3.3: Non-zero crossing angle without crab crossing(left) and with crab crossing(right).

Table 3.1: Beam parameters of KEKB and SuperKEKB [8]

LER/HER	KEKB Design	KEKB with crab	SuperKEKB Nano-Beam
Energy (GeV)	3.5/8.0	3.5/8.0	4.000/7.007
β_y^* (mm)	10/10	5.9/5.9	0.27/0.30
β_x^* (mm)	330/330	1200/1200	32/25
ϵ_x (nm)	18/18	18/24	3.2/4.3
σ_y^* (μm)	1.9	0.94	0.048/0.063
σ_x^* (μm)	77/77	147/170	10/10
ξ_y	0.052	0.129/0.090	0.0869/0.0807
σ_z (mm)	4	~ 6	6/5
2ϕ (rad)	22	22	83
I_{beam} (A)	2.6/1.1	1.64/1.19	3.6/2.6
$N_{bunches}$	5000	1584	2500
$\mathcal{L}$ ($10^{34}\mathrm{cm}^{-2}\mathrm{s}^{-1}$)	1	2.11	80

size at IP, ξ_y is the vertical beam-beam tune shift parameter, σ_z is the bunch length, 2ϕ is the beam crossing angle, I_{beam} is the beam current, $N_{bunches}$ is the number of bunches and $\mathcal{L}$ is the luminosity.

The essentials in luminosity upgrade are

- High beam current.
- Small beam size.

As shown in Tab. 3.1, beam size will be very small. To achieve this, the damping ring will be used before injection for LER, and wigglers will be used for HER. The idea of nano-beam scheme to obtain high luminosity is completely different from the current KEKB.

First of all, it does not use crab crossing, despite having a large crossing angle. Secondly, the vertical beta function is much smaller than bunch length, which seems to induce the "hourglass effect"; an effect that occurs when $\sigma_z \gtrsim \beta^*_{x,y}$ and furthermore decreases luminosity reduction coefficient. However having a crossing angle enables to decrease bunch length effectively and helps to avoid the hourglass effect with its small beta function of twiss parameter (figure 3.4). With a large non-zero crossing angle, the effective bunch length L becomes $L \sim \sigma^*_x/\phi$. Substituting $\sigma^*_x = 10\mu m$ and $\phi = 83/2$ mrad, L becomes 0.24 mm. Thus the hourglass effect can be small while $\beta^* \gtrsim L$, so the beta function of twiss parameter at IP can lessen up to 0.24 mm.

Besides, large crossing angle has another advantage. Very small β^* means a rapid increase in beam size near the IP (see eq.(A.46)). This means the quadrupoles that are closest to IP for focusing should be placed near IP as close as possible. Larger crossing angle is favorable to this requirement (For further detail of IR, see Chap. 5). However, there are both merits and demerits in anything, and small beam size causes serious problem. By upgrading, Touschek effect which makes beam particles deviate its orbit will increase. It makes beam life time short and causes large amount of radiation

damage and background to the detector. This is why beam energy is changed from 3.5 GeV v.s. 8 GeV to 4 GeV v.s. 7.0 GeV (The lower energy of the beam, the more significant Touschek effect will be. For detail, see Chap. 4). Although energy asymmetry was sacrificed for reducing Touschek effect, this effect is still large and this is one of the biggest problems of KEKB upgrade.

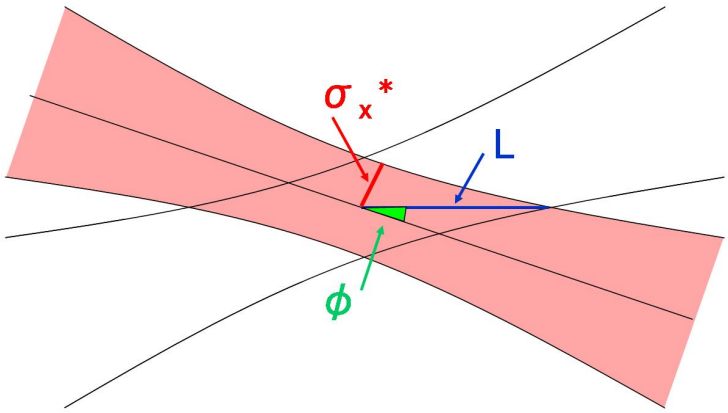

Figure 3.4: Illustration of effective bunch length L. $L \sim \sigma_x^*/sin\phi \sim \sigma_x^*/\phi$

Chapter 4

Beam background

In KEKB-factory upgrade, beam background is one of the most important issues. In this chapter beam background, especially beam-gas scattering and Touschek effect, is mentioned.

4.1 Beam background types

Beam particles emit synchrotron radiation (SR) when they are bent by magnet. SR background comes from both upper stream and down stream. This kind of background is especially important in HER beam because their beam energy is high. Beam particles are scattered by residual gas (beam-gas scattering) or they collide with each other within a bunch (Touschek effect). Scattered particles will hit beam pipe and make showers. These showers hit the detector and become background. In addition, when electron and positron beams collide at IP, background particles are also generated. The main background event is a electron-positron pair production. This background will increase because innermost detector get closer after upgrade. Illustration of these background events are shown in Fig. 4.1. Wave line (orange) means SR background. Line (blue) means scattered beam particle. Dash line (red) means electron-positron pair production.

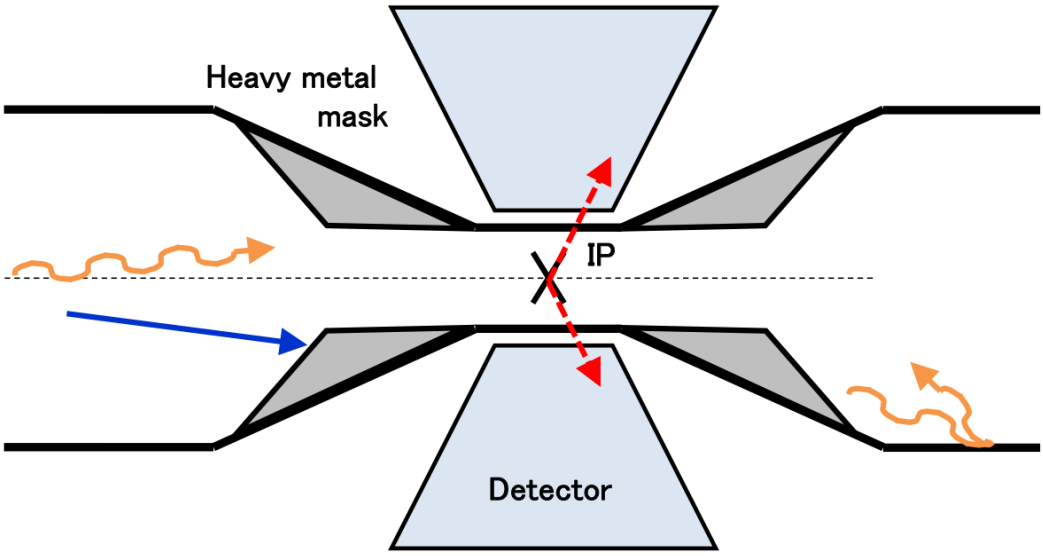

Figure 4.1: Beam background mechanism

4.2 Beam-gas scattering

Design value of pressure of the beam pipe is 10^{-7} Pa. Main constituents of the residual gas are H_2 and CO. When beam particles are scattered by the residual gas, particle's direction is changed (Coulomb scattering), or its energy is decreased with emitting photon (bremsstrahlung).

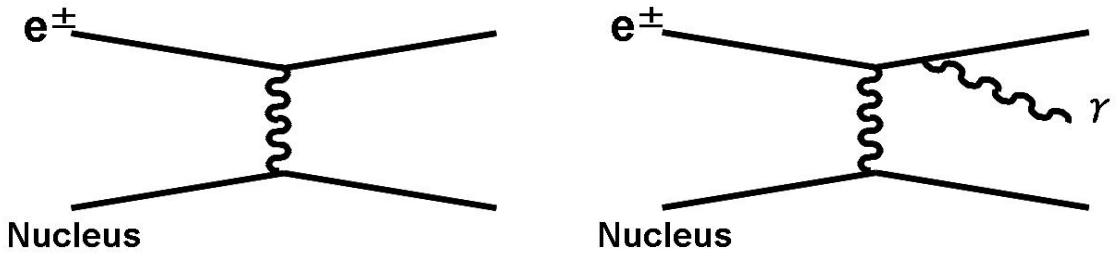

Figure 4.2: Feynman diagrams for Coulomb scattering (left) and bremsstrahlung (right).

4.2.1 Coulomb scattering

Coulomb scattering is caused by elastic scattering between electron (or positron) and gas nucleus. The energy of the electron is conserved while its direction is changed. Differential cross section of the scattering is,

$$\frac{d\sigma_{\text{coul}}}{d\Omega} = \frac{Z^2\alpha^2}{4\beta^2|\vec{p}|^2\sin^4\frac{\theta}{2}} \tag{4.1}$$

Where, Z is charge of the gas nucleus, α is fine structure constant, β and $\vec{p}$ are particle's velocity and momentum respectively, θ is the scattering angle [9]. Here, we can approximate $\beta \sim 1$ and θ is enough small to approximate $\sin\theta \sim \theta$. Integrate (4.1) from $\theta = \theta_{\text{min}}$ to $\theta = \theta_{\text{max}}$, we will get

$$\begin{aligned}
\sigma_{coul} &= \int_0^{2\pi} d\phi \int_{\theta_{\text{min}}}^{\theta_{\text{max}}} d\theta \frac{Z^2\alpha^2\sin\theta}{4\beta^2|\vec{p}|^2\sin^4\frac{\theta}{2}} \\
&= \int_{\theta_{\text{min}}}^{\theta_{\text{max}}} d\theta \frac{8\pi Z^2\alpha^2}{E^2\theta^3} \\
&= -\frac{4\pi Z^2\alpha^2}{E^2}[\theta^{-2}]_{\theta_{\text{min}}}^{\theta_{\text{max}}} \\
&= \frac{4\pi Z^2\alpha^2}{E^2}(\frac{1}{\theta_{\text{min}}^2} - \frac{1}{\theta_{\text{max}}^2})
\end{aligned} \tag{4.2}$$

4.2.2 Bremsstrahlung

By bremsstrahlung, an electron (or positron) emits photon and decreases its energy. Differential cross section for scattering is,

$$\frac{d\sigma_{\text{brem}}}{d\epsilon} = \frac{r_0^2\alpha Z[Z+\xi(Z)]}{\epsilon}\left\{[1+(1-\epsilon)^2][\Phi_1(\delta) - F(Z)] - \frac{2}{3}(1-\epsilon)[\Phi_2(\delta) - F(Z)]\right\} \tag{4.3}$$

Where, E is the electron energy, Z is the atomic number, ϵ is the fraction of E carried away by the photon(i.e. $\epsilon = \frac{\Delta E}{E}$), r_0 is the classical electron radius. ξ, F, Φ_1, Φ_2 and δ

are defined below [9].

$$\delta = \frac{136 m_e}{Z^{1/3} E} \cdot \frac{\epsilon}{1-\epsilon}$$

$$\left.\begin{aligned} \Phi_1 &= 20.867 - 3.242\delta + 0.625\delta^2 \\ \Phi_2 &= 20.209 - 1.930\delta - 0.086\delta^2 \end{aligned}\right\} \text{for } \delta \leq 1$$

$$\Phi_1 = \Phi_2 = 21.12 - 4.184 \ln(\delta + 0.952) \quad \text{for } \delta > 1$$

$$F(Z) = \begin{cases} 4/3 \ln ZE < 0.05 \text{ GeV} \\ 4/3 \ln Z + 4 f_c(Z) E \geq 0.05 \text{ GeV} \end{cases}$$

$$\xi(Z) = \frac{\ln(1440/Z^{2/3})}{\ln(183/Z^{1/3}) - f_c(Z)}$$

$$f_c(Z) = Z\alpha \left\{ \frac{1}{1+Z\alpha} + 0.20206 - 0.0369 Z\alpha + 0.0083 (Z\alpha)^2 - 0.002 (Z\alpha)^3 \right\}$$

4.2.3 Rate of gas-scattering

As we know cross sections of Coulomb scattering and bremsstrahlung, we can estimate scattering rate. First, from the equation

$$PV = N k_B T, \tag{4.4}$$

where P [Pa] is pressure, V [m^3] is volume, N is number of gas molecule, k_B is Boltzmann constant, 1.38×10^{-23} [J/K], and T [K] is absolute temperature. The number of gas molecules per 1 m^3 is $\dfrac{P}{k_B T}$ [m^{-3}]. Then, when the beam particles move at speed of light, the number of gas molecules seen from the beam particle per barn[1] per second N_{gas} is

$$N_{\text{gas}} = \frac{cP}{k_B T} \times 10^{-28} \text{ [barn}^{-1}\text{s}^{-1}\text{]}. \tag{4.5}$$

[1] 1 barn = 100 fm^2 = 10^{-28}m^2

Main components of remaining gas are H_2 and CO. They are diatomic molecules, thus the number of nuclei per barn per second $N_{\rm nuc}$ is twice that of $N_{\rm gas}$.

$$N_{\rm nuc} = 2N_{\rm gas} = 2\frac{cP}{k_B T} \times 10^{-28}[{\rm barn}^{-1}{\rm s}^{-1}] \tag{4.6}$$

The number of beam particles contained within one circuit of the ring $N_{\rm beam}$ is

$$N_{\rm beam} = \frac{I}{e} \times \frac{L}{c} \tag{4.7}$$

Here, I is beam current, L is the circumference of KEKB ring. Therefore, the scattering rate per second R [s^{-1}] is

$$\begin{aligned} R &= \sigma_{\rm gas} \times N_{\rm beam} \times N_{\rm nuc} \\ &= \sigma_{\rm gas} \times \frac{2PLI}{k_B T e} \times 10^{-28}[{\rm barn}^{-1}{\rm s}^{-1}] \end{aligned} \tag{4.8}$$

Here, $\sigma_{\rm gas}$ is total cross section of gas scattering, $\sigma_{\rm gas} = \sigma_{\rm coul} + \sigma_{\rm brem}$. From (4.1) and (4.3), $\sigma_{\rm gas}$ is depend on Z. Z = 1 for H_2 and Z = 7 for CO (taking the average, i.e. (6+8)/2). The larger the Z, the larger the $\sigma_{\rm gas}$ becomes, so scattering rate by CO $R_{\rm CO}$ is much larger than one by H_2 R_{H_2}. For simplification, R_{H_2} is ignored.

Substitute beam current of LER $I_{\rm LER}$ = 1.6 A, beam current of HER $I_{\rm HER}$ = 1.2 A, partial pressure of CO $P_{\rm CO} = 10^{-7}$ [Pa], length of beam pipe L = 3016 m, temperature T - 300K, we get

$$R[{\rm Hz}] = \begin{cases} 1.457 \times 10^8 \ \sigma_{\rm gas}\ [{\rm barn}] & ({\rm for\ LER}) \\ 1.093 \times 10^8 \ \sigma_{\rm gas}\ [{\rm barn}] & ({\rm for\ HER}). \end{cases} \tag{4.9}$$

For example, consider Coulomb scattering which scattering angle is greater than 0.4 mrad and bremsstrahlung which fraction of photon energy is 1 %. $\sigma_{\rm gas}$ for LER and HER

becomes

$$\sigma_{\rm gas}[\text{barn}] = \sigma_{\rm Coul} + \sigma_{\rm brem} = \begin{cases} 6.52 + 3.31 = 9.83 & \text{(for LER)} \\ 1.25 + 3.32 = 4.57 & \text{(for HER).} \end{cases} \tag{4.10}$$

Scattering rates of LER and HER are $1.4 \times 10^9[\text{s}^{-1}]$ and $5.0 \times 10^9[\text{s}^{-1}]$ respectively.

4.2.4 Gain of background due to upgrade

After upgrade, the beam current of LER and HER increase from 1.6 A to 3.6 A and 1.2 A to 2.6 A respectively. Scattering rate is proportional to the beam current and pressure, so scattering rate will increase about two times.

In addition, the geometry of the ring will change. Vacuum pressure is dependent on position of the rings; this changes vacuum pressure locally. For example, IP beam pipe radius changes from 1.5 cm to 1.0 cm. The vacuum conductance of a narrow pipe is small, so it is predicted that pressure at IP will be 100 - 1000 times higher than current pressure. And wiggler will be implemented for HER after upgrade. Vacuum pressure at wiggler area will be high because gas molecules are emitted when SR light hit beam pipe.

4.3 Touschek effect

4.3.1 Touschek effect

Beam particles circle the beam pipe forming a group (it is called bunch), which contains about $10^{10\sim11}$ beam particles. While circling, beam particles oscillate perpendicular to beam direction which is called "betatron oscillation (see appendix A)". When beam particles collide each other, their transverse momentum changes to longitudinal momentum. Thus the energy of the beam particle changed in laboratory frame. One collision always causes one particle to increase energy and one particle to decrease. A brief explanation

of the mechanism of Touschek effect is shown below.

To simplify, assume electron momentum in laboratory frame $p_{\rm lab}$ as

$$\pm p_{\rm lab} = (E/c,\ \pm p{\rm sin}\chi,\ 0,\ p{\rm cos}\chi). \tag{4.11}$$

Here, χ is an angle between electron direction and beam direction. Using ${\rm sin}\chi \sim \chi$ and ${\rm cos}\chi \sim 1$, $p_{\rm lab}$ can be written as

$$\pm p_{\rm lab} = (E/c,\ \pm p\chi,\ 0,\ p). \tag{4.12}$$

In bunch frame, momentum of electrons $p_{\rm bunch}$ is

$$\begin{aligned}
\pm p_{\rm bunch} &= (E/c,\ \pm p\chi,\ 0,\ p)\begin{pmatrix} \gamma & 0 & 0 & -\eta \\ 0 & 1 & 0 & 0 \\ 0 & 0 & 1 & 0 \\ -\eta & 0 & 0 & \gamma \end{pmatrix} && (4.13)\\
&= (\frac{p\gamma}{\beta} - p\beta\gamma,\ \pm p\chi,\ 0,\ -p\gamma + p\gamma) && (4.14)\\
&= (\frac{p}{\beta\gamma},\ \pm p\chi,\ 0,\ 0) && (4.15)
\end{aligned}$$

Here, $E = \gamma mc^2$ is beam energy in laboratory frame, $\gamma = \sqrt{1-\beta^2}$ is gamma factor, $\beta = v/c$ is particle velocity and $\eta = \beta\gamma$. After collision, electron's momentum $p_{\rm bunch}$ will be $p^{'}_{\rm bunch}$.

$$\begin{aligned}
\pm p_{\rm bunch} &= \pm p\chi(1,\ 0,\ 0) \\
&\downarrow \\
\pm p^{'}_{\rm bunch} &= \pm p\chi({\rm sin}\theta{\rm sin}\phi,\ {\rm sin}\theta{\rm cos}\phi,\ {\rm cos}\theta)
\end{aligned}$$

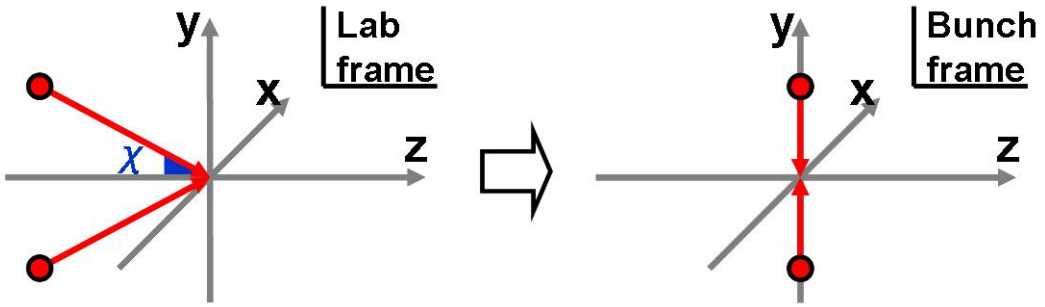

Figure 4.3: Illustration of momentum in laboratory frame and bunch frame.

Here, θ is the angle between scattering direction and bunch direction in the bunch frame. In the bunch frame, the absolute value of transverse momentum is changed from $p\chi$ to $p\chi\sin\theta$ and longitudinal momentum is changed from 0 to $p\chi\cos\theta$.

In the laboratory frame, the momentum after collision $p'_{\rm lab}$ is written as

$$\pm p'_{\rm lab} = \pm p'_{\rm bunch} \begin{pmatrix} \gamma & 0 & 0 & \eta \\ 0 & 1 & 0 & 0 \\ 0 & 0 & 1 & 0 \\ \eta & 0 & 0 & \gamma \end{pmatrix} \tag{4.16}$$

$$= \left(\frac{E}{c} \pm p\chi\beta\gamma\cos\theta,\ p\chi\sin\theta\sin\phi,\ p\chi\sin\theta\cos\phi,\ p \pm \gamma p\chi\cos\theta \right) \tag{4.17}$$

This means that the energy of the electron was changed from E to $E \pm pc\chi\beta\gamma\cos\theta$. If $E \pm pc\chi\beta\gamma\cos\theta$ exceeds the energy aperture, the electron will deviate from design orbit. In Fig. 4.4, the cones area shows region which exceeds the energy aperture. If the direction after scattering is within the area, the beam particle will be lost.

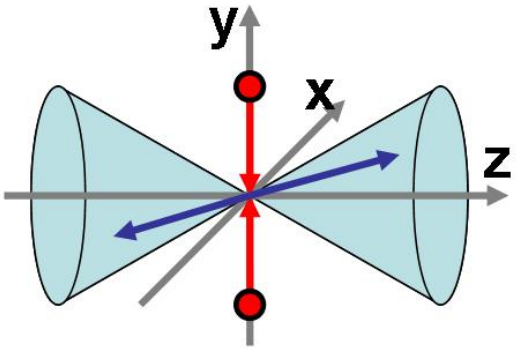

Figure 4.4: Illustration of Touschek effect in the bunch frame.

4.3.2 Rate of Touschek effect

The rate of Touschek effect per bunch which causes particles to exceed the energy aperture; R_{Tous} is

$$R_{\mathrm{Tous}} = \frac{r_p^2 c \beta_x \beta_y \sigma_h N_p^2}{8\sqrt{\pi}\beta^2\gamma^4\sigma_x^2\sigma_y^2\sigma_z\sigma_p}\int_{\tau_m}^{\infty} d\tau\left\{\left(2+\frac{1}{\tau}\right)^2\left(\frac{\tau/\tau_m}{1+\tau}-1\right)\right.$$
$$\left.+1-\sqrt{\frac{1+\tau}{\tau/\tau_m}}-\frac{1}{2\tau}\left(4+\frac{1}{\tau}\right)\ln\frac{\tau/\tau_m}{1+\tau}\right\}e^{-B_1\tau}I_0(B_2\tau)\sqrt{\frac{\tau}{1+\tau}}. \quad (4.18)$$

Where r_p is classical particle radius, $\beta_{x,y}$ is twiss parameter's beta of horizontal and vertical direction, N_p is number of beam particle per bunch, $\sigma_{x,y}$ is beam size for horizontal and vertical direction, σ_p and σ_z are relative momentum spread and bunch length respectively,

and I_0 is the modified Bessel function. σ_h, τ_m, B_1 and B_2 are given by

$$
\begin{aligned}
\frac{1}{\sigma_h^2} &= \frac{1}{\sigma_p^2} + \frac{D_x^2 + \tilde{D}_x^2}{\sigma_x^2} + \frac{D_y^2 + \tilde{D}_y^2}{\sigma_y^2} \\
B_1 &= \frac{\beta_x^2}{2\beta^2\gamma^2\sigma_x^2}\left(1 + \frac{\sigma_h^2\tilde{D}_x^2}{\sigma_x^2}\right) + \frac{\beta_y^2}{2\beta^2\gamma^2\sigma_y^2}\left(1 + \frac{\sigma_h^2\tilde{D}_y^2}{\sigma_y^2}\right) \\
B_2 &= \frac{1}{4\beta^4\gamma^4}\left(\frac{\beta_x^2}{\sigma_x^2}\left(1 - \frac{\sigma_h^2\tilde{D}_x^2}{\sigma_x^2}\right) - \frac{\beta_y^2}{\sigma_y^2}\left(1 - \frac{\sigma_h^2\tilde{D}_x^2}{\sigma_x^2}\right)\right)^2 + \frac{\sigma_h^4\beta_x^2\beta_y^2\tilde{D}_x^2\tilde{D}_y^2}{\beta^4\gamma^4\sigma_x^4\sigma_y^4} \\
\tau_m &= \beta^2\delta_m^2 \\
\tilde{D}_{x,y} &= \alpha_{x,y}D_{x,y} + \beta_{x,y}D'_{x,y}
\end{aligned}
$$

Where, D_x and D_y are dispersion. δ_m is the safety limit of energy aperture $\Delta E/E$ [10].

This formula looks complicated, but the essence is simple.

First of all, R_{Tous} is proportional not to N_p but N_p^2. This indicates that the scattering rate per particle is proportional to the bunch's particle density. Secondly, R_{Tous} is almost inversely proportional to beam sizes σ_x, σ_y and σ_z. That is because particle density increases when the beam size becomes small. Figure 4.5 to 4.7 show the relationships between beam size and beam life time τ. Here, definition of life time τ is

$$\tau[\text{min}] = \frac{N_{e^\pm}[e^\pm/\text{ring}]}{R_{\text{tous}}(\delta m)[\text{min}^{-1}]} \tag{4.19}$$

Where $N_{e^\pm}$ is the number of beam particles per ring and $R_{\text{Tous}}(\delta m)$ is the scattering rate when beam particle energy deviation is greater than δm. Beam life time is inversely proportional to scattering rate, and is proportional to beam size. For Fig. 4.5, vertical beam size $\sigma_y = \sqrt{\epsilon_y\beta_y}$ is modified by changing emittance ϵ_y for LER. As for Fig. 4.6, vertical beam size $\sigma_y = \sqrt{\epsilon_y\beta_y}$ is modified by changing beta function β_y for LER. These are correspondingly for horizontal direction. As for Fig. 4.7, longitudinal beam size σ_z is changed for LER.

And finally, R_{Tous} is roughly inversely proportional to the third power of γ. Figure 4.8

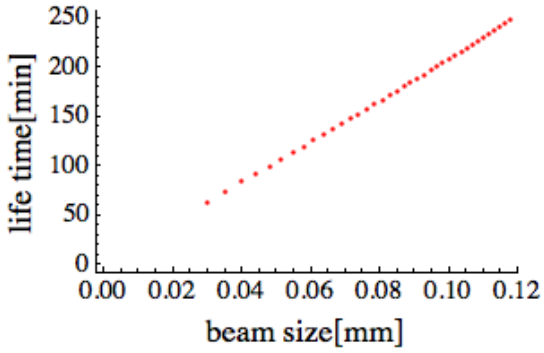

Figure 4.5: Relationship between vertical beam size and life time (Mathematica fonts by Wolfram Research, Inc.)

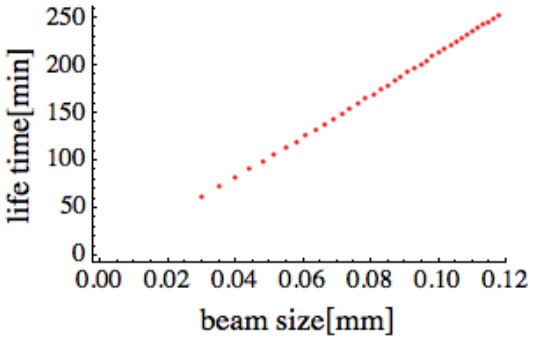

Figure 4.6: Relationship between vertical beam size and life time (Mathematica fonts by Wolfram Research, Inc.)

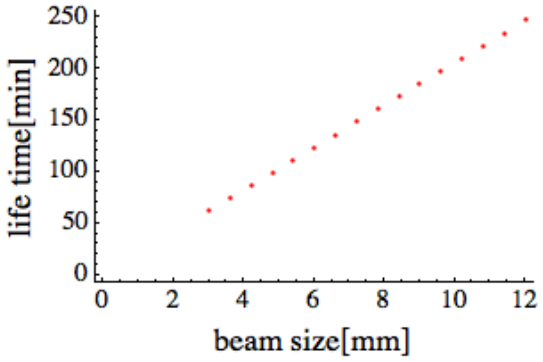

Figure 4.7: Relationship between longitudinal beam size and life time (Mathematica fonts by Wolfram Research, Inc.)

shows this relationship. This comes from two relativistic effects. The first effect comes from the fact that although both LER and HER bunch sizes σ_z are the same ($\sigma_z = 6$ mm) in "laboratory frame", they do not much in the bunch frame. Bunch size in bunch frame is $\sigma_z\gamma$. Thus, R_{Tous} has a factor of $1/\gamma$. The second effect comes from the fact that both LER and HER have same betatron tune per ring (about 40 times) whice means that the number of betatron oscillation that occurs per one cycle of the ring are the same. In the bunch frame, the time that beam particle feels per one cycle is inversely proportional to γ. This means oscillation speed in bunch frame is proportional to γ. From equation (4.2), elastic scattering rate is inversely proportional to the square of energy. So, R_{Tous} has a factor of $1/\gamma^2$.

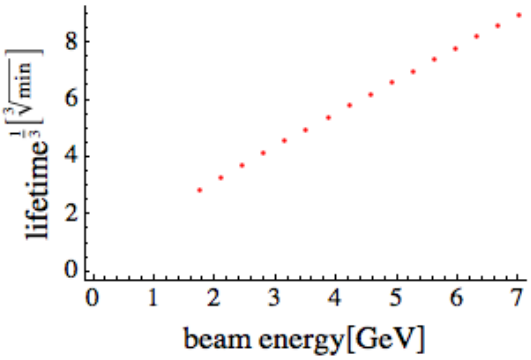

Figure 4.8: Relationship between cube root of beam energy and life time (Mathematica fonts by Wolfram Research, Inc.)

Scattering rate of LER and HER with beam particle energy deviation δ_m greater than 1 % are $1.4 \times 10^{10}[\text{s}^{-1}]$ and $6.6 \times 10^{8}[\text{s}^{-1}]$ respectively, and the touschek life times are 124 [min] and 1900 [min] respectively. In this section, for calculating scattering rate, beam parameters of table 3.1 and averaged twiss beta $\beta_x = 17.18$ m (LER), 20.58 m (HER) and $\beta_y = 23.35$ m (LER), 25.33 m (HER) were used. Twiss alpha $\alpha_{x,y}$, dispersion $D_{x,y}$ and dispersion prime $D'_{x,y}$ are treated as 0.

4.3.3 Gain of background due to upgrade

Beam parameters of SuperKEKB are shown in table 3.1, and the averaged twiss betas are β_x = 19.26 m (LER),24.63 m (HER) and β_y =44.95 m (LER),60 m (HER). With a rough estimation, the increments of Touschek scattering $\frac{R_{\text{Tous\_after}}}{R_{\text{Tous\_before}}}$ are

$$\left(\frac{2500}{1500}\right)\left(\frac{3.6/2500}{1.64/1584}\right)^2\left(\frac{\sqrt{18\times 17.18}\sqrt{150\times 23.35}}{\sqrt{3.2\times 19.26}\sqrt{8.84\times 24.63}}\right)\left(\frac{3.5}{4}\right)^3 \sim 18$$

$$\left(\frac{2500}{1500}\right)\left(\frac{2.6/2500}{1.19/1584}\right)^2\left(\frac{\sqrt{24\times 20.58}\sqrt{150\times 25.33}\ 6}{\sqrt{5.3\times 44.95}\sqrt{12.7\times 60}\ 5}\right)\left(\frac{8}{7}\right)^3 \sim 24$$

for LER and HER respectively. Indeed, by calculating scattering rate of LER and HER with the beam particle energy deviation δ_m is greater than 1 % using equation (4.18), R_{Tous} becomes 2.85×10^{11} (20.4 times greater) and 1.84×10^{10} (27.9 times greater) respectively.

4.4 Movable masks

If the scattered particles can be stopped before they reach IR, background is reduced. Scattered particle changes its direction and energy as mentioned above and deviate its orbit. There are 16 movable masks to stop these scattered particles in each LER and HER. Movable masks can collimate beam with operating mask as shown in Fig. 4.9. Table 4.1 shows the positions of each of the movable masks. "D" stands for "Dengen (power source in Japanese)", and it represents the area in the KEKB rings. From the north, KEKB rings are divided in 12 areas and numbered clockwise as shown in Fig. 4.10. "H" and "V" mean horizontal and vertical respectively. Every horizontal mask is placed in the inner side because they have to avoid SR light damage. Although there are no horizontal masks in the outer side, beam particles oscillate through betatron oscillation, so they can collimate both tails as shown in Fig. 4.11.

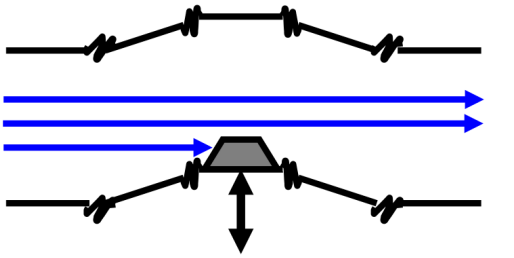

Figure 4.9: Movable mask

Table 4.1: Movable mask information

HER			LER		
Name	Side	Depth [mm]	Name	Side	Depth [mm]
D09H1	inner	16.	D06H1	inner	17.
D09H2	inner	16.	D06H2	inner	17.
D09H3	inner	16.	D06H3	inner	17.
D09H4	inner	17.	D06H4	inner	17.
D09V1	lower	3.0	D06V1	upper	6.4
D09V2	lower	5.5	D06V2	lower	4.0
D09V3	lower	3.0	D06V3	upper	7.0
D09V4	lower	5.0	D06V4	lower	7.0
D12H1	inner	17.	D03H1	inner	17.
D12H2	inner	17.	D03H2	inner	17.
D12H3	inner	17.	D03H3	inner	17.
D12H4	inner	19.	D03H4	inner	17.
D12V1	upper	4.5	D03V1	upper	6.5
D12V2	lower	5.0	D03V2	lower	10.
D12V3	upper	4.7	D03V3	upper	4.5
D12V4	lower	5.0	D03V4	lower	5.5

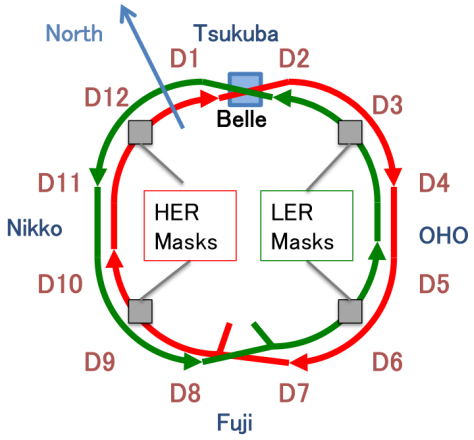

Figure 4.10: Movable masks position

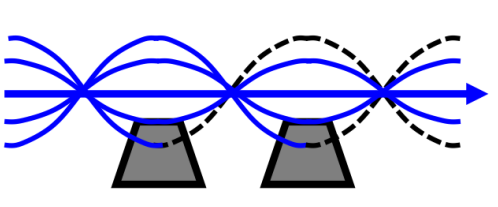

Figure 4.11: How to stop tails on both sides

Chapter 5

Interaction region

In this chapter, the interaction region (IR) is mentioned. First, we will explain the current IR and requirements for IR designing. And next, IR design for SuperKEKB is mentioned.

5.1 KEKB IR

5.1.1 Belle detector and IR

Figure 5.1 shows the section of the Belle detector. From inside, detectors which are called "SVD", "CDC", "ACC", "TOF", "ECL", "KLM" are placed. SVD (Silicon Vertex Detector) is the silicon strip detector with four layers. It measures decay position of B mesons and time difference of decay between them. CDC (Central Drift Chamber) is a drift chamber with low-Z gas which consist of 50 % He and 50 % C_2H_6. From particle track and $\frac{dE}{dx}$, it identifies particles. ACC and TOF help CDC to identify particles between $\pi^{\pm}$ and $K^{\pm}$. That is because it is difficult to distinguish $\pi^{\pm}$ and $K^{\pm}$ by using only CDC. ECL is an electromagnetic calorimeter made from thallium doped CsI crystal. It has the length of about 16 X_0. KLM (K Long and Muon detector) detects particles which could not be stopped by ECL,K_L and μ. IR is the innermost area that contains beam pipe and SVD detector.

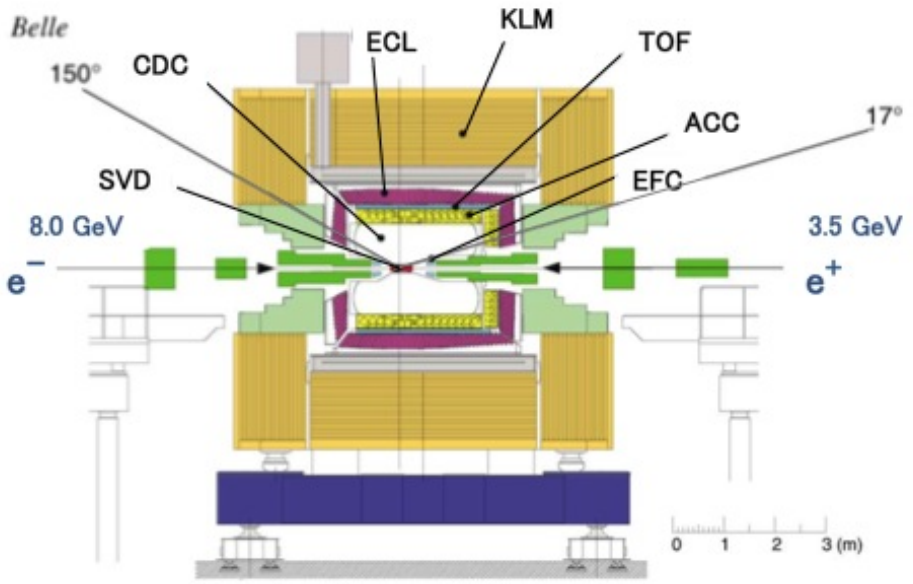

Figure 5.1: Section of the Belle detector [5]

5.1.2 IR design

For making IR, various metals are used, and thus there are restrictions, such as affinity for welding. There are many other aspects to consider for in construction as well. For example, pass space for cable and coolant, how to insert the IR beam pipe in belle detector, etc.

Belle detector has 1.5 T magnetic field generated by superconducting solenoid. For the purpose of decreasing the effect on the beam from the magnetic field, the superconducting compensation solenoid is placed. The magnetic field strength of solenoid and compensation solenoid along belle detector axis is shown in Fig. 5.2. A cryostat which contains compensation solenoid is shown in Fig. 5.3. It also contains superconducting final focusing magnet, QCS. The meaning of "S" in QCS is "shared". QCS works as a quadrupole magnet for the incoming beam towards IP and works as a bending magnet for the outgoing beam from IP to the separation of the electron and positron beam.

Heating caused by beam current must also be considered. The main cause of heating

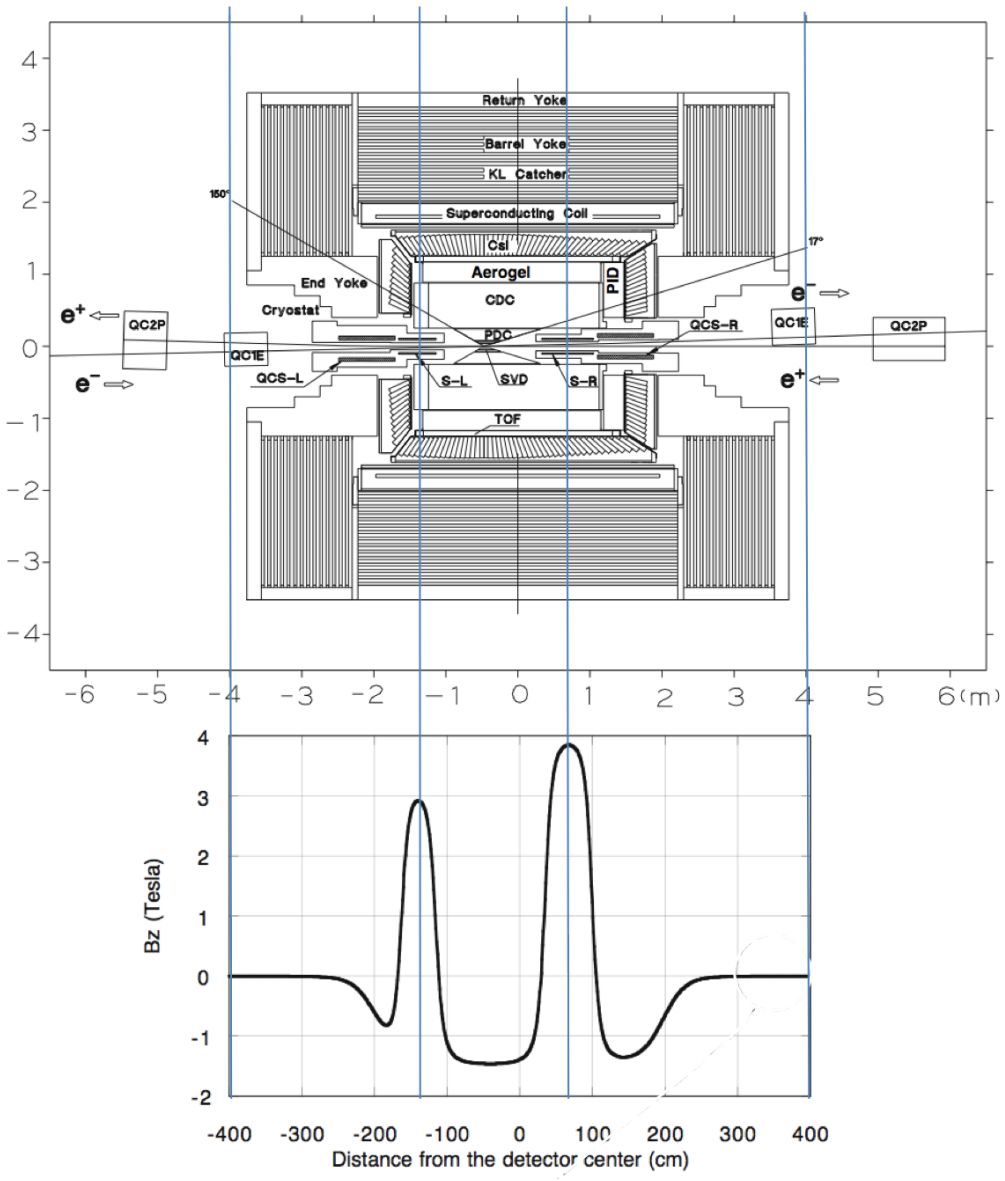

Figure 5.2: Magnetic field strength and solenoid position of KEKB [6]

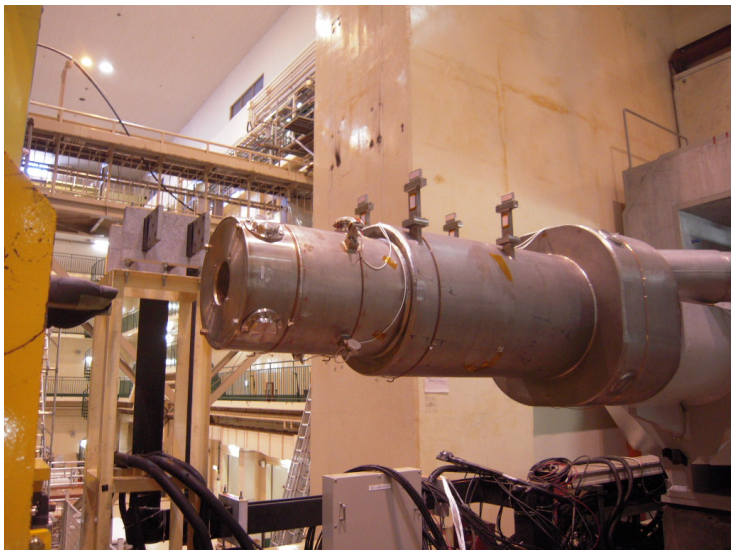

Figure 5.3: Cryostat for compensation solenoid and QCS

is image current, Higher Order Mode (**HOM**) made by wakefield of beam bunch and irradiation of synchrotron radiation (**SR**) light. Thus, cooling is important.

The purpose of SVD is the measurement of the decay positions of B mesons decay. Thus, to decrease reconstruction error caused by multiple scattering, beam pipe should be made as thin as possible. Beam pipe at IP is made of Be because of its long radiation length, $X_0 = 35$ cm. Small beam pipe radius allows SVD to be placed closer to the IP. It also improves measurement resolution of the decay position. Figure 5.4 shows cross section of the Be beam pipe and SVD detector. Be pipe has a double-layered structure. The inner Be pipe thickness is 0.6 mm and the outer Be pipe thickness is 0.4 mm. Between them there is a 0.5 mm space and paraffin flows to cool Be pipe.

Decreasing background is also very important. Figure 5.5 and 5.6 shows the IR beam pipe design and its illustration respectively. SR light from HER is especially serious, so SR mask is placed upstream of HER (left side) to prevent SR light from hitting Be pipe directly. SR mask is absent for upstream of LER (right side). Although SR background increase, this avoids generating HOM at Be pipe. In addition, inner surface of taper pipe part made of tantalum (X_0 =0.43 cm) shaped like "saw tooth". This shape prevents

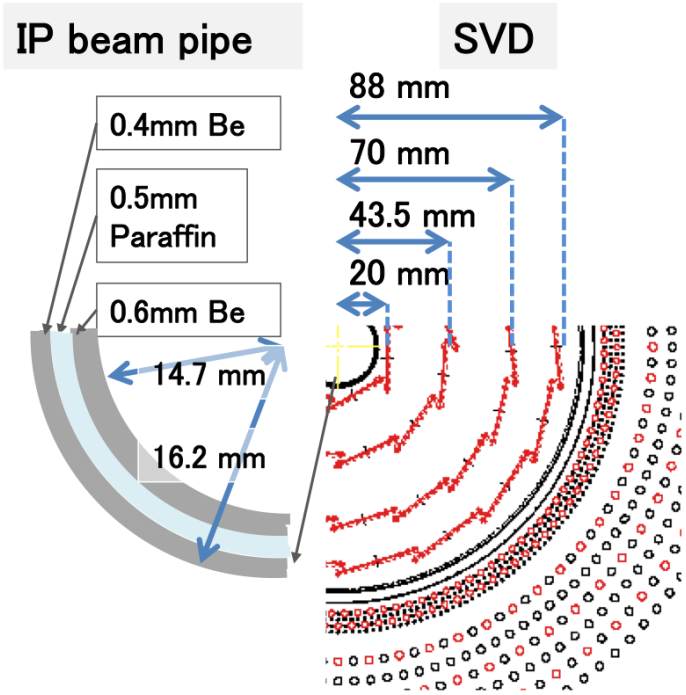

Figure 5.4: Be beam pipe and inner detector of KEK and Belle

SR light (which were emitted from HER and bounced off of the taper part) from hitting Be pipe. Heavy metal masks made of tungsten (X_0 =0.35 cm) are placed around the taper pipe part to compensate for the particle background which could not be stopped by movable masks.

5.2 Super KEKB IR

In current KEKB, when the beam is bent by QCS after crossing at IP, SR light is emitted. Some of them backscatter down stream of beam pipe and hit Be pipe. Such SR backgrounds are one of the problems in KEKB. On the other hand, in SuperKEKB optics, each ring places its final quadrupole magnet as shown in Fig. 5.7 (thanks to having 83 mrad crossing angle which is about four times larger than KEKB). Crotch part position of the beam pipe will be much closer than before. Figure 5.8 shows the magnetic

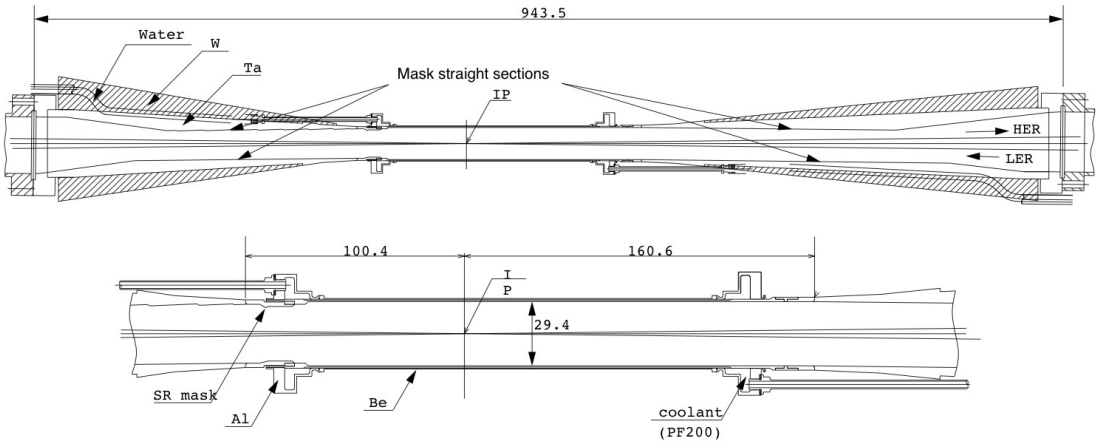

Figure 5.5: IR beam pipe design

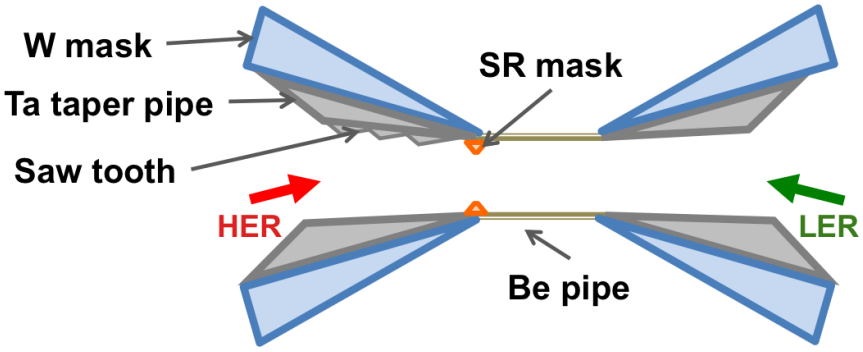

Figure 5.6: illustration of IR beam pipe design

field strength of solenoid and compensation solenoid along BelleII detector axis and each magnet position. Table 5.1 shows comparison of IR quadrupole magnets position in the current KEKB and SuperKEKB optics. In order to place QC1 magnet as close as possible to IP, beam pipe radius should be small. The beam pipe radius at the quadrupole magnet is 1 cm. For the purpose of avoiding HOM trap at Be pipe, Be pipe radius is also 1 cm. Upstream of IP, beam pipe has a taper shape to protect Be pipe from SR background as shown in Fig. 5.9. Figure 5.10 shows the section of Be pipe and inner detectors, PXD and SVD. In order to design tantalic heavy metal mask, simulation study of Touschek and beam-gas backgrounds is necessary; result of the simulation study for particle background is urgent.

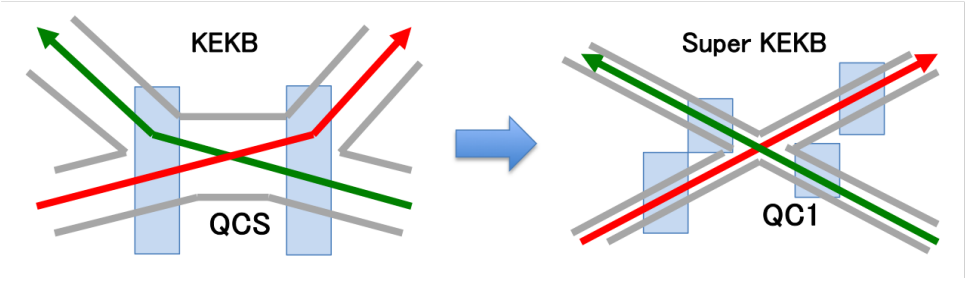

Figure 5.7: Final focusing magnets for KEKB and SuperKEKB

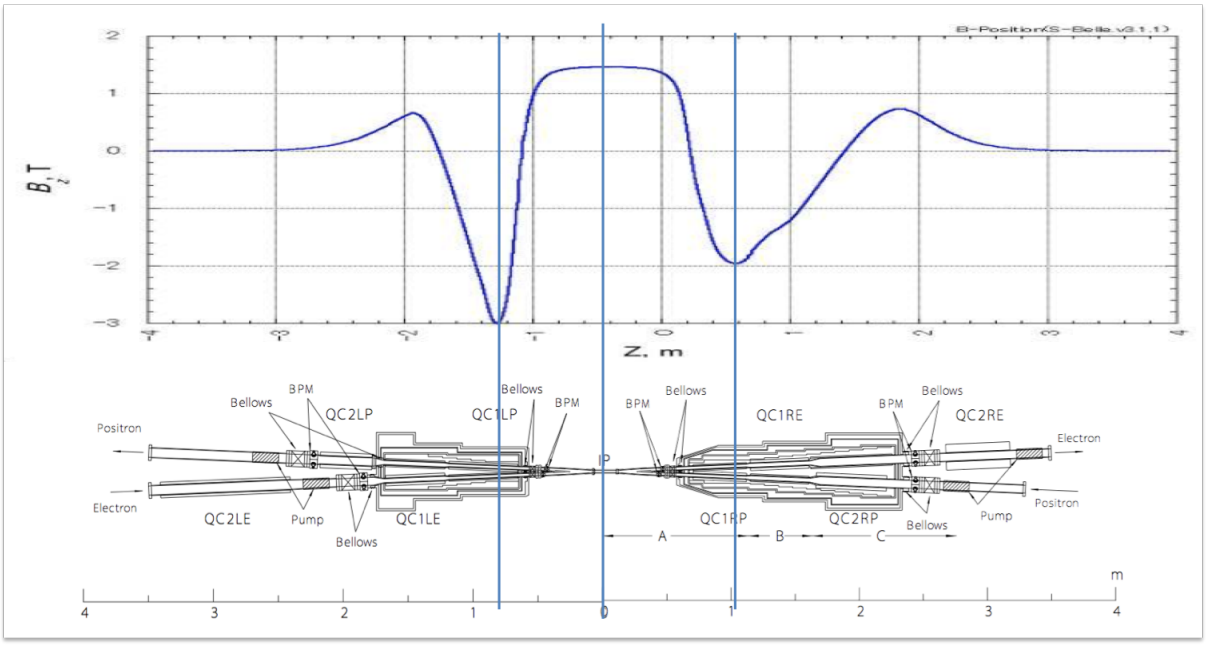

Figure 5.8: Magnetic field strength and solenoid position of SuperKEKB [7]

Table 5.1: Magnets positions of KEKB and effective positions of SuperKEKB [6] [7]

Current KEKB			
LER		HER	
Left side [m]			
QCSL	1.35 ∼ 1.85	QCSL	1.35 ∼ 1.85
QC2LP	4.4 ∼ 5.0	QC1LE	3.0 ∼ 3.6
		QC2LE	7.2 ∼ 8.0
Right side [m]			
QCSR	1.685∼ 2.185	QCSR	1.685∼ 2.185
QC2RP	5.4 ∼ 6.4	QC1RE	4.0 ∼ 4.6
		QC2RE	7.2 ∼ 7.8
SuperKEKB			
LER		HER	
Left side [m]			
QC1LP	0.53 ∼ 1.31	QC1LE	1.10 ∼ 1.82
QC2LP	1.63 ∼ 2.33	QC2LE	2.3 ∼ 3.5
Right side [m]			
QC1RP	0.63 ∼ 1.19	QC1RE	1.02 ∼ 1.74
QC2RP	1.59 ∼ 2.29	QC2RE	2.53 ∼ 3.33

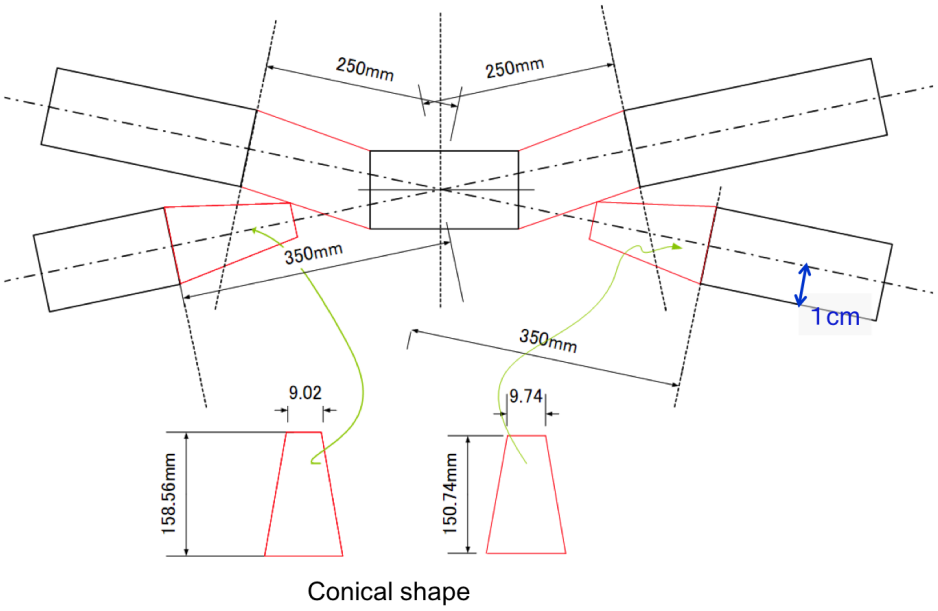

Figure 5.9: IR beam pipe design

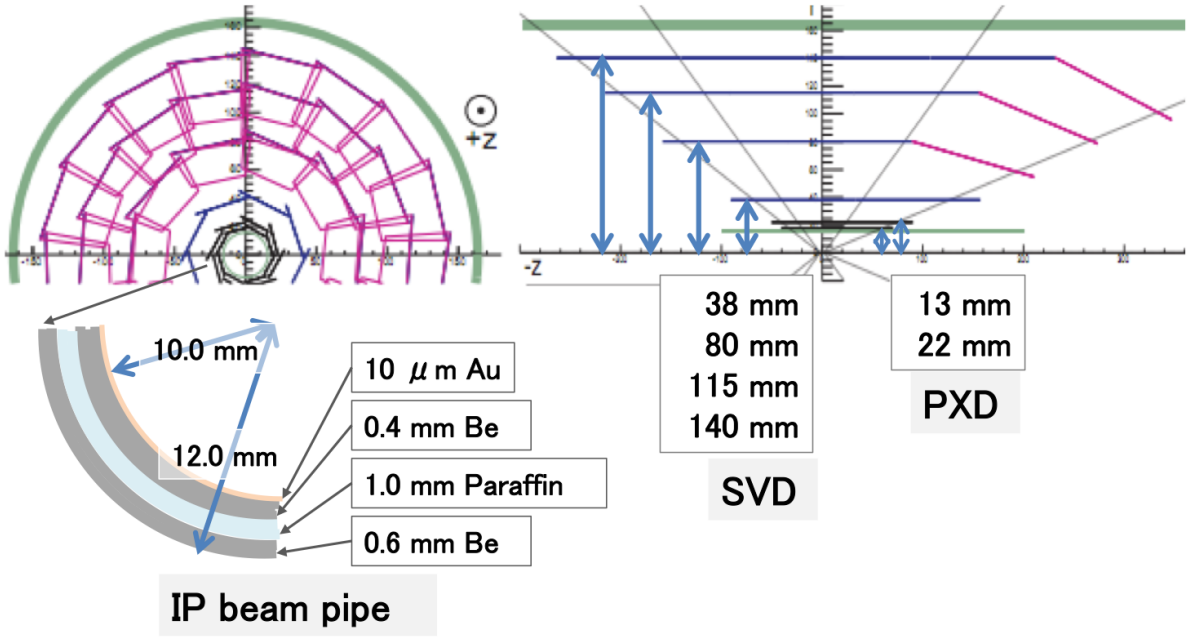

Figure 5.10: Be pipe and inner detector of SuperKEKB and Belle II

Chapter 6

Beam background simulation

After KEKB upgrade, the amount of beam background is expected to increase seriously. Simulation study is necessary in order to design IR, especially heavy metal mask. To confirm simulation framework validity, Belle detector simulation was done. In this chapter, radiation dose and occupancy of SVD for KEKB and SuperKEKB are mentioned.

6.1 Overview of background simulation

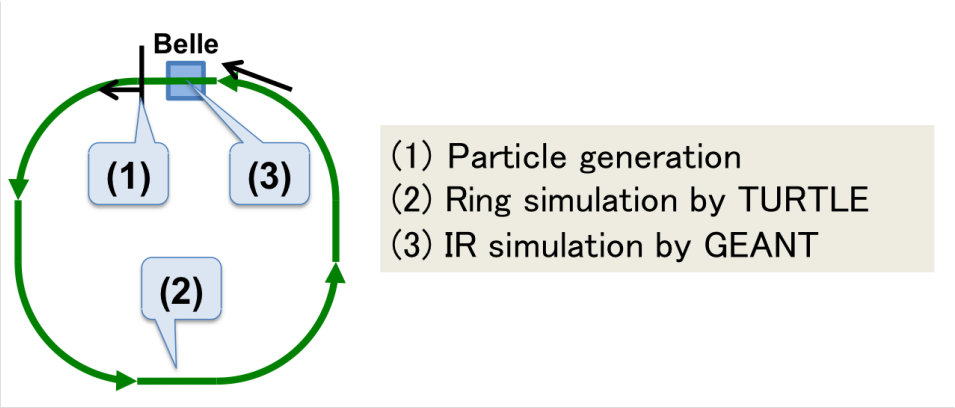

Figure 6.1: Overview of background simulation

Figure 6.1 shows overview of background simulation.

First, initial position of beam particle is decided using random number. Scattering position and scattering amount are also decided in advance.

Second, beam particle is transported with "Decay TURTLE (Trace Unlimited Rays Through Lumped Elements) [11]" from initial position to scattering position. Then, beam particle is changed its direction or momentum as decided before. After the "scattering", beam particle transported by Decay TURTLE again.

Finally, after beam particle circled KEKB ring, scattered beam particle motion near the Belle detector is simulated with GEANT3.

6.2 Assumption and method for KEKB simulation

It is impossible to simulate everything completely; we have to make some assumptions. Accuracy and precision are needed for the simulation, but we have time limitation. A trade-off between perfection and quickness is needed. Assumption and method for each step of the simulation are described in this section.

6.2.1 Beam particle generation

How to generate beam particle

Pairs of value in phase space $(x, x^{'})$ and $(y, y^{'})$ are generated randomly. In order to generate these values, twiss alpha $\alpha_{x,y}$ and beta $\beta_{x,y}$ of initial position and emittance $\epsilon_{x,y}$ are needed. These random number pairs are generated by two-dimensional gaussian distribution random number generator, and they satisfy an equation:

$$\epsilon = \gamma\sigma_x^2 + 2\alpha\sigma_x\sigma_{x'} + \beta\sigma_{x'^2}. \tag{6.1}$$

From Chap. 4, scattering rate R is estimated as $R \sim 10^{8\sim10}$. The beam current of KEKB is $\mathcal{O}$(1A) order, so particle number times circuit per second is $1/e \sim 10^{19}$

[particles·circuit/s]. Then, scattering rate per circuit per particle is $10^{-9\sim-11}$ [/particle·circuit]. It is clear that beam particle is seldom scattered more than two times in one circuit; each beam particle is scattered one time in the simulation. Three things are decided before Decay TURTLE beam transportation: scattering type, position where beam particle will be scattered, scattering amount (angle θ or energy deviation $\delta(\equiv \Delta E/E)$).

Three kinds of scattering, Coulomb scattering, bremsstrahlung and Touschek effect are generated with the simulation.

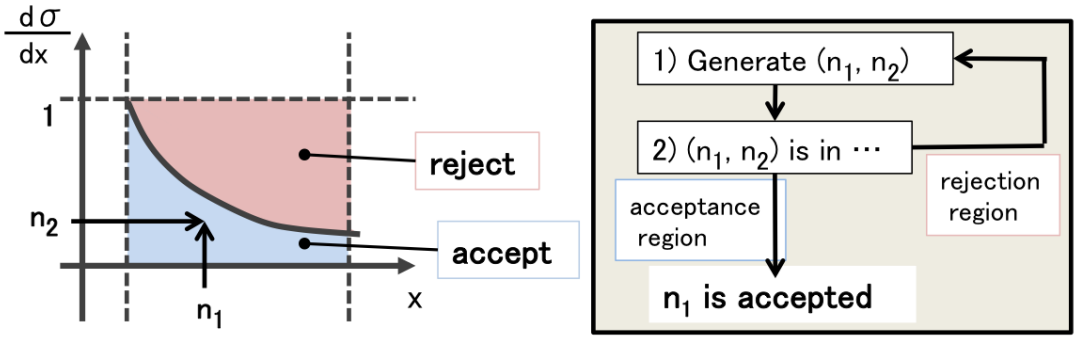

Figure 6.2: Illustration of acceptance-rejection method

For generating Coulomb scattering and bremsstrahlung particles, "acceptance-rejection" method is used. This method is one of a method to get random number. Figure 6.2 describes the acceptance-rejection method. First, random number pair n_1 and n_2 are produced. Second, position of (n_1, n_2) and differential cross section line are compared. If the position is lower than the line, the value n_1 is accepted. If the position is higher than the line, the value n_1 is rejected, and random number pair are produced again. Here, differential cross section of Coulomb scattering $\dfrac{d\sigma}{d\theta}$ is inversely proportional to θ^2 and differential cross section of bremsstrahlung $\dfrac{d\sigma}{d\delta}$ is almost inversely proportional to δ. Then, function $f(\theta) \propto \theta^{-2}$ and $f(\delta) \propto \delta^{-1}$ are used for generating Coulomb scattering particle and bremsstrahlung, respectively. Finally, accepted value n_1 is used for the amount of scattering.

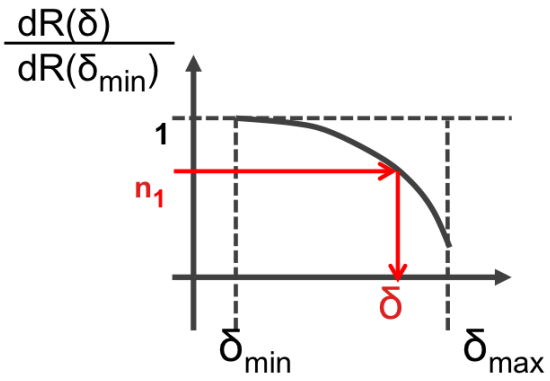

Figure 6.3: Illustration of δ generation for Touschek simulation

For generating scattered particle by Touschek effect, probability density function is used. First, random number n_1 is produced. n_1 satisfies the condition: $0 \leq n_1 \leq 1$. Second, find a value δ which satisfies $n_1 = R(\delta)/R(\delta min)$. Here, $R(\delta)$ is defined as $R(\delta) \equiv \int_{\delta min}^{\infty} d\delta \, \frac{dR}{d\delta}$. Figure 6.3 describes this method. The reason why this method is used is differential scattering rate of Touschek effect $\frac{dR}{d\delta}$ is complicated; only we can get easily is $\int_{\delta}^{\infty} d\delta \, \frac{dR}{d\delta}$. Finally, the value δ is used for the amount of energy deviation δ.

Determination of the cutoff

Differential cross section of scattering $\left(\frac{d\sigma}{d\delta} \text{ or } \frac{d\sigma}{d\theta}\right)$ will diverge at zero-scattering ($\delta \to 0$ or $\theta \to 0$). This means we have to set cut-off value at some point; too small scattering do not simulated. When we choose cut-off value, we have to be careful. If the cut-off value is too large, we will make miss count. If the cut-off value is too small, statistics of the result will decrease. Simulation ranges are defined from 1 % to 70 % for bremsstrahlung, from 0.1 mrad to 3.0 mrad for Coulomb scattering and from 0.9 % to 20 % for Touschek effect. A validity of selection of cut-off value were checked. Figure 6.5 shows the scattering amount range vs background occupancy for 1st layer. They show the ranges for 1st layer are valid. In these figures, horizontal axes are taken in logarithmic scale; their cut-off

values are set to zero.

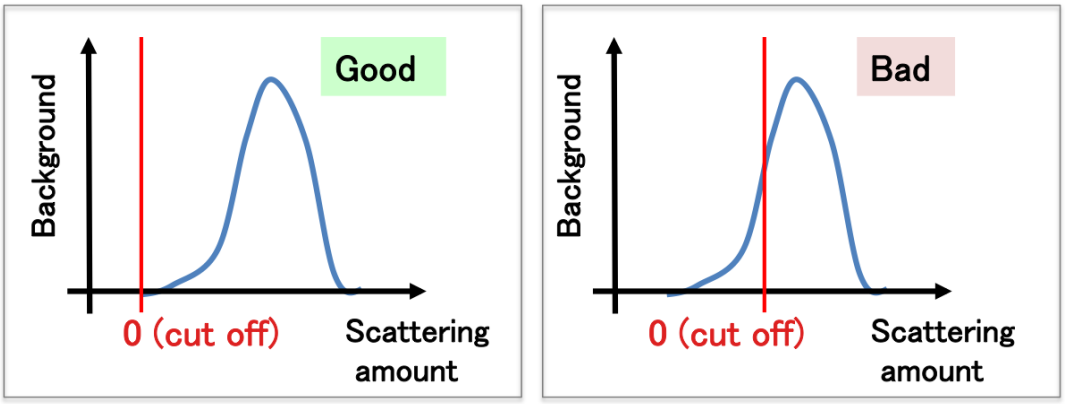

Figure 6.4: Explanation of good and bad cut-off value

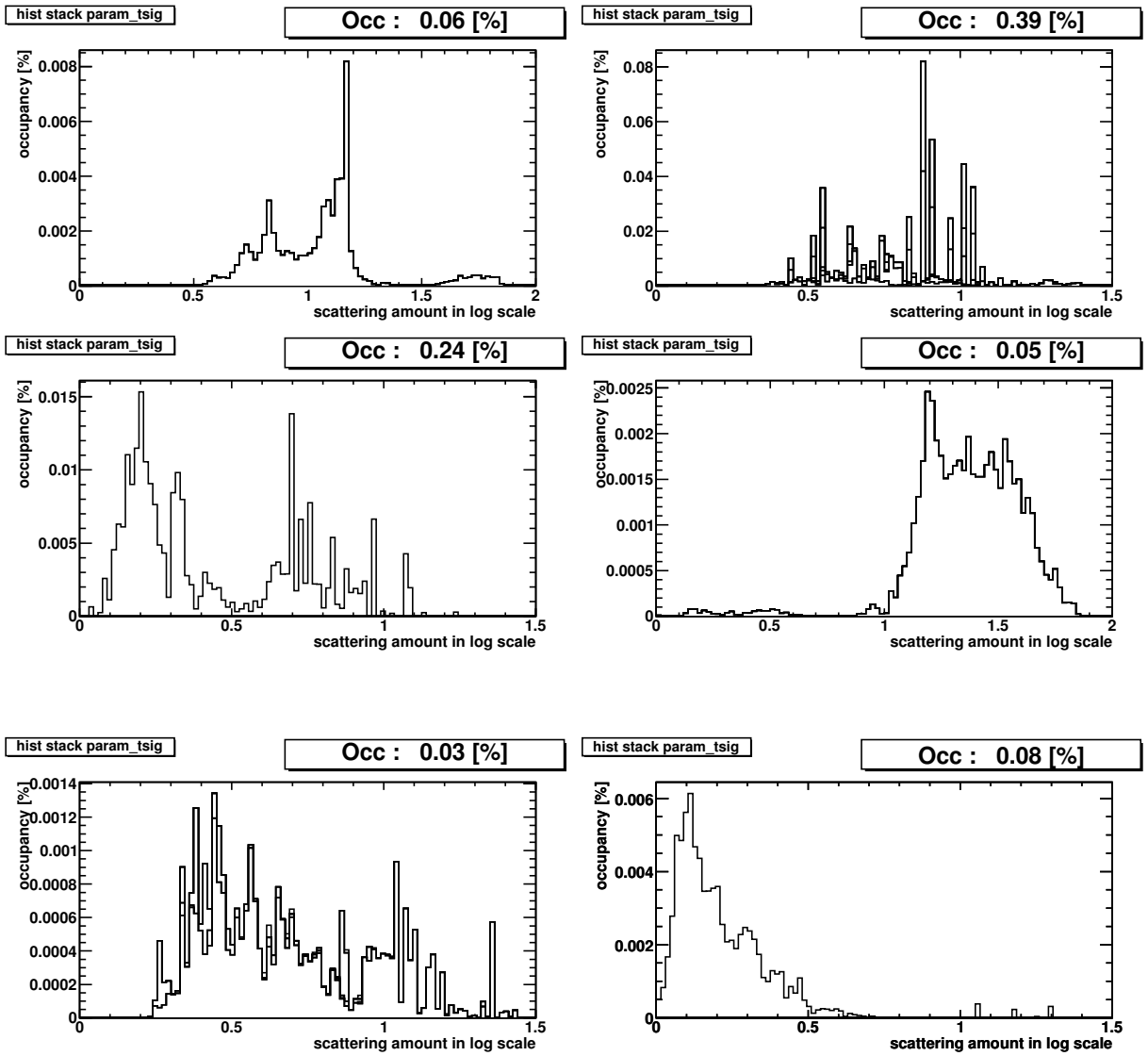

Figure 6.5: Parameter vs radiation dose for SVD 1st layer. LER bremsstrahlung (top left). LER Coulomb (top right). LER Touschek (middle left). HER bremsstrahlung (middle right). HER Coulomb (bottom left). HER Touschek (bottom right).

6.2.2 Simulation of ring optics part by Decay TURTLE

Decay TURTLE's ring simulation

Using Decay TURTLE, beam particle is traced along accelerator optics. Decay TURTLE calculates particle trajectory by multiplying matrices for each components to particle information, (x, x', y, y', s, p). At the end of tracking, particle's position and momentum are taken over to GEANT simulation. Figure 6.7 and 6.8 shows alignments of optics elements for LER and HER, respectively.

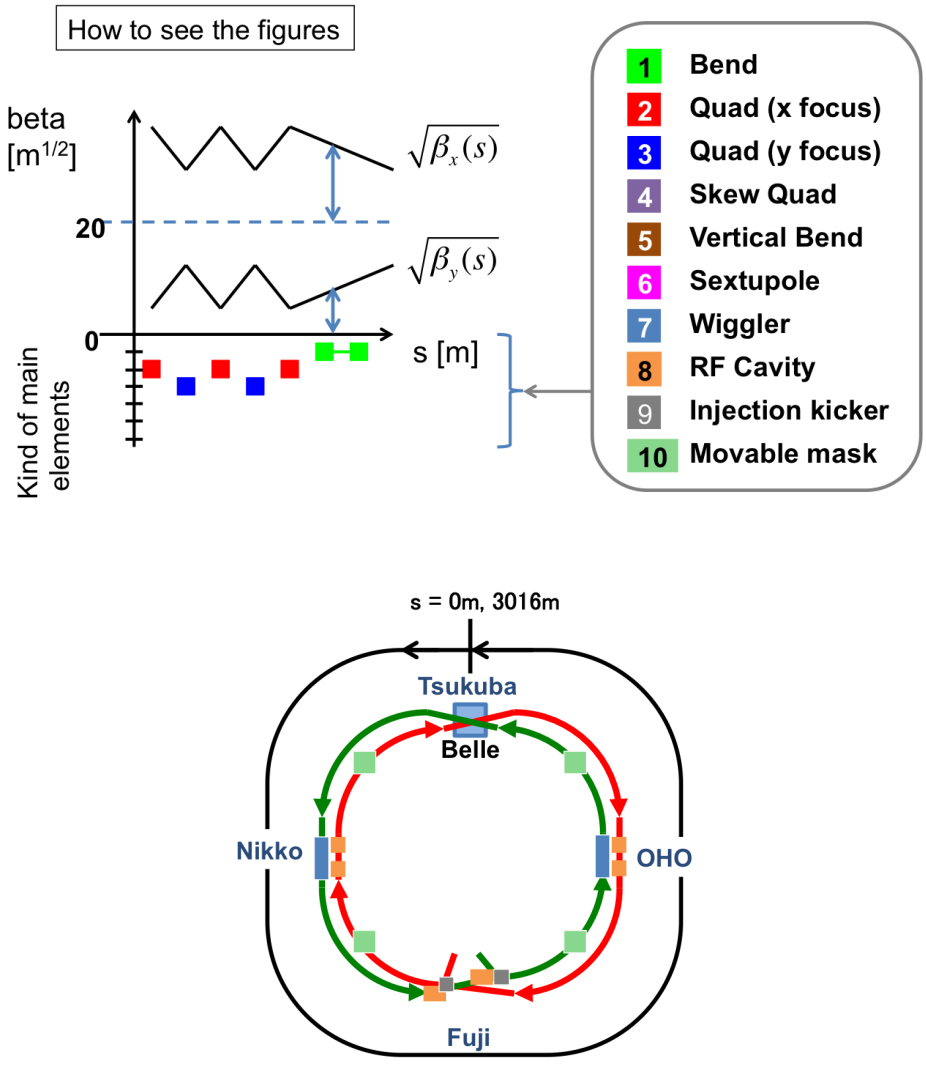

Figure 6.6: Explanation of Fig. 6.7 and 6.8

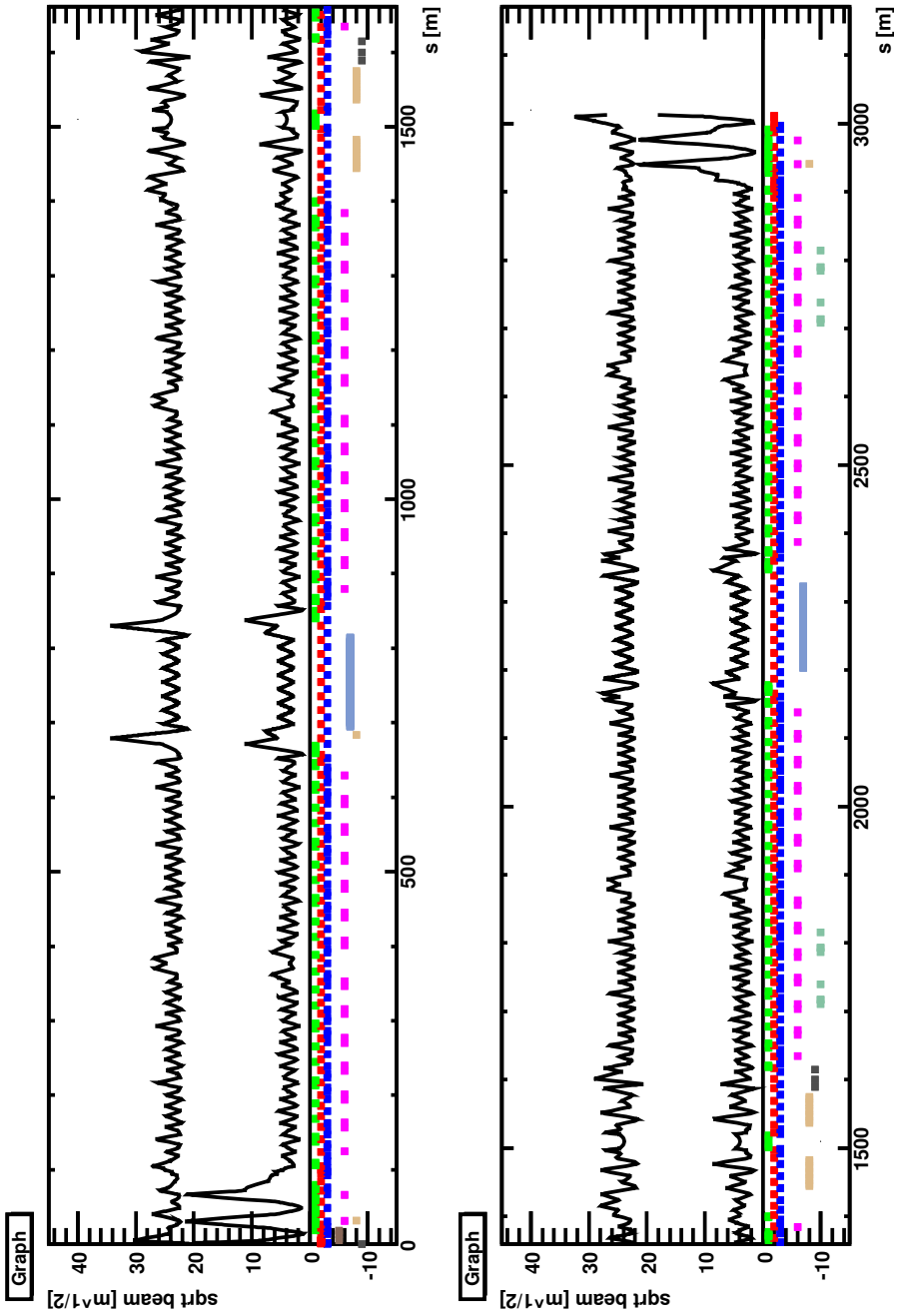

Figure 6.7: Elements and beta size for LER of KEKB

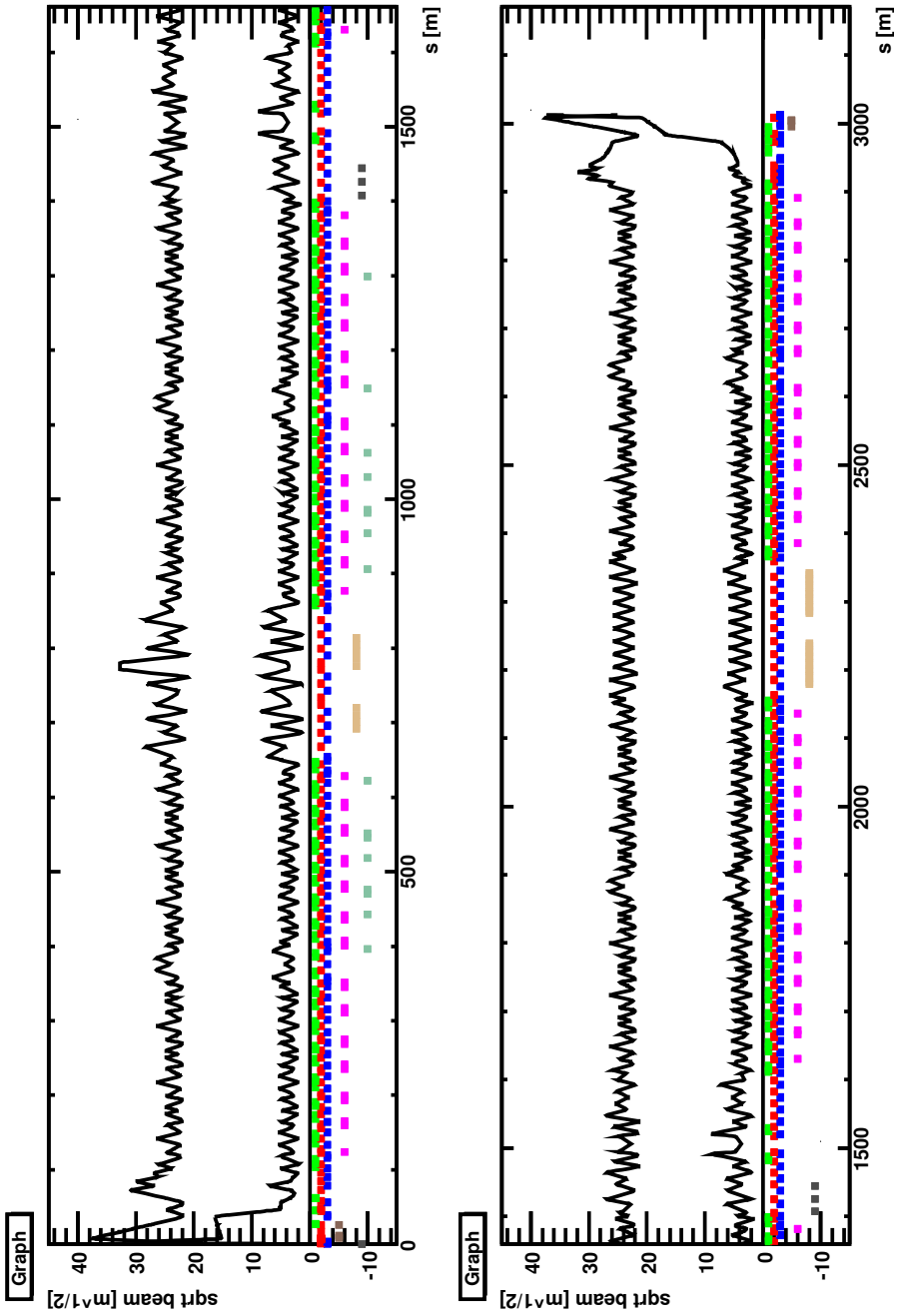

Figure 6.8: Elements and beta size for HER of KEKB

Movable mask setting

In the simulation, movable mask position is set to the setting when beam background study had been done. The setting is shown in Tab. 6.1

Table 6.1: Movable mask parameters for background study

HER			LER		
Name	Collimation depth		Name	Collimation depth	
D09H1	20. mm	$(23.8\sigma_x)$	D06H1	20. mm	$(22.3\sigma_x)$
D09H2	20. mm	$(23.6\sigma_x)$	D06H2	20. mm	$(27.3\sigma_x)$
D09H3	20. mm	$(23.8\sigma_x)$	D06H3	20. mm	$(22.3\sigma_x)$
D09H4	20. mm	$(23.6\sigma_x)$	D06H4	20. mm	$(27.3\sigma_x)$
D09V1	3.0 mm	$(26.6\sigma_y)$	D06V1	6.4 mm	$(58.9\sigma_y)$
D09V2	5.5 mm	$(37.1\sigma_y)$	D06V2	4.0 mm	$(36.5\sigma_y)$
D09V3	3.0 mm	$(26.6\sigma_y)$	D06V3	7.0 mm	$(64.4\sigma_y)$
D09V4	5.0 mm	$(44.4\sigma_y)$	D06V4	7.0 mm	$(63.8\sigma_y)$
D12H1	20. mm	$(23.0\sigma_x)$	D03H1	20. mm	$(23.1\sigma_x)$
D12H2	20. mm	$(23.0\sigma_x)$	D03H2	20. mm	$(23.1\sigma_x)$
D12H3	20. mm	$(23.0\sigma_x)$	D03H3	20. mm	$(23.1\sigma_x)$
D12H4	19. mm	$(21.8\sigma_x)$	D03H4	20. mm	$(23.1\sigma_x)$
D12V1	4.5 mm	$(40.0\sigma_y)$	D03V1	6.5 mm	$(59.8\sigma_y)$
D12V2	5.0 mm	$(44.4\sigma_y)$	D03V2	10. mm	$(91.2\sigma_y)$
D12V3	4.7 mm	$(41.8\sigma_y)$	D03V3	4.5 mm	$(41.4\sigma_y)$
D12V4	5.0 mm	$(33.7\sigma_y)$	D03V4	5.5 mm	$(50.1\sigma_y)$

Position dependence of the scattering rate

Vacuum pressure is dependent on position of the rings; scattering rate of gas-scattering is dependent on the position z. Beam size is also dependent on position; scattering rate of Touschek effect is dependent on the position. But position dependence of Touschek effect is too complicated. Then, we assumed that scattering rate of Touschek effect is uniform. In the simulation, only position dependence of gas scattering was considered.

LER and HER have 300 CCG vacuum pressure gauges per about 10 m in 3 km of circumference. These gauges are placed near ion pump; pressures of these places are lower than the pressure at beam pipe. Figure 6.9 shows illustration of beam pipe and CCG

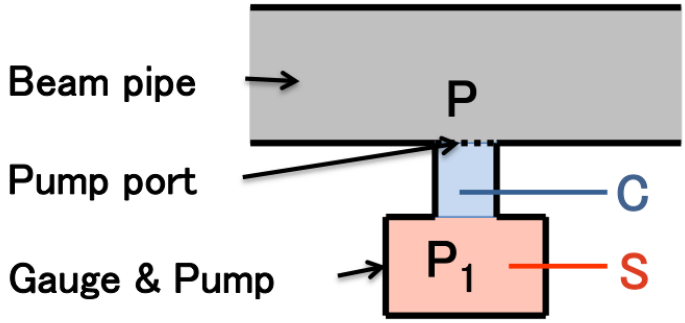

Figure 6.9: Illustration of beam pipe, pressure pump and vacuum gauge.

gauge. In this condition, relationship between pressure of CCG gauge P_1 and pressure of beam pipe at pump port P is

$$P_1 = \frac{C}{S+C}P. \tag{6.2}$$

Here, C is vacuum conductance of the port and S is pumping speed of ion pump as shown in Fig. 6.9 [12]. In KEKB, C and S are $C \sim S \sim 200\ l/sec$, equation (6.2) becomes $P_1 = \frac{1}{2}P$. The pressure of beam pipe near pump port is lower than the one far from pump port also. Average pressure of beam pipe calculated by using a model becomes 3 times higher than P_1. So, CCG pressure gauges output 3 times higher values than they measured: $3P_1$.

It is assumed that gas component is N_2 when CCG pressure gauge measure the pressure. However, main components of the gas of beam pipe are CO and H_2. We have to correct the value using the ratio of "absolute sensitivity coefficient (the degree of easiness of ionization)" between N_2 and particular molecule. The value for CO is 0.92, and the value for H_2 is 2.4. It means H_2 is about two times more difficult to be ionized than N_2 and CO.

Unfortunately, partial pressure gauge had been broken and not repaired [1]; a ratio of composition between CO and H_2 cannot be measured. Assuming that the ratio is

[1]Partial pressure gauge is placed near the IP. It is not good to open vacuum near the IP. So broken pressure gauge should be left.

$P_{\mathrm{CO}} : P_{\mathrm{H_2}} = 5 : 7$: the data of 2001 at 600 mA.

Using these information, when pressure gauge indicates P_{CCG}, partial pressures of $\mathrm{H_2}$ and CO satisfy that

$$\begin{cases} \frac{P_{CO}}{0.92} + \frac{P_{H_2}}{2.4} = P_{\mathrm{CCG}} \\ \frac{P_{CO}}{P_{H_2}} = \frac{5}{7}. \end{cases} \tag{6.3}$$

Solving this, we get $P_{\mathrm{CO}} = 0.6 P_{\mathrm{CCG}}$ and $P_{H_2} = 0.84 P_{\mathrm{CCG}}$. The values $P_{\mathrm{CO}} = 0.6 P_{\mathrm{CCG}}$ from CCG gauge monitors when background study had done are used.

Figure 6.10 and 6.11 are CCG gauge value for LER and HER respectively. CCG monitor values are plotted clockwise order from Oho side IR to Nikko side IR. The limit of monitoring of CCG is up to around 10^{-8} Pa, so the value lower than 10^{-8} Pa is output as 10^{-8} Pa. Then, the value 10^{-8} Pa is treated as $5{\times}10^{-9}$ Pa: middle value between max value 10^{-8} and minimum value 0. As written in figures, some areas of vacuum pressure are higher ($10^{-5\sim-7}$ Pa) than the other area ($10^{-7\sim-8}$ Pa). At RF cavity areas, vacuum pressure is designed as 10^{-6} Pa from the biginning. At Wiggler areas, much more SR light hitting beam pipe wall, beam pipe emit much more gas. In addition, because of the space limitation, short number of pumps were placed. At Test region area, new beam pipes emit much more gas. Then, average value for each areas are used for gas scattering background simulation. Table 6.2 shows that average CCG value and definition of the area.

About the area of Super conducting RF cavity (SC-RF cavity) of HER, there is no CCG monitor of vacuum group, so CCG monitor values are not plotted on Fig. 6.11. The temperature of inner surface of SC-RF cavity is 4.4 K; gas molecules are condensed on the surface except for $\mathrm{H_2}$. Therefore main component of gas is $\mathrm{H_2}$ in SC-RF cavity. Cross section of Coulomb scattering is proportional to Z^2, so cross section of $\mathrm{H_2}$ is about 50 times smaller than one of CO. Gas scattering at SC-RF cavity is negligible if the pressure is not higher 50 times than the other area. CCG monitors ($\sim$300K) near SC-RF cavity indicate around 10^{-8} Pa. In addition, SC-RF cavities work as cryopump. Then, in this

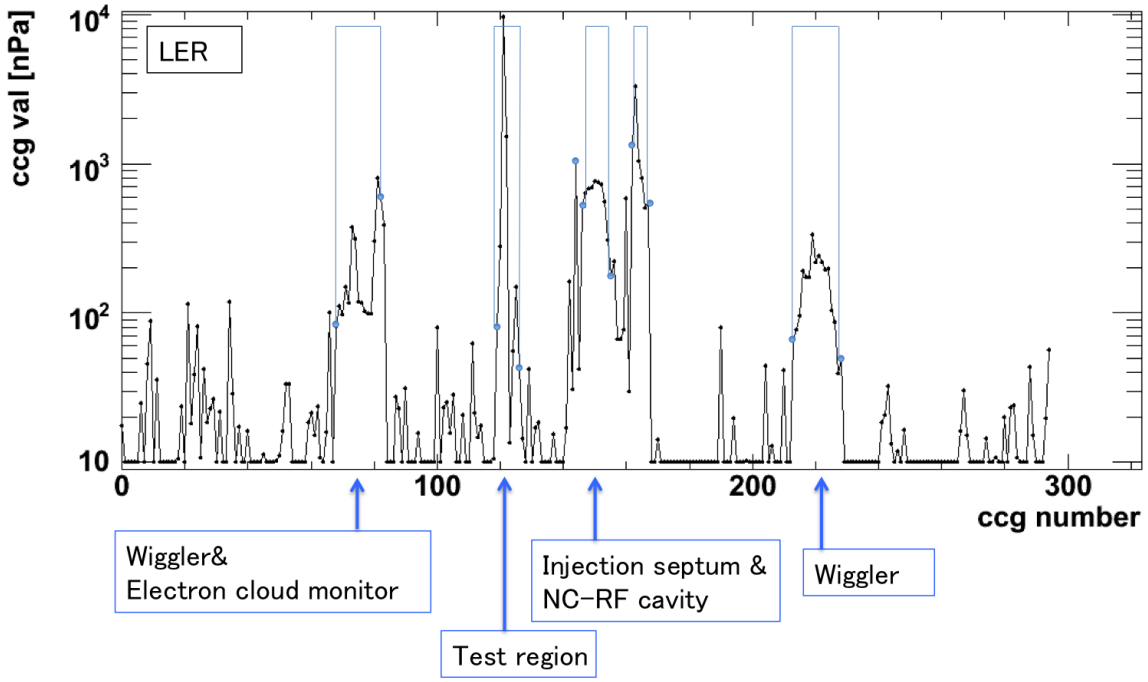

Figure 6.10: CCG monitor for LER

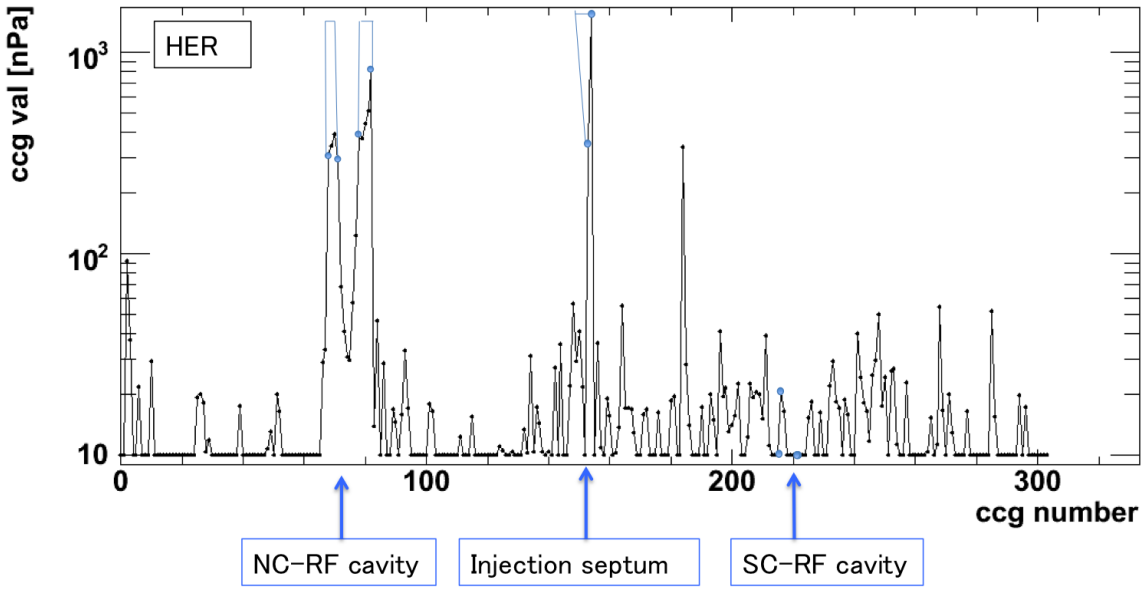

Figure 6.11: CCG monitor for HER

simulation, scattering from SC-RF cavity area is neglected. However, we do not have to forget the possibility that pressure of SC-RF cavity is high. Gas molecule velocity is low at low temperature; it makes vacuum conductance lower.

Table 6.2: Average CCG value and their area

LER		HER	
P_{CCG} [nPa]	Comment	P_{CCG} [nPa]	Comment
IP (end)			
19.6		12.4	
232.7	Wiggler	–	SC-RF
25.4		12.8	
1463.7	Test region	–	SC-RF
21.4		19.3	
645.3	NC-RF	934.1	Inject
9.2		11.9	
154.0	Wiggler	265.1	NC-RF
9.9		9.7	
IP (start)			

6.2.3 Simulation of IR part by GEANT

GEANT3 Belle detector geometry

Belle detector and beam pipe around the detector are implemented as shown in Fig. 6.12 and 6.13. Beam particles are injected from 942 cm upstream for LER and 840 cm upstream for HER. Figure 6.13 shows IR beam pipe and SVD detector. Information of deposited energy and raw data-like ADC for each channel of SVD are stored [13].

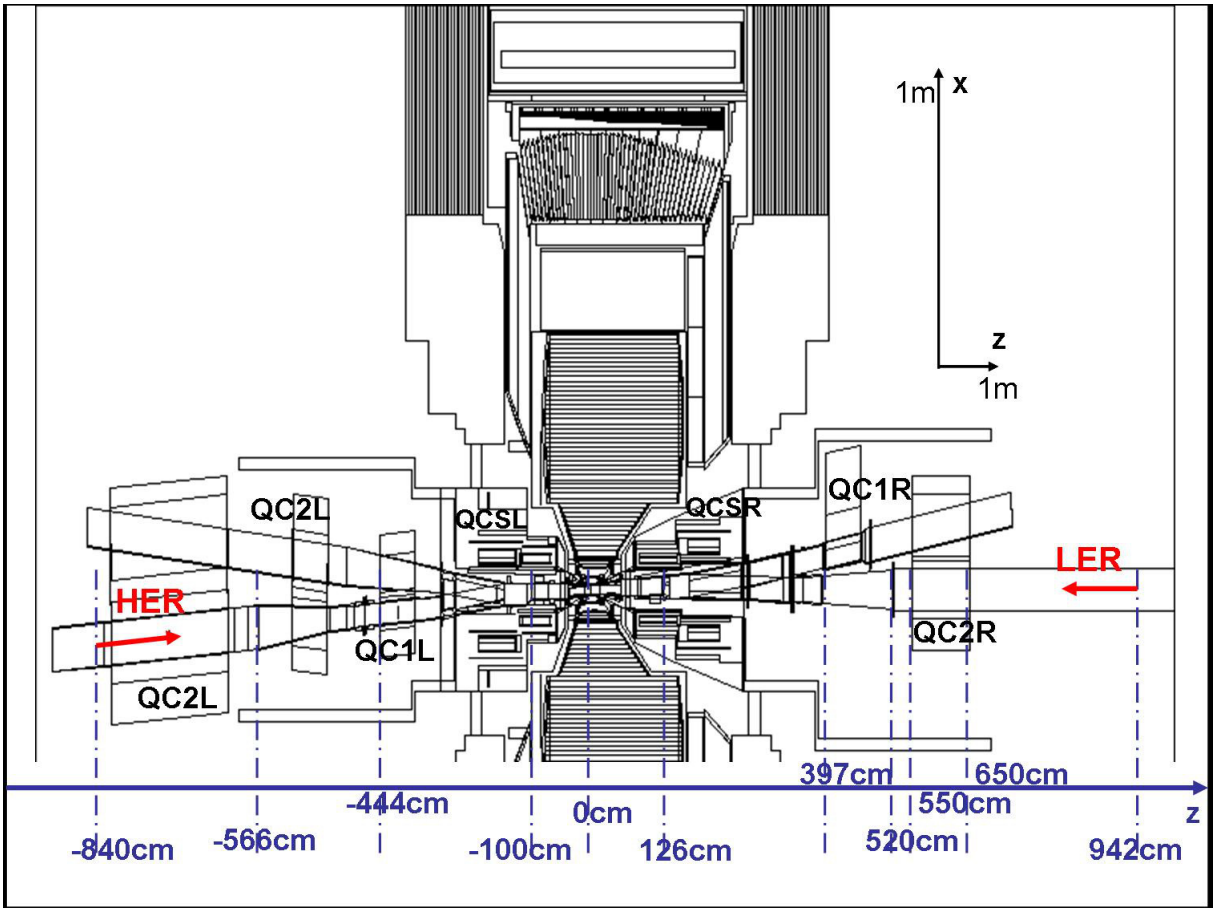

Figure 6.12: GEANT3 belle detector

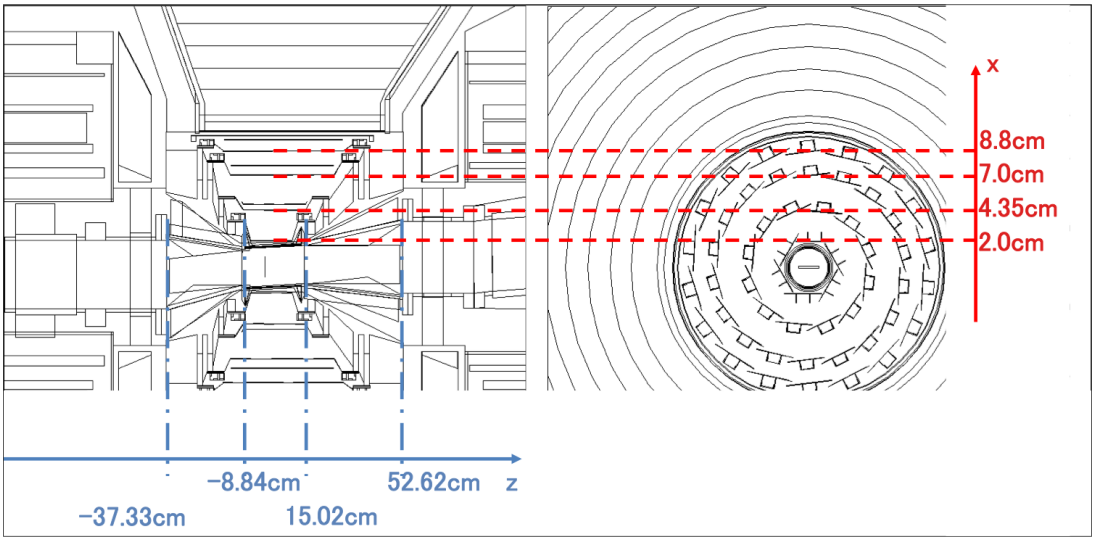

Figure 6.13: GEANT3 interaction region

Region to be simulated by GEANT

Beam background process is described in three steps. First, scattered beam particle hits beam pipe. Second, secondary particles are generated. Finally, some of secondary particles hit the detector

While Decay TURTLE cannot simulate secondary shower generation, GEANT simulation area should be large enough. In order to check where secondary particles are generated, hit positions of scattered particles were checked. The routes of secondary particle from hit position to the detector were understood using event display. If the GEANT volume is not enough, correction is needed for the result. Understanding beam background generation mechanism is not only useful for checking simulation validity but also necessary for IR designing.

Figure 6.14 and 6.15 show histograms of contribution to occupancy background for 1st SVD layer; horizontal axis means hit position of scattered particle. Each peak of the histogram was checked by using event display. The mechanism of becoming background was divided into two ways.

First one is that the scattered particle hit IR heavy metal mask directly as shown in Fig. 6.16. Most of bremsstrahlung events are categorized into this way.

Second one is that the scattered particle hit upstream beam pipe or graze on corner of the beam pipe, and secondary particle hit IR mask as shown in Fig. 6.17; photons can reach IR mask even if they were made at far from IP because they do not feel magnetic field. For LER Touschek background, most of the events of which hit points are greater than 650 cm (like Fig. 6.18) are caused by secondary photon. This peak seems distributed over GEANT geometry; it means geometry length is not enough. Correction for the result is needed. Two assumptions for correction are made. First, beam particles hit uniformly on the region where z is greater than 650 cm and make photon. Second, solid angle of IR from the position where photon generated is proportional to z^{-2}. From these assumptions,

background contribution from upper than QC2 (650 cm) $D_{>650cm}$ is written as

$$D_{>650cm} = \int_{650cm}^{942cm} dx \frac{\alpha}{z^2} \tag{6.4}$$

Here, α is coefficient. If this contribution is extrapolated to far enough, $D_{>650cm}$ will be

$$D_{>650cm} = \int_{650cm}^{\infty} dx \frac{\alpha}{z^2} \tag{6.5}$$

On the other hand, background contribution from lower than QC2 $D_{<650cm}$ is not changed. Then, background from LER Touschek effect is corrected as

$$\begin{aligned}
D_{tot} &= D_{<650cm} + D_{>650cm} && (6.6)\\
&\downarrow && (6.7)\\
D_{tot} &= D_{<650cm} + \frac{\int_{650cm}^{\infty} dz \frac{\alpha}{z^2}}{\int_{650cm}^{942cm} dx \frac{\alpha}{z^2}} D_{>650cm} && (6.8)\\
&= D_{<650cm} + \frac{\frac{1}{650}}{\frac{1}{650} - \frac{1}{942}} D_{>650cm} && (6.9)\\
&\sim D_{<650cm} + 3.23\ D_{>650cm} && (6.10)
\end{aligned}$$

However, as shown in Fig. 6.19 and 6.20, some Touschek effect events for 3rd layer do not fit the mechanism as mentioned. Then, this correction may cause over estimation for 3rd layer result.

Figure 6.21 concludes that the illustration of background generation mechanism.

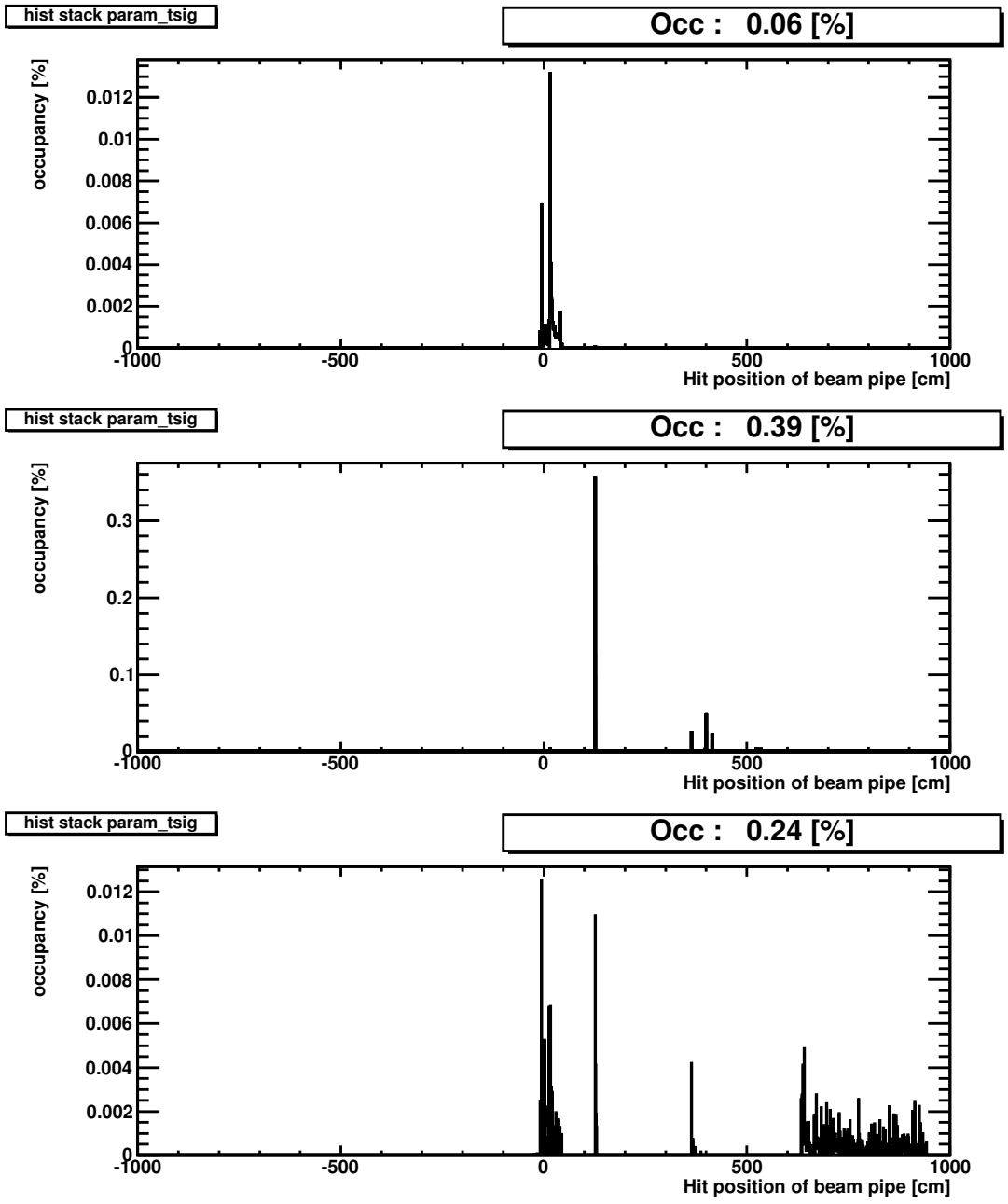

Figure 6.14: Histograms of hit position vs occupancy for 1st layer from LER: bremsstrahlung (top), Coulomb scattering (middle), Touschek effect (bottom).

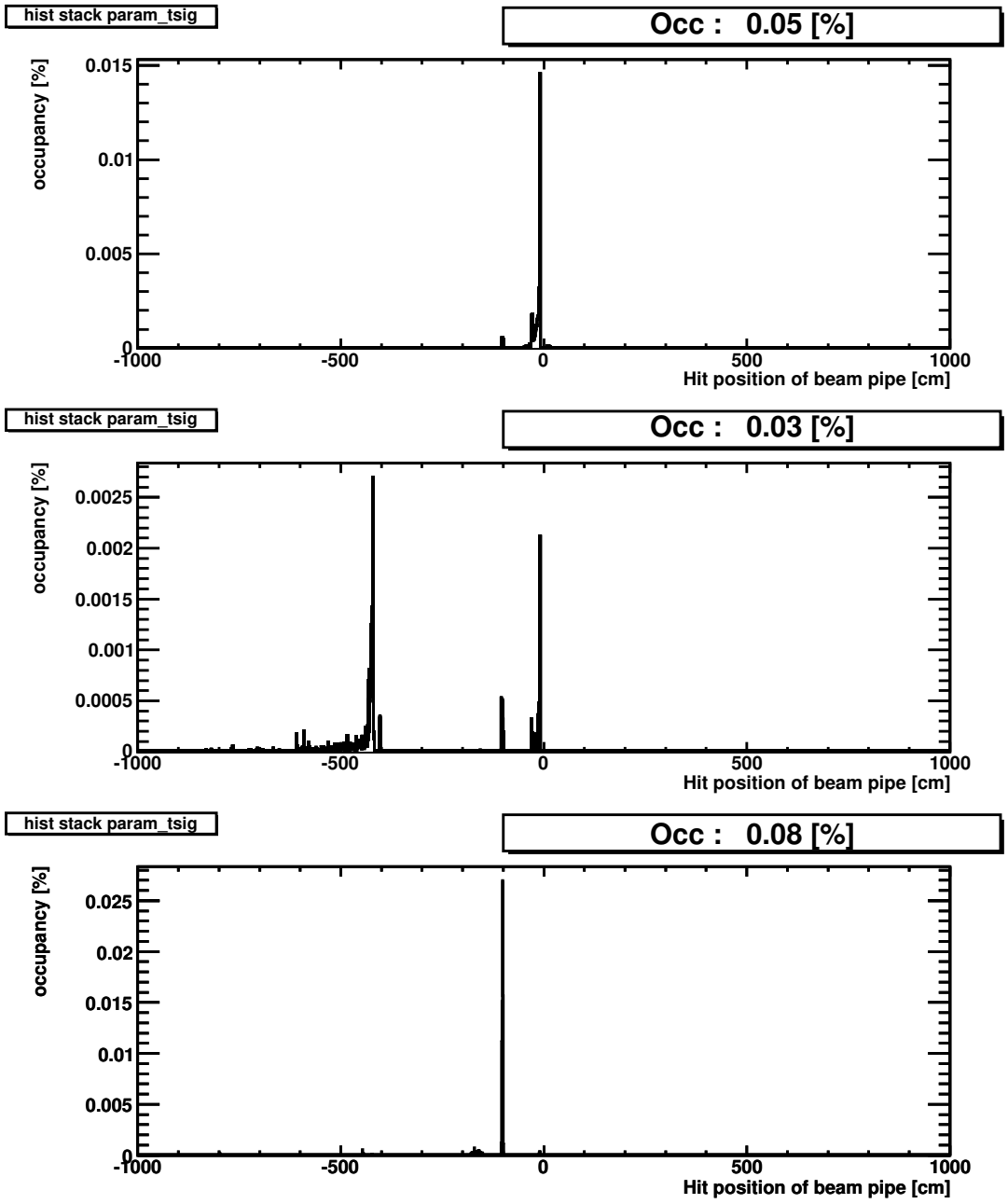

Figure 6.15: Histograms of hit position vs occupancy for 1st layer from HER: bremsstrahlung (top), Coulomb scattering (middle), Touschek effect (bottom).

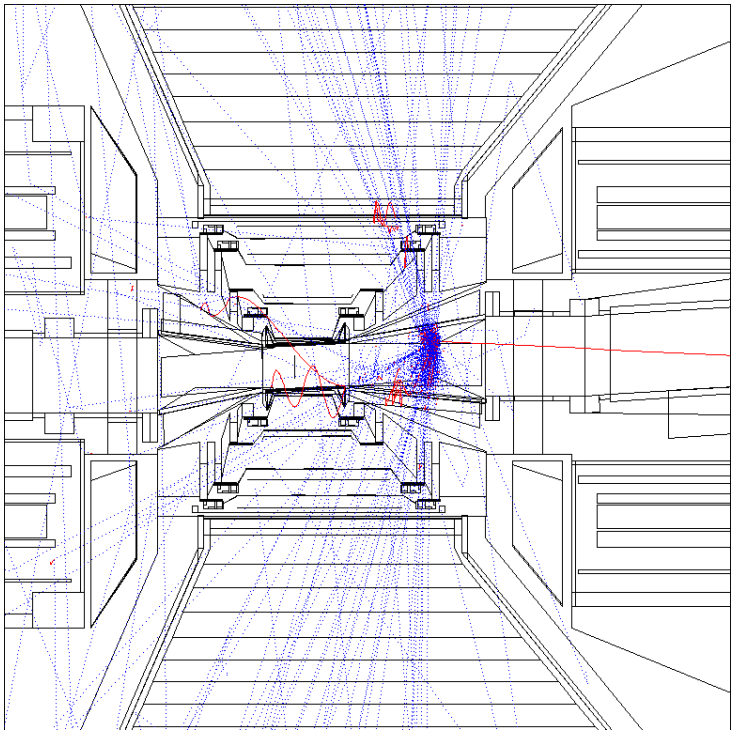

Figure 6.16: Beam particle hit the IR mask directly.

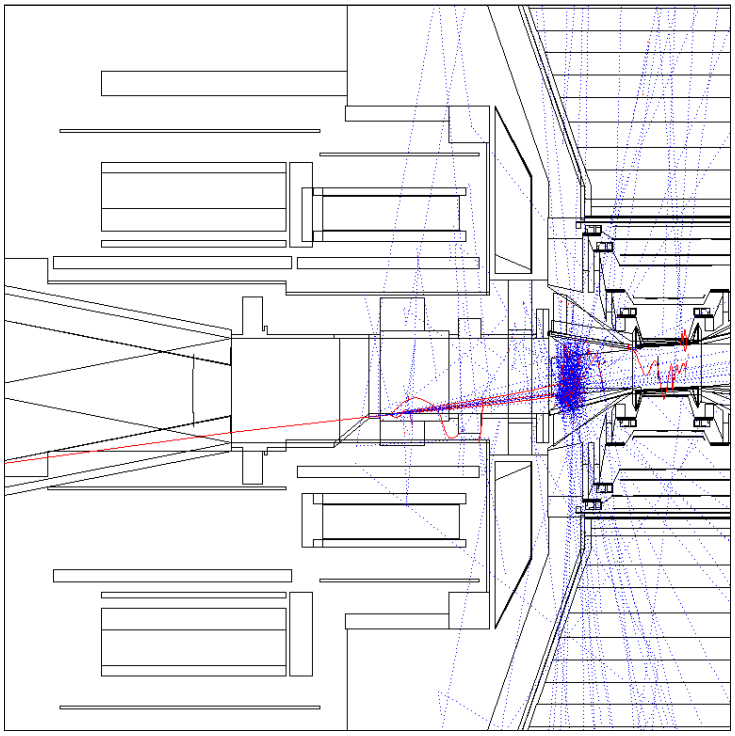

Figure 6.17: Beam particle graze on the corner of the beam pipe.

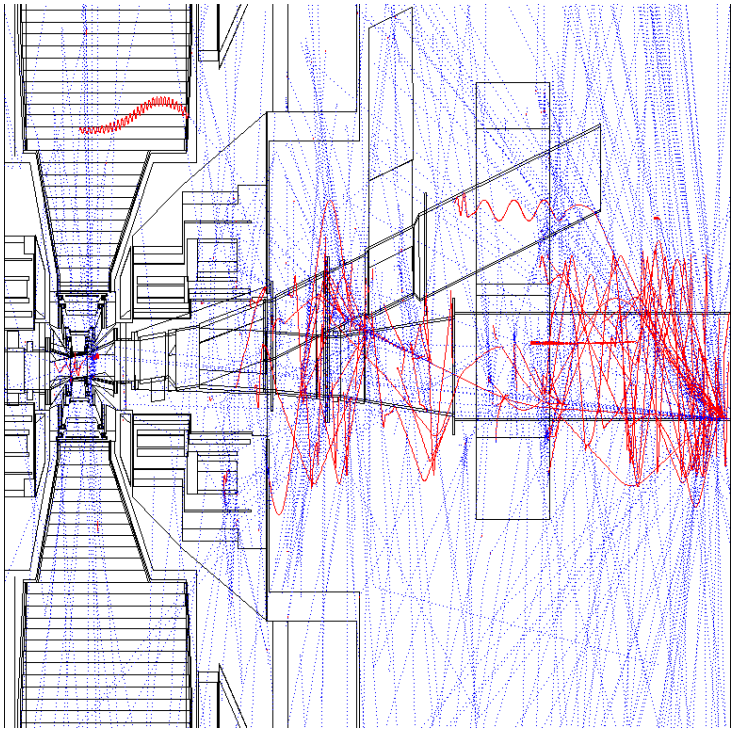

Figure 6.18: An event display of LER Touschek effect. Beam particle hit beam pipe and make shower; one of a photon reach IR mask.

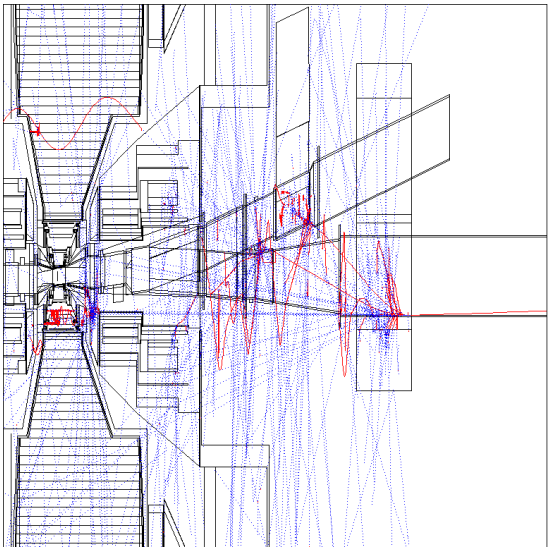

Figure 6.19: LER Touschek effect background of SVD 3rd layer. Photon become background from outside of the beam pipe.

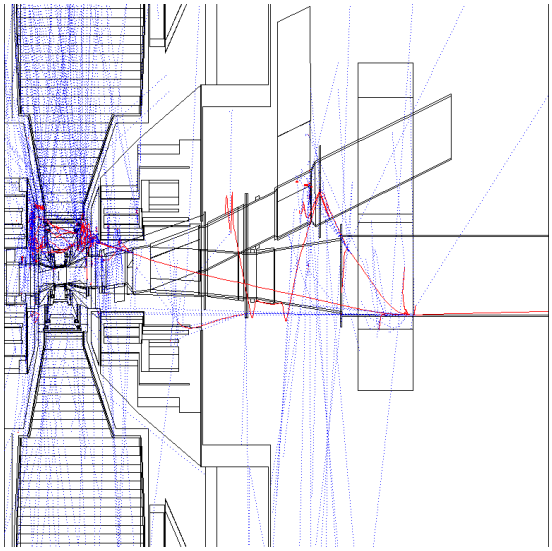

Figure 6.20: LER Touschek effect background of SVD 3rd layer. Positron become background from outside of the beam pipe.

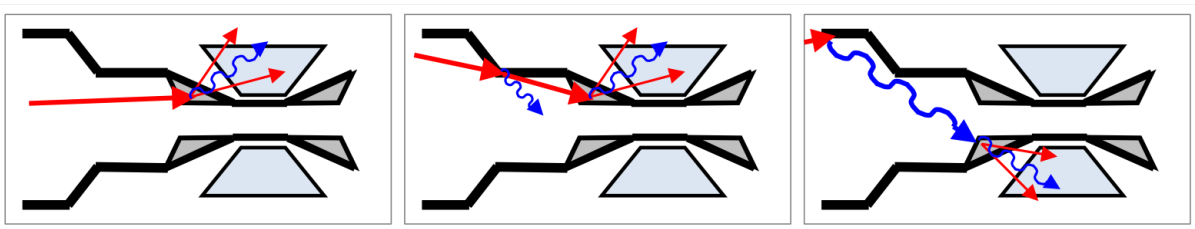

Figure 6.21: Illustrations of Background mechanism: Hitting IR mask directly(left), Grazing on corner of the beam pipe (middle), Photons in generated shower hitting IR mask(right).

6.3 Results of KEKB simulation

6.3.1 Assumption used associated systematic errors

Three types of beam background were simulated: bremsstrahlung, Coulomb scattering and Touschek effect. Cut-off values are decided as $\delta = 1$ % for bremsstrahlung, $\theta = 0.1$ mrad for Coulomb scattering and $\delta = 0.9$ % for Touschek effect.

Presumptive value of vacuum pressure was obtained by using CCG pressure gauge.

For the simulations of occupancy and radiation dose beam parameter was set for background study as shown in Tab. 6.3. Horizontal and vertical emittances are corresponding to IP beam size of $\sigma_x^* = 200$ [μm] and $\sigma_y^* = 2$ [μm], respectively. For occupancy simulation, beam current for LER and HER were set as $I_{\mathrm{LER}} = 1.45$ A and $I_{\mathrm{HER}} = 0.85$ A respectively. For radiation dose simulation, beam current for LER and HER were set as $I_{\mathrm{LER}} = 1.64$ A and $I_{\mathrm{HER}} = 1.19$ A respectively. Assuming that vacuum pressure is proportional to beam current, pressure was increased. In addition, scattering ratio of Touschek effect was also increased because particle density was increased. It means that the factors $(1.64/1.45)^2$ and $(1.19/0.85)^2$ were multiplied to the each scattering rate of LER and HER, respectively. 10^7 s/year was assumed for KEKB run time in a year. Beam particles just after injection are unstable. This effect is not considered in the simulation.

Error of CCG gauge is about factor 2. As CCG gauge is used, so the discharge current of CCG gauge decreases; this effect is not considered. Considering that pressure from CCG values can be different by a factor of 10 while in same area, error of beam-gas scattering could be about factor 10.

Table 6.3: Beam parameters for the simulation

parameters (LER)/(HER)	Occupancy	Radiation dose
horizontal emittance ϵ_x [nm]	44.4	
vertical emittance ϵ_y [nm]	0.678	
beam current I [A]	1.45 / 0.85	1.64 / 1.19
# of bunch N_{bunch}	1584	

6.3.2 Statistical error of random number

To estimate statistical error, a standard deviation of simulation results was calculated. The way of calculating standard deviation is,

1. Divide the simulation statistics into 10. We get 10 results which has tenth of statistics.
2. Calculate standard deviation $\sigma_{\frac{1}{10}} = \sqrt{\dfrac{\Sigma(\ (each\ value) - (average)\ )^2}{10}}$
3. The statistical error σ is calculated as $\sigma = \frac{1}{\sqrt{10}}\ \sigma_{\frac{1}{10}}$.

Each scattering (bremsstrahlung, Coulomb scattering and Touschek effect for LER and HER) had been simulated ten million times. For example, standard deviations of radiation dose of 1st layer SVD by Coulomb scattering background are shown in Tab. 6.4.

6.3.3 Occupancy simulation

How to simulate occupancy

"Occupancy" is an amount which describes how many channels of detector has signals. Usually, it is defined as (# of signal channel)/(# of total channel) for each event. Occupancy should not exceed 10 % to get useful data. Estimation of occupancy is necessary

Table 6.4: Standard deviation for 10^5 and 10^6 events

Radiation dose [krad/yr]		
	10^5 events	10^6 events
1	1.04	5.63
2	10.7	5.38
3	1.58	6.37
4	3.56	5.24
5	13.8	3.97
6	7.22	5.94
7	7.93	6.66
8	7.73	4.68
9	1.98	12.93
10	0.77	3.32
Average	5.63	6.01
σ	$\sigma_{1/100} = 4.28$	$\sigma_{1/10} = 2.51$

for IR design. This simulation framework can get raw data-like output for each "event". But the "event" in the simulation is not "one trigger (actual)" but "one scattered particle (simulation)".

Here, a value "t_{sig}" is used to get occupancy from simulation. t_{sig} is a length of time which the signal of the pulse exceeds threshold. MIPs (Minimum Ionizing Particles) deposit 116 keV energy when they go through 300 μm thick Si. An electron/hole pair is produced per 3.6 eV, so MIP makes about 32 kilo e/h pairs. Correction factor of SVD is about 75 %. ADC of MIP signal is corresponding to $\sim$ 24 kilo e/h pairs. Signal/noise ratio is about 20, so noise is corresponding to about 1 kilo e/h pairs.

Threshold ADC is set as corresponding to three times higher than noise level, $3\sigma \sim 3$ kilo e/h pairs. And signal pulse shape $f(t)$ is assumed that $f(t) \propto te^{-t/\tau}$. Here, τ is shaping time and $\tau = 800$(ns). Figure 6.22 shows 20 kilo e/h pair signal and 3 kilo e/h pair threshold. Because the value $f(t = \tau)$ is obtained by simulation, we can get t_{sig}. In this simulation, occupancy is defined as the ratio of the sum of t_{sig} per unit time. A

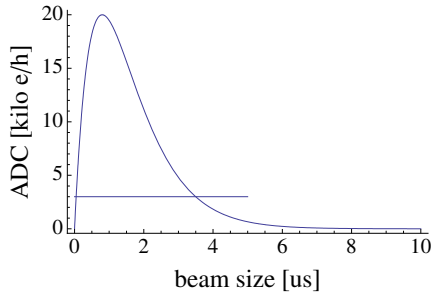

Figure 6.22: Pulse shape of SVD signal (Mathematica fonts by Wolfram Research, Inc.)

formula of the occupancy will be

$$\text{Occupancy } [\%] = \frac{(\text{Average } t_{\text{sig}} \text{ per scattering } [\text{s/e}^{\pm}]) \times (\text{Scattering rate } [\text{e}^{\pm}/\text{s}])}{(\#\text{ of channel})} \times 100 \tag{6.11}$$

Number of channels of each SVD layer is 12288, 24576, 36864 and 36864 from 1st layer to 4th layer, respectively [14]. In this formula, it is assumed that there is no pile up of signals because of few % of occupancy in real. From this assumption, GEANT simulation do not have to simulate shower particle which energy is less than ~ 10 keV because they cannot make more than 3000 e/h pairs. The threshold ADC of background study data is corresponding to 3000 electron-hole pairs also. Average t_{sig} value is about 2 μs; it is much more longer than crossing rate $\frac{3000[m]}{\sim 1500[bunch] \times 3 \times 10^8[m/s]} \sim 7\ ns$. There is no need to consider whether the trigger is corresponding to bunch crossing or not.

On June 2010, machine study had done. The simulated occupancies of 1st from 3rd SVD layers were compared with the data from the study. The data is obtained from master's thesis written by S. Sugihara [15].

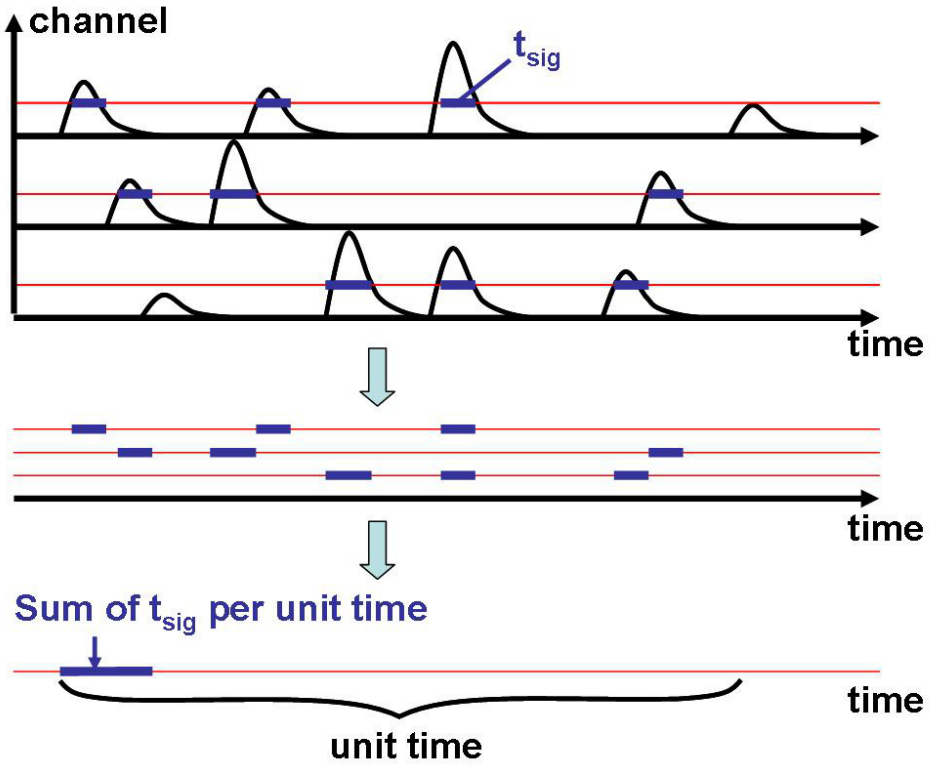

Figure 6.23: An illustration of occupancy definition.

Simulation result of occupancy

Simulation results for occupancy and background study data for 1st layer to 3rd layer of SVD are shown in Tab. 6.5. "Other" background of simulation only contains beam-gas scattering. SR background or other background is not included. For the simulation result, only statistical error was written in table. Systematic error was not obtained precisely.

From the data, Touschek background is main background for LER; on the other hand, contribution of Touschek background to HER is almost nothing.

Table 6.5: Occupancy simulation results and experimental data. HER SR backgrounds are not simulated.

1st layer occupancy [%]		simulation	data
LER	Touschek	0.52 ± 0.03	0.47 ± 0.07
	other	0.45 ± 0.05	0.19 ± 0.07
HER	Touschek	0.083 ± 0.001	0.006 ± 0.002
	other	0.082 ± 0.002	0.49 ± 0.003
Total		1.14 ± 0.06	1.2 ± 0.1

2nd layer occupancy [%]		simulation	data
LER	Touschek	0.32 ± 0.01	0.14 ± 0.03
	other	0.17 ± 0.02	0.06 ± 0.04
HER	Touschek	0.024 ± 0.0003	0.01 ± 0.01
	other	0.025 ± 0.0005	0.18 ± 0.01
Total		0.54 ± 0.03	0.38 ± 0.05

3rd layer occupancy [%]		simulation	data
LER	Touschek	0.74 ± 0.02	0.08 ± 0.02
	other	0.10 ± 0.01	0.10 ± 0.02
HER	Touschek	0.022 ± 0.0003	0.01 ± 0.01
	other	0.017 ± 0.0003	0.14 ± 0.01
Total		0.88 ± 0.03	0.33 ± 0.03

6.3.4 Radiation dose simulation

How to simulate radiation dose

Radiation damage is also important issue to simulate. Detector will lose its performance under long time irradiation. An unit for radiation dose "**krad**" is used in the simulation.

$$1\ [\text{krad}] = 10\ [\text{Gy}] = 10\ [\text{J/kg}] = \frac{10}{1.6 \times 10^{-19}}\ [\text{eV/kg}] \tag{6.12}$$

Mass of each SVD layer is 18.9 g, 56.8 g, 142 g and 200 g from 1st layer to 4th layer, respectively.

Data of radiation dose is obtained from "RADFET monitor". This data is shown in Fig. 6.24. "Recovery" can be seen while KEKB run had been stopped; this is caused by annealing. From the monitor, 1st layer of SVD is irradiated about 100 $\sim$ 200 krad/year. 2nd and 3rd layers of SVD is irradiated about 10 $\sim$ 20 krad/year.

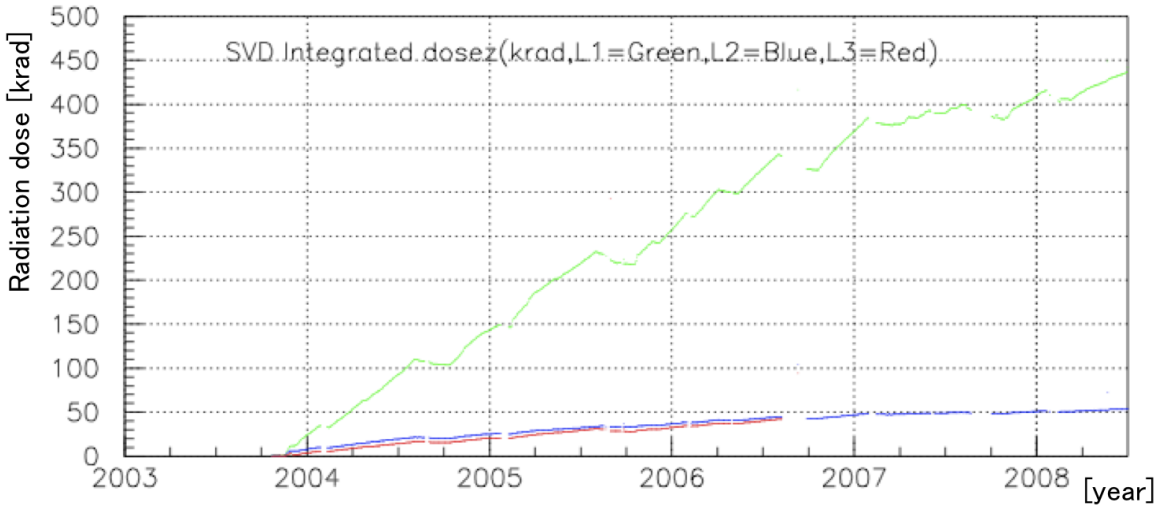

Figure 6.24: SVD radiation dose from RADFET monitor

simulation result of radiation dose

Simulation results for radiation dose and the data obtained from RADFET monitor for 1st layer to 3rd layer of SVD are shown in Tab. 6.6. "Other" background of simulation only contains beam-gas scattering. SR background or other background is not included. For the simulation result, only statistical error was written in table. Systematic error was not obtained precisely.

Table 6.6: Radiation dose simulation results and RADFET radiation dose monitor value. HER SR backgrounds are not simulated.

layer 1 dose [krad/yr]		simulation	data
LER	Touschek	10.5 ± 0.6	
	Coulomb	7.6 ± 1.0	
	brems	1.24 ± 0.02	
HER	Touschek	2.60 ± 0.05	
	Coulomb	0.98 ± 0.04	
	brems	1.60 ± 0.03	
Total		24.5 ± 1.2	$100 \sim 200$

layer 2 dose [krad/yr]		simulation	data
LER	Touschek	4.4 ± 0.1	
	Coulomb	1.9 ± 0.3	
	brems	0.21 ± 0.006	
HER	Touschek	0.49 ± 0.01	
	Coulomb	0.19 ± 0.01	
	brems	0.33 ± 0.006	
Total		7.5 ± 0.3	$10 \sim 20$

layer 3 dose [krad/yr]		simulation	data
LER	Touschek	6.9 ± 0.2	
	Coulomb	0.8 ± 0.1	
	brems	0.05 ± 0.001	
HER	Touschek	0.30 ± 0.005	
	Coulomb	0.11 ± 0.004	
	brems	0.12 ± 0.002	
Total		8.2 ± 0.2	$10 \sim 20$

6.4 Considerations

6.4.1 Validity of the simulation

The ratio of contribution to background is almost same as one of occupancy. Comparing the simulation results of occupancy with background study data, simulation result of "HER other" is much smaller than data. This is because SR background is not counted on the simulation. Backscattered SR background of HER is about 10 $\sim$ 30 % of total background amount, and other SR contribution is small [16]. Simulation result of "LER Touschek" for 3rd layer is much larger than the data. It seems to be over estimation as discussed in Sec. 6.2.3.

Then, it can be said that the simulation results agree with the data.

6.4.2 Function of movable mask

Figure 6.25 and 6.26 shows where background particles of 1st layer were scattered. Background particles for 2nd and 3rd layer were also checked. Movable masks are placed at about 1700 to 1800 m and 2700 to 2800 m. Beam particles scattered by bremsstrahlung are stopped by movable masks. Particles scattered after movable masks become background. For Coulomb scattering background, particles scattered after 1st movable mask become background. About the background caused by Touschek effect, movable mask seems to be not working. That is because how deviate beam orbit is different from kind of scattering. Figure 6.27 shows that how deviate beam orbit by each scattering process. Particles scattered by Coulomb scattering change its direction randomly, so they spread uniform direction. Particles scattered by bremsstrahlung decrease its energy, so they deviate inner direction just after bending magnet. Particles scattered by Touschek effect are divided into two groups. One is energy-decreased particles group; they deviate inner direction like bremsstrahlung. And the other is energy-increased particles group; they

deviate outer direction just after bending magnet. Figure 6.28 shows the distribution in energy deviation vs scattering position plane. We can see that movable mask cannot stop energy-increased particles. That is because movable masks are placed at arc (see Fig. 4.10). From this result, outer horizontal mask is necessary in order to stop Touschek background.

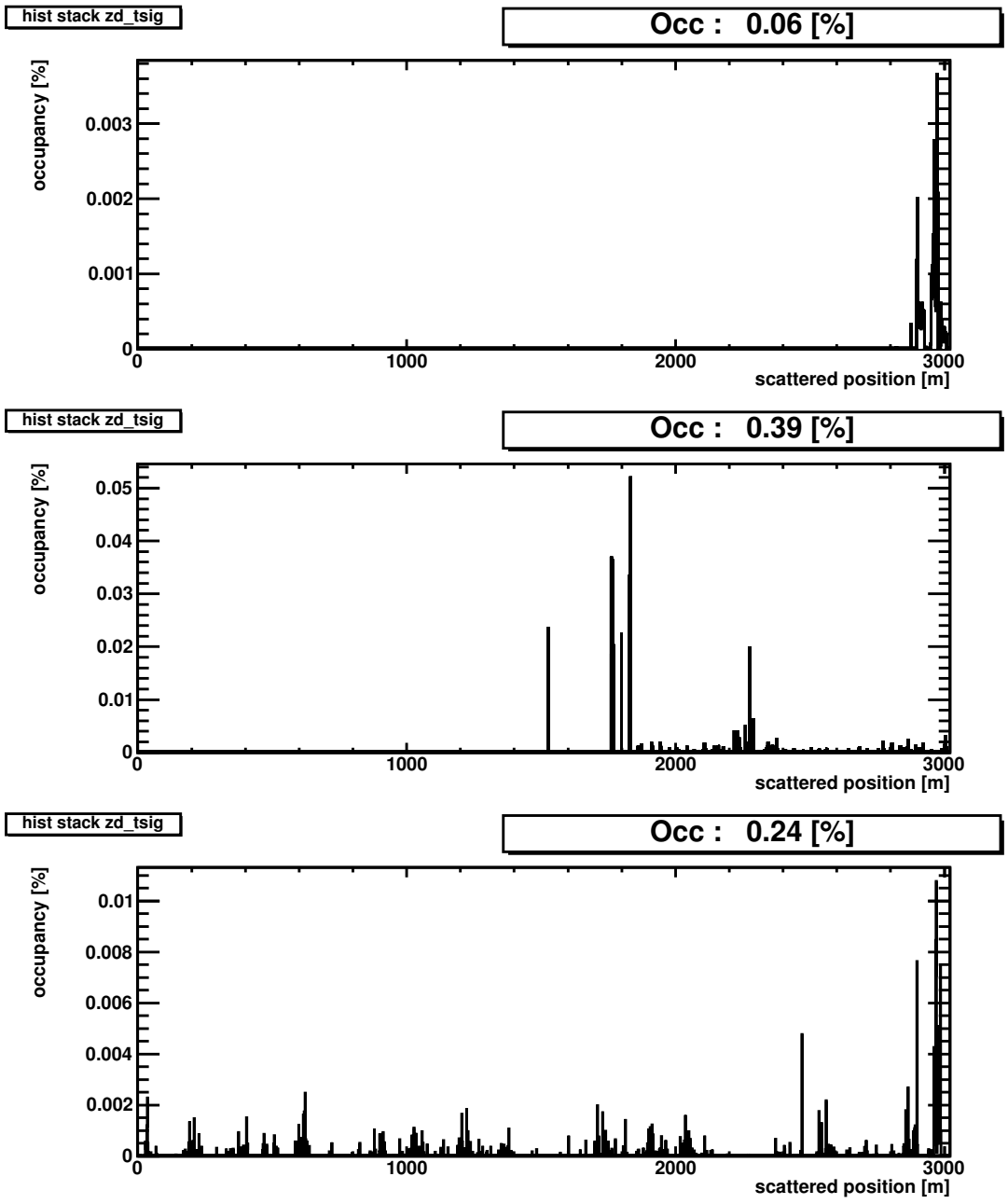

Figure 6.25: Scattering position vs occupancy for 1st layer from LER. 1st layer (top). 2nd layer (middle). 3rd layer (bottom).

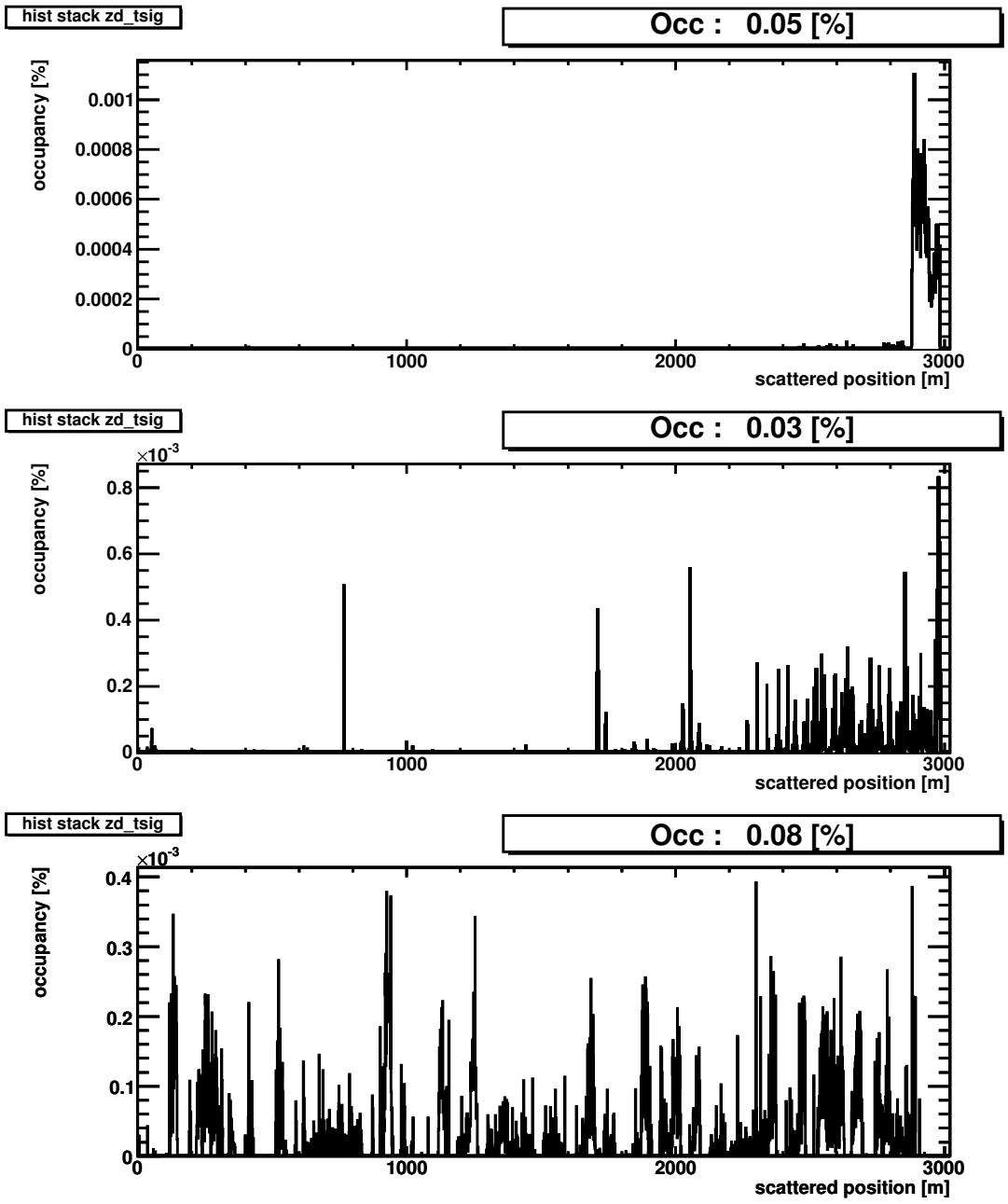

Figure 6.26: Scattering position vs occupancy for 1st layer from HER. 1st layer (top). 2nd layer (middle). 3rd layer (bottom).

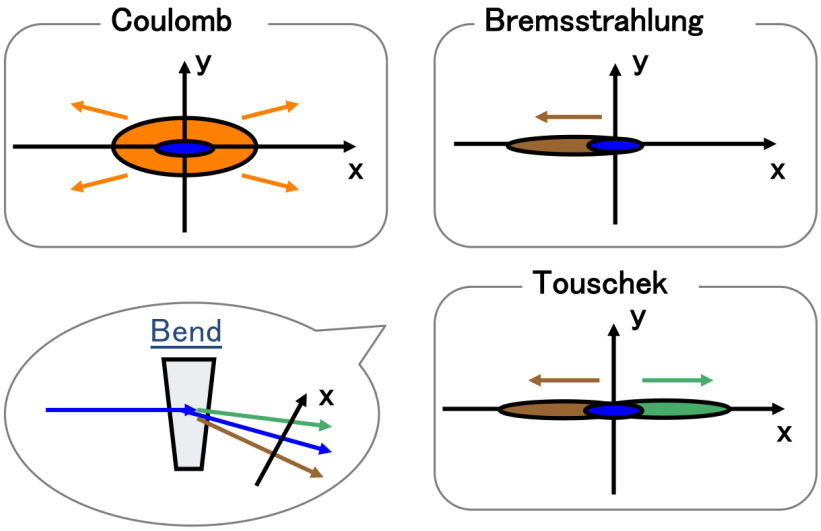

Figure 6.27: Scattered beam profiles

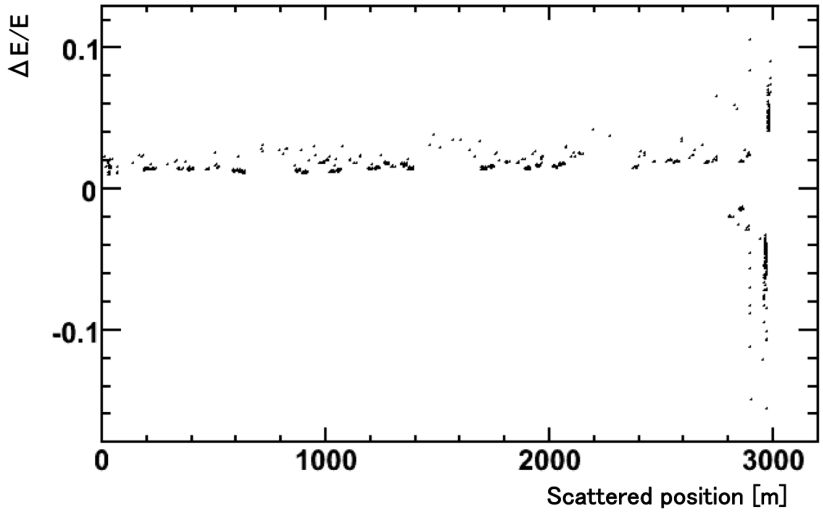

Figure 6.28: Scattering amount vs position for Touschek background

6.5 Beam background simulation of SuperKEKB

Preliminary results for SuperKEKB beam background were obtained by using SuperKEKB optics and Belle detector geometry. In other words, background flux of SuperKEKB applied to current Belle detector. Several assumptions are applied. 10^{-7} Pa vacuum pressure is assumed. Assuming that beam particles which had been scattered at more than 300 m upstream from IP were stopped by "ideal" movable mask; beam particles which had been scattered after 300 m upstream from IP were counted. Beam particles were injected to GEANT geometry from 4 m upstream from IP.

Table 6.7: Radiation dose with SuperKEKB background flux

		layer 1	layer 2	layer 3
LER	Touschek	1060 ± 150	430 ± 35	460 ± 16
	Coulomb	150 ± 10	43 ± 2	37 ± 1
	brems	1.6 ± 0.2	0.60 ± 0.06	0.54 ± 0.07
HER	Touschek	0.02 ± 0.02	0.003 ± 0.003	0.006 ± 0.003
	Coulomb	102 ± 6	42 ± 2	45 ± 1.5
	brems	5.8 ± 0.4	2.0 ± 0.1	0.93 ± 0.06
Total		1300 ± 150	520 ± 35	540 ± 16

Comparing these results with KEKB's ones, we can expect that radiation amount from background will be an order of 1 Mrad/year from 100 krad/year.

Chapter 7

Summary and future prospects

7.1 Summary

Estimation and understanding of beam background are necessary in order to design interaction region (IR) of SuperKEKB collider and Belle-II detector. We simulate the beam background from beam-gas scattering and Touschek effect. KEKB simulation using TURTLE and GEANT shows consistent results with experimental data taken in machine study in June 2010. Therefore we confirm the validity of our simulation framework.

In this simulation study, we obtain detailed understanding of the background mechanism. Scattered beam particles can be a source of detector background in two ways, mainly. First, scattered beam particles hit IR mask directly, generate shower particles, and they reach the detector and become background. Secondly, scattered beam particles hit upstream beam pipe and secondly particle hit IR mask. Especially, photons in generated shower can reach IR mask far from IP since they do not feel magnetic field.

We start the SuperKEKB simulation and obtained preliminary results. According to background mechanism studied with the simulation, it is expected that the dominant background source at SuperKEKB will be the shower generated at taper-shaped part, where beam particles are grazed as shown in Fig. 7.1. This prediction is consistent with

the optics simulation by accelerator group.

Further study on SuperKEKB simulation is ongoing.

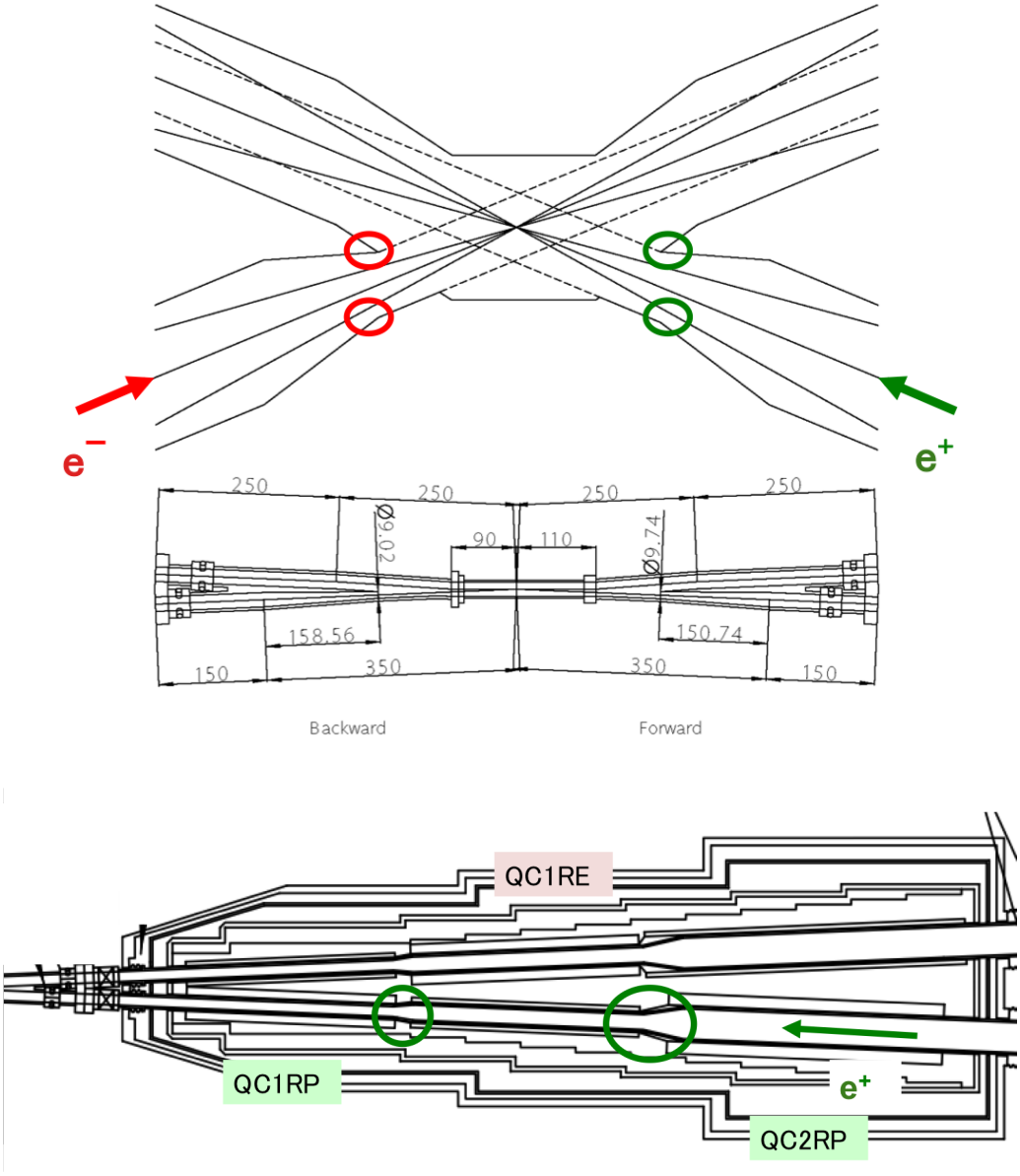

Figure 7.1: Expected shower source position of new IR

7.2 Future prospects

First priority is to complete SuperKEKB simulation and to prepare its documentation. For more credible background estimation including showers from upstream, GEANT simulation should cover wider range. Further geometry implementation is important. The design of heavy-metal mask to protect the PXD and SVD should be optimized based on the simulation results. Position and collimation depth of movable mask should also be optimized.

Appendix A

Accelerator

A.1 Beam transportation and magnets

A.1.1 Coordinate system in accelerator physics

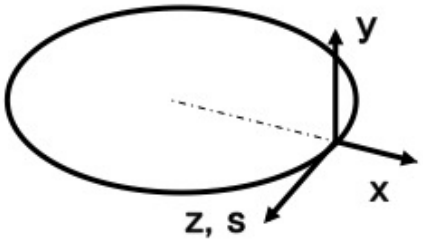

Figure A.1: Coordinate system in accelerator physics

In accelerator physics, local Cartesian coordinate system is generally used. In this system, x axis is taken at the horizontal direction, y axis is taken at the vertical direction and z (or s) axis is taken at the beam direction as shown in Fig. A.1. Coordinates will be defined in this system from now on.

A.1.2 Drift space

The direction of beam particle can only be changed by the existence of a magnetic field. The displacement of position is proportional to beam angle $x^{'}$ ($\equiv \frac{dx}{ds}$) and space length. Therefor the motion in drift space can be illustrated as Fig. **??**, and the transfer matrix can be written as Where L is the horisontal direction.

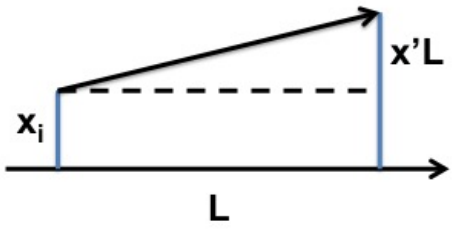

Figure A.2: Illustration of drift space

$$\begin{pmatrix} x_f \\ x_f^{'} \end{pmatrix} = \begin{pmatrix} 1 & L \\ 0 & 1 \end{pmatrix} \begin{pmatrix} x_i \\ x_i^{'} \end{pmatrix}. \tag{A.1}$$

Here, the subscript "i" represents initial beam status, and "f" represents final beam status. The same stands for the vertical direction $(y, y^{'})$.

A.1.3 Bending magnet

Basically, the transfer matrix is the same as drift space except the length is replaced by $\rho\theta$.

$$\begin{pmatrix} x_f \\ x_f^{'} \end{pmatrix} = \begin{pmatrix} 1 & \rho\theta \\ 0 & 1 \end{pmatrix} \begin{pmatrix} x_i \\ x_i^{'} \end{pmatrix}. \tag{A.2}$$

Here, ρ is the radius and θ is the bending angle.

If there is a non-zero angle between beam direction and pole-face, the bending magnet has a lens effect. For example, let's think about situation where a positron beam enters

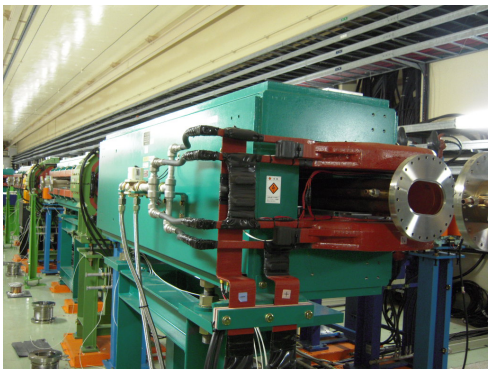

Figure A.3: KEKB bending magnet

and exits rectangular shape magnetic field area (as shown in Fig. A.4) with a pole-face angle of $\theta/2$. Such a magnetic field is considered as a summation of magnetic fields as

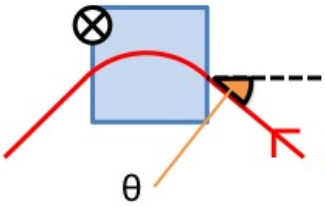

Figure A.4: Pole-face angle of bending magnet

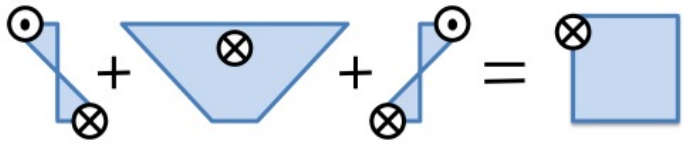

Figure A.5: Summation of magnet

shown in Fig.A.5. From the effect of additional field, a defocusing force is generated.

On the other hand, the change in y direction is caused by fringe field. As shown in Fig. A.6, there is magnetic field which is perpendicular to x direction at the corner of the magnet. Here, positron beams enter the area from the front of the page to the back. So, if beam particle is placed at $y > 0$, the particle feels negative y direction force. And if beam particle is placed at $y < 0$, the particle feels positive y direction force. Thus, a focusing force is generated for y direction. Such a fringe effect is also considered in my background simulation.

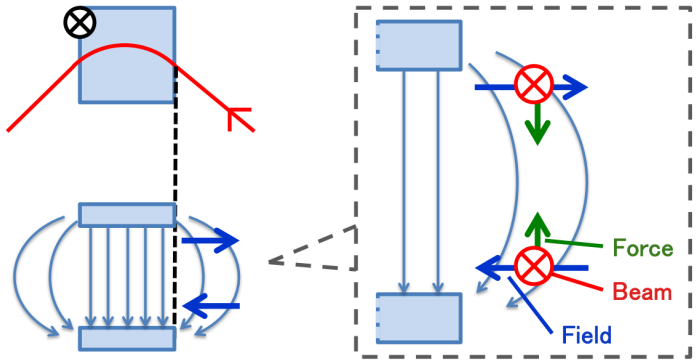

Figure A.6: Fringe field

A.1.4 Quadrupole

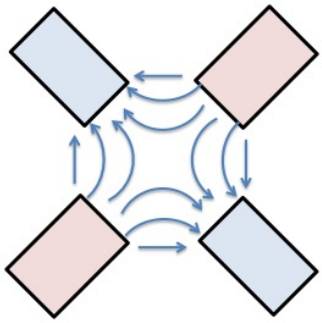

Figure A.7: Quadrupole magnet

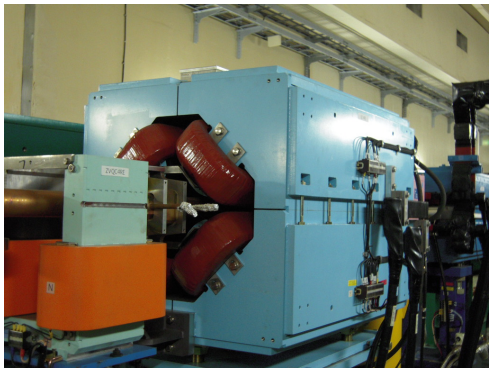

Figure A.8: KEKB quadrupole magnet

Quadrupole has a magnetic field as shown in Fig.A.7. It acts as a focusing lens for one direction, and defocusing lens for another direction. With a thin lens assumption, these lens effect are written as

$$\mathbf{M_f} = \begin{pmatrix} 1 & 0 \\ -\frac{1}{f} & 1 \end{pmatrix} \tag{A.3}$$

$$\mathbf{M_d} = \begin{pmatrix} 1 & 0 \\ \frac{1}{f} & 1 \end{pmatrix} \tag{A.4}$$

Here, $\mathbf{M_f}$ and $\mathbf{M_d}$ are transfer matrix for focusing lens and defocusing lens respectively, where f is focal length. When the beam particles start upstream $a(> f)$, they will be focused at downstream $b(> f)$ as shown in Fig.A.9. The relationship between a and b is

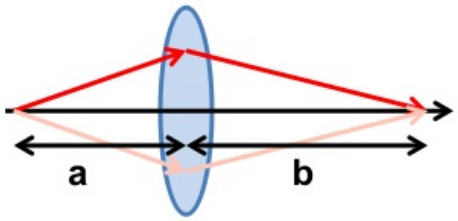

Figure A.9: Relationship between a and b

$$\begin{pmatrix} 1 & b \\ 0 & 1 \end{pmatrix} \begin{pmatrix} 1 & 0 \\ -\frac{1}{f} & 1 \end{pmatrix} \begin{pmatrix} 1 & a \\ 0 & 1 \end{pmatrix} \begin{pmatrix} 0 \\ x' \end{pmatrix} = \begin{pmatrix} a+b-\frac{ab}{f} \\ 1-\frac{a}{f} \end{pmatrix} x' \tag{A.5}$$

$$\Big\downarrow \quad a+b-\frac{ab}{f}=0$$

$$\frac{1}{f} = \frac{1}{a}+\frac{1}{b} \tag{A.6}$$

Therefore by placing focusing magnets periodically, a beam can be transported safety. However we have keep in mind that in quadrupoles when focused in one direction, it defocus in the other. So, FODO lattice is used for beam transportation. FODO lattice is an alignment of a focusing and a defocusing magnet. It has focusing effect totally. Transfer matrices for focusing-drift-defocusing alignment $\mathbf{M_{FODO}}$ and defocusing-drift-focusing alignment $\mathbf{M_{DOFO}}$ as shown in Fig.A.10 and A.11 are

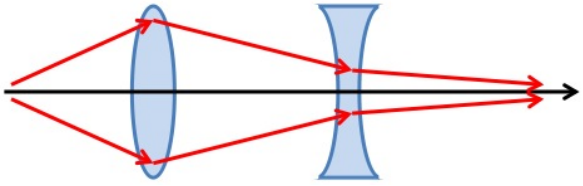

Figure A.10: Illustration of FODO lattice

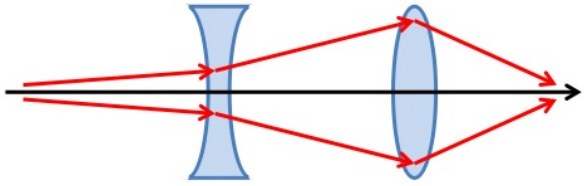

Figure A.11: Illustration of DOFO lattice

$$
\begin{aligned}
\mathbf{M_{FODO}} &= \begin{pmatrix} 1 & L_1 \\ 0 & 1 \end{pmatrix} \begin{pmatrix} 1 & 0 \\ \frac{1}{f} & 1 \end{pmatrix} \begin{pmatrix} 1 & L_2 \\ 0 & 1 \end{pmatrix} \begin{pmatrix} 1 & 0 \\ -\frac{1}{f} & 1 \end{pmatrix} \begin{pmatrix} 1 & L_1 \\ 0 & 1 \end{pmatrix} \\
&= \begin{pmatrix} 1 - \frac{L_2}{f} + \frac{L_1 L_2}{f^2} & (2L_1 - L_2) - \frac{L_1^2 L_2}{f^2} \\ -\frac{L_2}{f^2} & 1 + \frac{L_2}{f} - \frac{L_1 L_2}{f^2} \end{pmatrix} \qquad \text{(A.7)} \\
\mathbf{M_{DOFO}} &= \begin{pmatrix} 1 & L_1 \\ 0 & 1 \end{pmatrix} \begin{pmatrix} 1 & 0 \\ -\frac{1}{f} & 1 \end{pmatrix} \begin{pmatrix} 1 & L_2 \\ 0 & 1 \end{pmatrix} \begin{pmatrix} 1 & 0 \\ \frac{1}{f} & 1 \end{pmatrix} \begin{pmatrix} 1 & L_1 \\ 0 & 1 \end{pmatrix} \\
&= \begin{pmatrix} 1 + \frac{L_2}{f} - \frac{L_1 L_2}{f^2} & (2L_1 - L_2) - \frac{L_1^2 L_2}{f^2} \\ -\frac{L_2}{f^2} & 1 - \frac{L_2}{f} - \frac{L_1 L_2}{f^2} \end{pmatrix}. \qquad \text{(A.8)}
\end{aligned}
$$

A.1.5 Sextupole

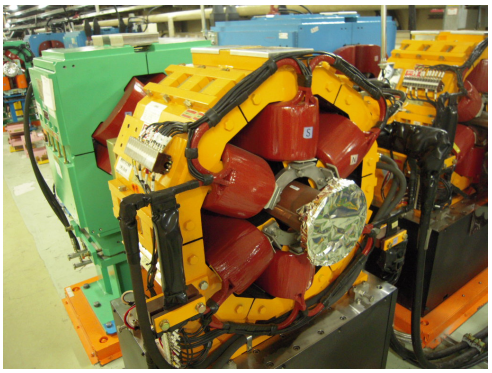

Figure A.12: KEKB sextupole magnet

Sextupole is a magnet which has six poles as shown in Fig. A.12. They are used for chromaticity correction. Chromaticity is the difference of bend angle caused by difference of particle energies.

A.2 Beam dynamics

In this section, for the purpose of understanding main beam parameters, general transfer matrix and Courant-Snyder invariant will be derived from equation of motion of the beam. Equation of motion for beam optics can be written as

$$\frac{d^2x}{ds^2} + k_x(s)x = 0 \tag{A.9}$$

This also stands for y. Here, $k_x(s)$ and $k_y(s)$ are

$$\begin{aligned} k_x(s) &= \frac{1}{\rho^2} + \frac{e}{p_0}\frac{\partial B_y}{\partial x} \\ k_y(s) &= -\frac{e}{p_0}\frac{\partial B_x}{\partial y} = -\frac{e}{p_0}\frac{\partial B_y}{\partial x} \end{aligned}$$

Equation (A.9) is called Hill's equation. When $k(s)$ is constant, the equation is a harmonic oscillator. To say roughly, this equation shows existence of the force which keeps beam particle within design orbit. The general solution of Hill's equation is

$$x(s) = A\omega(s)cos\Psi(s) + B\omega(s)sin\Psi(s) \tag{A.10}$$

This oscillation which is perpendicular to beam direction is called betatron oscillation. In equation (A.10), the first term and the second term satisfy Hill's equation (A.9) independently. Therefore by substituting $x(s) = A\omega(s)cos\Psi(s)$ for eq.(A.9), we get

$$Acos\Psi(s)\left\{\omega''(s) - \omega(s)\Psi'^2(s) + k(s)\omega(s)\right\} - Bsin\Psi(s)\left\{2\omega'(s)\Psi'(s) + \omega(s)\Psi''(s)\right\} = 0 \tag{A.11}$$

Then,

$$\begin{cases} \omega''(s) - \omega(s)\Psi'^2(s) + k(s)\omega(s) = 0 \\ 2\omega'(s)\Psi'(s) + \omega(s)\Psi''(s) = 0 \end{cases} \tag{A.12}$$

From the second equation, we get the relationship between $\omega(s)$ and $\Psi(s)$.

$$\begin{aligned} 2\omega^{'}(s)\Psi^{'}(s)+\omega(s)\Psi^{''}(s) &= \frac{\frac{d}{ds}(\omega^2(s)\Psi^{'}(s))}{\omega(s)}=0 \\ &\Big\downarrow \quad \omega^2(s)\Psi^{'}=const \\ \Psi^{'}(s) &= \frac{1}{\omega^2(s)} \end{aligned} \tag{A.13}$$

Here, the integration constant is normalized. Differentiation of eq.(A.10) gives

$$\begin{aligned} x^{'}(s) &= A\left(\omega^{'}(s)cos\Psi(s)-\omega(s)\Psi^{'}(s)sin\Psi(s)\right)+B\left(\omega^{'}(s)sin\Psi(s)+\omega(s)\Psi^{'}(s)cos\Psi(s)\right) \\ &= A\left(\omega^{'}(s)cos\Psi(s)-\frac{sin\Psi(s)}{\omega(s)}\right)+B\left(\omega^{'}(s)sin\Psi(s)+\frac{cos\Psi(s)}{\omega(s)}\right) \end{aligned} \tag{A.14}$$

Then, we get $x(s)$ and $x^{'}(s)$. Let's derive general transfer matrix $\mathbf{M}$ which satisfy

$$\begin{pmatrix} x(s) \\ x^{'}(s) \end{pmatrix} = \mathbf{M} \begin{pmatrix} x(s_0) \\ x^{'}(s_0) \end{pmatrix}. \tag{A.15}$$

By substituting $x(s_0)=x_0$,$x^{'}(s_0)=x_0^{'}$,$\Psi^{'}(s_0)=\Psi_0$ and $\omega(s_0)=\omega_0$ for eq.(A.10) and (A.14), we get

$$x_0 = A\omega_0 cos\Psi_0 + B\omega_0 sin\Psi_0 \tag{A.16}$$

$$x_0^{'} = A\left(\omega_0^{'}cos\Psi_0-\frac{sin\Psi_0}{\omega_0}\right)+B\left(\omega_0^{'}sin\Psi_0+\frac{cos\Psi_0}{\omega_0}\right) \tag{A.17}$$

Solving these equations for A and B, we get

$$A = \left(\omega_0^{'}sin\Psi_0+\frac{cos\Psi_0}{\omega_0}\right)x_0-\left(\omega_0 sin\Psi_0\right)x_0^{'} \tag{A.18}$$

$$B = -\left(\omega_0^{'}cos\Psi_0-\frac{sin\Psi_0}{\omega_0}\right)x_0+\left(\omega_0 cos\Psi_0\right)x_0^{'} \tag{A.19}$$

Substituting these equations (A.18) and (A.19) for (A.10) and (A.14), we get

$$\begin{aligned} x(s) &= \left\{ \frac{\omega(s)}{\omega_0} cos[\Psi(s) - \Psi_0] - \omega(s)\omega_0^{'} sin[\Psi(s) - \Psi_0] \right\} x_0 \\ &\quad + \omega(s)\omega_0 sin[\Psi(s) - \Psi_0] x_0^{'} \qquad \text{(A.20)} \\ x^{'}(s) &= \left\{ -\frac{1 + \omega(s)\omega_0\omega^{'}(s)\omega_0^{'}}{\omega(s)\omega_0} sin[\Psi(s) - \Psi_0] - \left(\frac{\omega_0^{'}}{\omega(s)} - \frac{\omega^{'}(s)}{\omega_0} \right) cos[\Psi(s) - \Psi_0] \right\} x_0 \\ &\quad + \left\{ \omega_0\omega^{'}(s) sin[\Psi(s) - \Psi_0] + \frac{\omega_0}{\omega(s)} cos[\Psi(s) - \Psi_0] \right\} x_0^{'} \qquad \text{(A.21)} \end{aligned}$$

Defining $\beta(s)$, $\alpha(s)$ and $\Delta\Psi(s)$ as

$$\begin{aligned} \beta(s) &= \omega^2(s) \qquad \text{(A.22)} \\ \alpha(s) &= - = -\omega(s)\omega^{'}(s) \qquad \text{(A.23)} \\ \Delta\Psi(s) &= \Psi(s) - \Psi_0, \qquad \text{(A.24)} \end{aligned}$$

eq.(A.20) and (A.21) become

$$\begin{aligned} x(s) &= \left\{ \sqrt{\frac{\beta(s)}{\beta_0}} [cos\Delta\Psi(s) + \alpha_0 sin\Delta\Psi(s)] \right\} x_0 + \left\{ \sqrt{\beta_0\beta(s)} sin\Delta\Psi(s) \right\} x_0^{'} \qquad \text{(A.25)} \\ x^{'}(s) &= \left\{ -\frac{[\alpha(s) - \alpha_0] cos\Delta\Psi(s) + [1 + \alpha_0\alpha(s)] sin\Delta\Psi(s)}{\sqrt{\beta_0\beta(s)}} \right\} x_0 \\ &\quad + \left\{ \sqrt{\frac{\beta_0}{\beta(s)}} [cos\Delta\Psi(s) - \alpha(s) sin\Delta\Psi(s)] \right\} x_0^{'} \qquad \text{(A.26)} \end{aligned}$$

Then, $\mathbf{M}$ is obtained as

$$\mathbf{M} = \begin{pmatrix} \sqrt{\frac{\beta(s)}{\beta_0}} [cos\Delta\Psi(s) + \alpha_0 sin\Delta\Psi(s)] & \sqrt{\beta_0\beta(s)} sin\Delta\Psi(s) \\ -\frac{[\alpha(s) - \alpha_0] cos\Delta\Psi(s) + [1 + \alpha_0\alpha(s)] sin\Delta\Psi(s)}{\sqrt{\beta_0\beta(s)}} & \sqrt{\frac{\beta_0}{\beta(s)}} [cos\Delta\Psi(s) - \alpha(s) sin\Delta\Psi(s)] \end{pmatrix} \qquad \text{(A.27)}$$

In addition, if we describe

$$\frac{x_0}{\sqrt{\beta_0}} = \sqrt{c_1} cos c_2 \tag{A.28}$$

$$-\left(\frac{x_0}{\sqrt{\beta_0}}\alpha_0 + \sqrt{\beta_0}x_0^{'}\right) = \sqrt{c_1} sin c_2 \tag{A.29}$$

using arbitrary value c_1 and c_2, eq.(A.25) and (A.26) can be written as

$$x(s) = \sqrt{c_1\beta(s)} cos[\Delta\Psi(s) + c_2] \tag{A.30}$$

$$x^{'}(s) = -\sqrt{\frac{c_1}{\beta(s)}}\left\{\alpha(s) cos[\Delta\Phi(s) + c_2] + sin[\Delta\Phi(s) + c_2]\right\}. \tag{A.31}$$

Then, by using $\gamma(s) = \dfrac{1+\alpha^2(s)}{\beta(s)}$, $x(s)$ and $x^{'}(s)$ satisfies

$$\begin{aligned}
& \gamma(s)x^2(s) + \beta(s)x^{'2}(s) + 2\alpha(s)x(s)x^{'}(s) \\
= \; & \left\{c_1 cos^2[\Delta\Psi(s) + c_2] + c_1\alpha^2(s) cos^2[\Delta\Psi(s) + c_2]\right\} \\
& + \left\{c_1\alpha^2(s) cos^2[\Delta\Psi(s) + c_2] + 2\alpha sin[\Delta\Psi(s) + c_2] cos[\Delta\Psi(s) + c_2] + sin^2[\Delta\Psi(s) + c_2]\right\} \\
& + \left\{-2\alpha^2 c_1 cos^2[\Delta\Psi(s) + c_2] - 2\alpha c_1 sin[\Delta\Psi(s) + c_2] cos[\Delta\Psi(s) + c_2]\right\} \\
= \; & c_1
\end{aligned} \tag{A.32}$$

This invariant is called Courant-Snyder invariant. The group of $(x(s), x^{'}(s))$ with arbitrary c_1 and s distributes on an ellipse, and when there 1σ of beam particles in the ellipse, such a c_1 is called emittance, ϵ [17].

A.3 Beam parameters

In last section, we studied beam particle dynamics. Then, we are ready to understand meaning of the beam parameters. In this section, beam parameters which are important for accelerator are described.

A.3.1 N_b : number of bunches

In accelerator, beam particles accelerated forming a group called "bunch". In KEKB, radio frequency of accelerator cavity is 508 MHz. This means 508 million bunchs can be accelerated per second. There are accelerator cavities in LER and HER for compensating lost energy from synchrotron radiation. KEKB ring has the circumference of 3000 m and the beam velocity is almost speed of light, 3.0×10^8 m/s. Beam particle circles 10^5 times per second. Then, accelerator cavity can accelerate a maximum $\dfrac{508 \times 10^6}{10^5} \sim 5000$ bunches. These 5000 places for bunch acceleration are called "buckets". However, if the distance from a bunch to the next bunch becomes short, the following bunch is strongly effected by HOM or electron cloud and becomes unstable. Thus, at current KEKB, each bunch is separated 2 or 3 buckets and about 1600 bunches circle totally.

A.3.2 $\alpha_{x,y}, \beta_{x,y}, \gamma_{x,y}, \sigma_{x,y}$: twiss parameters and beam size

The equation of Courant-Snyder invariant ,Eq. (A.32), is a formula of an ellipse. Figure

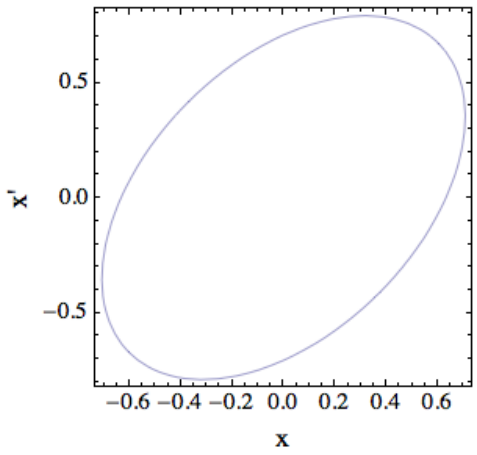

Figure A.13: Phase space of beam particle(Mathematica fonts by Wolfram Research, Inc.)

A.13 shows the ellipse with $\epsilon = 0.5$, $\beta = 1$ and $\alpha = -0.5$. Here, the maximum value of $x(s)$ is $\sqrt{\epsilon\beta(s)} \equiv \sigma_x(s)$, so $\sigma_x(s)$ means beam size at the position s. The maximum value

of $x^{'}(s)$ is $\sqrt{\epsilon\gamma(s)} \equiv \sigma_{x'}(s)$, and it describes width of $x^{'}$ distribution. Thus, $\sqrt{\beta(s)}$ is proportional to beam size, $\alpha(s) \equiv -\frac{1}{2}\beta^{'}(s)$ indicates whether beam size is increasing or decreasing. $\alpha(s) > 0$ means beam size is decreasing (focused), at s. $\alpha(s) < 0$ means beam size is increasing (defocused), at s. For example, looking at Fig.A.13, most of positive x particle has $x^{'} > 0$, and most of negative x particle has $x^{'} < 0$. The beam is indeed focused at the position s.

Betatron oscillation is described as circular motion on the ellipse. As $\beta(s)$ is dependent on position s, beam particles rotate on the periodical variable ellipse orbit in the phase space.

A.3.3 $\nu_{x,y}$: betatron tune

Betatron tune is the frequency of betatron oscillation per cycle. So, $\nu = \Delta\Psi$ (1 cycle) should not take an integer or a half integer. If the betatron tune is an integer, beam particle traces the same orbit every cycle. If the betatron tune is a half integer, beam particle traces same orbit every two cycles. This means the beam particle undergoes the same miss alignment of elements in optics causing bean instability. This is why betatron tune should be set as a "halfway" value.

A.3.4 $\xi_{x,y}$: beam beam tune shift parameter

To obtain high luminosity, beam beam tune shift parameters $\xi_{x,y}$ are important. These parameter describes the effect on opposite bunch at IP when they cross each other. For positrons in positive charged bunch, negative charged bunch acts as focusing lens for both horizontal and vertical directions. It is correspondingly for electrons in negative charged bunch. Now, for example, let's consider the effect on positron from negative charged bunch at IP.

As the bunch moves at the speed of light, electric field of the bunch shrink along

the beam direction because of Lorentz contraction. Thus, the number of lines of electric force per unit z direction is proportional to the amount of charge per unit z direction. Which means that it is proportional to number of electrons per bunch N_-, and inversely proportional to bunch length $\sigma_{z,-}$. Here, the subscript "-" means negative charged bunch. Now, in the x-y plane, density of lines of electric force is inversely proportional to the circumference of the beam profile, thus being inversely proportional to $\sigma^*_{x,-} + \sigma^*_{y,-}$.

The force from negative charged bunch is dependent on position of the positron. For simplification, if we consider the electric field along the y direction to be shown as in Fig.A.14. Then, the gradient of field strength $\dfrac{\partial E}{\partial y}$ for $0 \leq y \lesssim \sigma^*_{y,-}$ becomes $\sigma^*_{y,-}$.

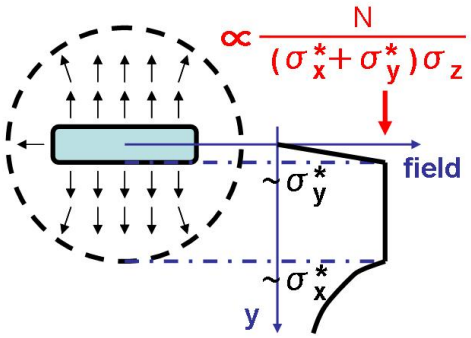

Figure A.14: Illustration of electric field along y direction

The length of time which positron feel force from negative charged bunch is propor-

tional to bunch length $\sigma_{z,-}$. From equation of motion,

$$\begin{aligned}
\gamma_+ m_e \frac{d^2y}{dt^2} &\propto -\frac{e^2 N_-}{\sigma^*_{y,-}(\sigma^*_{x,-}+\sigma^*_{y,-})\sigma_{z,-}} y \\
&\Big\downarrow \int dt \\
\Delta\frac{dy}{dt} &\propto -\frac{e^2 N_-}{\gamma_+ m_e \sigma^*_{y,-}(\sigma^*_{x,-}+\sigma^*_{y,-})\sigma_{z,-}} yt \\
&\Big\downarrow \frac{dy}{dt} = cy^{'}, t \propto \sigma_{z,-} \\
\Delta y^{'} &\propto -\frac{r_e N_-}{\gamma_+ \sigma^*_{y,-}(\sigma^*_{x,-}+\sigma^*_{y,-})} y
\end{aligned} \tag{A.33}$$

Here, γ_+ is the gamma factor of positron (not twiss parameter), m_e and e are mass and electric charge of positron respectively, and r_e is classical electron radius, $r_e \equiv \frac{e^2}{4\pi\epsilon_0 mc^2}$.

Using an analogy of thin focusing lens as shown in Fig.A.15,

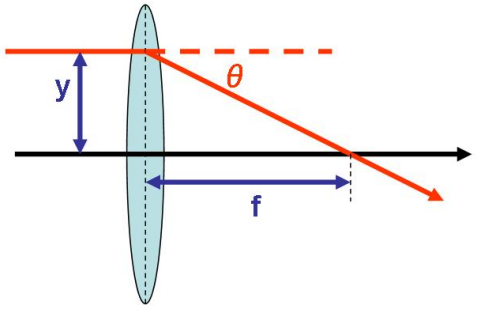

Figure A.15: Illustration of thin lens and focal length

$$-\frac{y}{f} \sim \theta = \Delta y^{'} \tag{A.34}$$

$$-\frac{1}{f} \propto -\frac{r_e N_-}{\gamma_+ \sigma^*_{y,-}(\sigma^*_{x,-}+\sigma^*_{y,-})} \tag{A.35}$$

Then, transfer matrix for $(y, y^{'})$ of positron $\mathbf{M}$ can be written as

$$\mathbf{M} = \begin{pmatrix} 1 & 0 \\ -C\dfrac{r_e N_-}{\gamma_+ \sigma^*_{y,-}(\sigma^*_{x,-} + \sigma^*_{y,-})} & 1 \end{pmatrix} \tag{A.36}$$

Here, C is an arbitrary constant. Now, if we recall Eq. (A.27) and consider $s = s_i$ as the position just before bunch crossing and $s = s_f$ as just after, substituting $\beta(s_i) \sim \beta(s_f) \sim \beta^*_{y,+}$, $\alpha(s_i) \sim \alpha(s_f) \sim 0$ and $\Phi(s_f) - \Phi(s_i) \equiv \xi_{y,+}$, we get

$$\mathbf{M} = \begin{pmatrix} cos\xi_{y,+} & \beta^*_{y,+} sin\xi_{y,+} \\ -\dfrac{sin\xi_{y,+}}{\beta^*_{y,+}} & cos\xi_{y,+} \end{pmatrix} \sim \begin{pmatrix} 1 & 0 \\ -\dfrac{\xi_{y,+}}{\beta^*_{y,+}} & 1 \end{pmatrix}. \tag{A.37}$$

Comparing between Eq. (A.36) and Eq. (A.37), tune shift by bunch crossing (i.e. beam beam effect) $\xi_{y,+}$ is

$$\xi_{y,+} \propto \frac{r_e N_- \beta^*_{y,+}}{\gamma_- \sigma^*_{y,-}(\sigma^*_{x,-} + \sigma^*_{y,-})} \tag{A.38}$$

The value $\xi_{y,+}$ represents focus strength of the opposite bunch and is called beam beam tune shift parameter. To be precise, $\xi_{y,+}$ is defined as

$$\xi_{y,+} \equiv \frac{r_e N_- \beta^*_{y,+}}{2\pi\gamma_- \sigma^*_{y,-}(\sigma^*_{x,-} + \sigma^*_{y,-})} R_{\xi_y} \tag{A.39}$$

Here, R_{ξ_y} is correction coefficient for geometrical factor such as non-zero crossing angle and hourglass effect [8].

A.3.5 $\mathcal{L}$: Luminosity

Luminosity $\mathcal{L}$ is proportional to the number of events per unit time. The number of events can be written as,

$$(\#\ of\ events) = \sigma \times \int dt\ \mathcal{L}. \tag{A.40}$$

Where, σ is the cross section of the event, and luminosity is integrated over operation time. $\int dt\ \mathcal{L}$ is called "integrated luminosity" and its unit is inverse area. Luminosity $\mathcal{L}$ can be written as

$$\mathcal{L} = \frac{N_+ N_- f_c}{2\pi\sqrt{(\sigma^{*2}_{x,+} + \sigma^{*2}_{x,-})(\sigma^{*2}_{y,+} + \sigma^{*2}_{y,-})}} R_{\mathcal{L}} \tag{A.41}$$

Where, $N_\pm$ is the number of beam particles per bunch, f_c is crossing frequency, σ^* is beam size at interaction point (IP) and R_L is "luminosity reduction coefficient" which is related with crossing angle and geometrical (hourglass) effect [18], [19]. If the beam size of positive charged beam and negative charged beam at IP are same, equation (A.41) can be written as

$$\mathcal{L} = \frac{N_+ N_- f_c}{4\pi\sigma^*_x\sigma^*_y} R_L \tag{A.42}$$

Let's describe luminosity $\mathcal{L}$ using $\xi_{y,+}$,

$$\begin{aligned} \frac{\mathcal{L}}{\xi_{y,+}} &= \left(\frac{N_+ N_- f_c}{4\pi\sigma^*_x\sigma^*_y} R_L\right) \Big/ \left(\frac{r_e N_- \beta^*_y}{2\pi\gamma_+\sigma^*_y(\sigma^*_x + \sigma^*_y)} R_{\xi_y}\right) \\ &\Big\downarrow \quad N_+ f_c = I_+/e \\ \mathcal{L} &= \frac{\gamma_+}{2er_e}\left(1 + \frac{\sigma^*_y}{\sigma^*_x}\right)\left(\frac{I_+\xi_{y,+}}{\beta^*_y}\right)\left(\frac{R_L}{R_{\xi_y}}\right) \end{aligned} \tag{A.43}$$

Here, I_+ is positive beam current [8] [19].

A.3.6 R_L : Luminosity reduction coefficient

Luminosity reduction coefficient R_L is mainly consists of two parts, non-zero crossing angle and hourglass effect.

$$R_L = R_{cross} \times R_{hourglass} \tag{A.44}$$

Where, R_{cross} and $R_{hourglass}$ are reduction coefficient from non-zero crossing angle and hourglass effect respectively.

The reduction coefficient R_{cross} for a symmetric-collider (while KEKB is asymmetric-collider) with $\sigma_y^* \ll \sigma_x^*$ is [18]

$$R_{cross} = \sqrt{\frac{2}{\pi}} a e^b K_0(b) \tag{A.45}$$

$$a = \frac{\beta_y^*}{\sqrt{2}\sigma_z}, \qquad b = a^2\left[1 + \left(\frac{\sigma_z}{\sigma_x^*} tan\phi\right)^2\right]$$

Where, K_0 is a Bessel function, β_y^* is vertical beta function of twiss parameter at IP, σ_z is horizontal beam size at IP and ϕ is half crossing angle. For reference, substituting $\beta_y^* = 10mm$, $\sigma_z = 4mm$, $\sigma_x^* = 77\mu m$ and $\phi = 11$ mrad (KEKB design value(from table 3.1)) in equation (A.45), R becomes 0.84.

Hourglass effect is named after beam size shape at IP. Figure A.16 shows an image of hourglass effect. Around the IP, horizontal and vertical beam size $\sigma_{x,y}(s)$ can be written as

$$\sigma_{x,y}(s) = \sqrt{\epsilon_{x,y}\left(\beta_{x,y}^* + \frac{s^2}{\beta_{x,y}^*}\right)} \tag{A.46}$$

Where s is the distance from IP. This means that the stronger the focusing, the faster beam size enlarges from IP. Even if we decreased the beam size at IP, if beam sizes at other positions were to increase we couldn't gain luminosity. If only beam size at IP is small and beam size at other position is large, luminosity doesn't become high. This is called the hourglass effect. When the bunch length σ_z is greater than twiss beta at IP β^*, this effect strengthens. Thus causing luminosity reduction. The reduction coefficient $R_{hourglass}$ with $\sigma_z \lesssim \beta^*$ is [18]

$$R(t_x, t_y) = \int_{-\infty}^{\infty} \frac{dt}{\sqrt{pi}} \frac{e^{-t^2}}{\sqrt{\left(1 + \frac{t^2}{t_x^2}\right)\left(1 + \frac{t^2}{t_y^2}\right)}} \tag{A.47}$$

$$t_x^2 = \frac{2(\sigma_{x,+}^{*2} + \sigma_{x,-}^{*2})}{\left(\sigma_{z,+}^2 + \sigma_{z,-}^2\right)\left(\frac{\sigma_{x,+}^{*2}}{\beta_{x,+}^{*2}} + \frac{\sigma_{x,-}^{*2}}{\beta_{x,-}^{*2}}\right)}$$

and correspondingly for t_y. If we assume that the bunch size of positive beam and negative beam are the same, t_x is

$$t_x^2 = \frac{\beta_x^{*2}}{\sigma_z^2} \tag{A.48}$$

(and it is correspondingly for t_y). Substituting beam parameters of luminosity record $\beta_x^* = 1200mm$, $\beta_y^* = 5.9mm$ and $\sigma_z = 6mm$ in the equation (A.47), R becomes 0.86. From this effect, vertical beta function at IP β_y^* cannot become any smaller than bunch length σ_z.

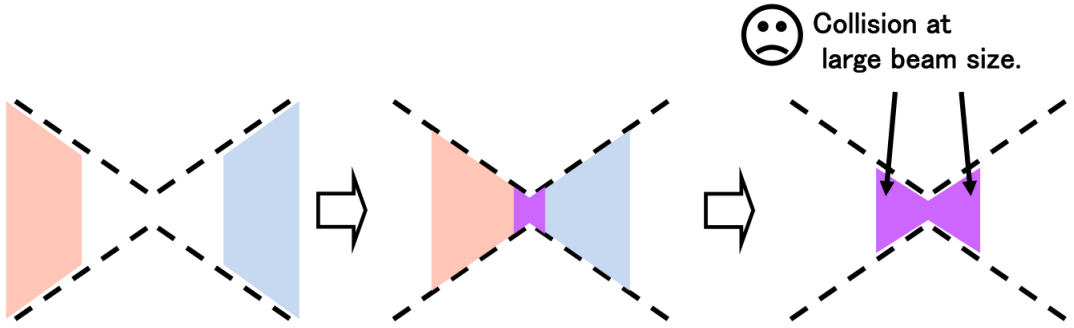

Figure A.16: Illustration of hourglass effect.

A.4 Accelerator components

A.4.1 Damping ring

Although it is said that emittance is a constant, there is a way to change emittance. The way to decrease emittance is first, decrease beam particle momentum by emitting SR. Second, using accelerating cavity only increases momentum in the beam direction. Thus, only the momentum perpendicular to beam direction is decreased as shown in Fig. A.17. The storage ring which plays a roll for damping is called damping ring.

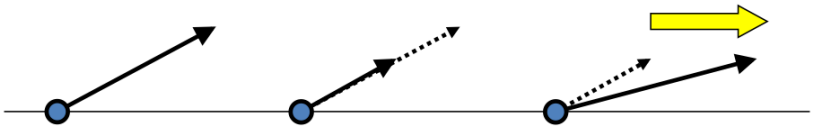

Figure A.17: Damping mechanism

Bibliography

[1] Heavy Flavor Averaging Group. http://www.slac.stanford.edu/xorg/hfag/triangle/moriond2010/index.shtml.

[2] KEK. Physics at super b factory. http://belle2.kek.jp/physics.html, February 2010.

[3] BELLE HOME PAGE. http://belle.kek.jp/.

[4] KEKB HOME PAGE. http://acc-physics.kek.jp/OHO/OHO05/kekbtour.htm.

[5] A. Abashian et al. The belle detector. *Nucl. Inst. Meth. A*, 479:117, (2002).

[6] KEK. Kekb design report.

[7] KEK. Belle ii technical design report. http://b2comp.kek.jp/~twiki/pub/Organization/B2TDR/B2TDR.pdf, Nov 2010.

[8] Naoko Ida. status of superkekb project. *High energy news*, 29-1:20, (2010).

[9] S K Sahu T E Browder, editor. *Proceedings of the Second Workshop on BACKGROUNDS AT THE MACHINE-DETECTOR INTERFACE.* World Scientific, (1998).

[10] A. Piwinski. The touschek effect in strong focusing storage rings, Mar 1999.

[11] Ch. Iselin D. C. Carey, K. L. Brown. Decay turtle. http://www.slac.stanford.edu/pubs/slacreports/slac-r-246.html.

[12] Kenichi Kanazawa. Basic of vacuum technology and accelerator. http://accwww2.kek.jp/oho/oho09/text.html, (2009).

[13] H. Ozaki. (d)ssd signal generator. *Belle note*, (110), February (1996).

[14] T. Hara. Numbering rules for svd2.0. *Belle note*, (464).

[15] Shinya Sugihara. Design study of belle ii interaction region, 2011.

[16] O. Tajima. http://www.phys.hawaii.edu/~superb04/slides.html.

[17] William W MacKay Mario Conte. *An Introduction to the Physics of Particle Accelerators*. World Scientific, (2008).

[18] Maury Tigner Alexander Wu Chao, editor. *Handbook of Accelerator Physics and Engineering 3rd Printing*. World Scientific, (2009).

[19] Yukiyoshi Ohnishi. Superkekb factory. *BUTSURI*, 63:10, (2008).